ORNL/SUB-4450-1
MIT-EL 76-005

MASSACHUSETTS INSTITUTE OF TECHNOLOGY

APPLIED TECHNOLOGY

ANY FURTHER DISTRIBUTION BY ANY HOLDER OF THIS DOCUMENT OR OF THE DATA THEREIN TO THIRD PARTIES REPRESENTING FOREIGN INTERESTS, FOREIGN GOVERNMENTS, FOREIGN COMPANIES AND FOREIGN SUBSIDIARIES OR FOREIGN DIVISIONS OF U.S. COMPANIES SHOULD BE COORDINATED WITH THE DIRECTOR, DIVISION OF REACTOR RESEARCH AND DEVELOPMENT, U.S. ENERGY RESEARCH AND DEVELOPMENT ADMINISTRATION.

ORNL/SUB/4450-1
MIT-EL 76-005

WATER TESTS FOR DETERMINING POST VOIDING BEHAVIOR IN THE LMFBR

by
William D. Hinkle

MASTER

June, 1976

ORNL/SUB/4450-1
MIT-EL 76-005

Final Report

WATER TESTS FOR DETERMINING POST-VOIDING BEHAVIOR IN THE LMFBR

by
William D. Hinkle

Energy Laboratory
Massachusetts Institute of Technology
Cambridge, Massachusetts 02139

sponsored by
The Union Carbide Corporation, Nuclear Division
under Subcontract No. 4450 of
Contract No. W-7405-eng-26
with
The United States Energy Research and
Development Administration

June, 1976

ABSTRACT

The most serious of the postulated accidents considered in the design of the Liquid Metal Cooled Fast Breeder Reactor (LMFBR) is the Loss of Pipe Integrity (LOPI) accident. Analysis models used to calculate the consequences of this accident assume that once boiling is initiated film dryout occurs in the hot assembly as a result of rapid vapor bubble growth and consequent flow stoppage or reversal. However, this assumption has not been put to any real test.

Once boiling is initiated in the hot assembly during an LMFBR LOPI accident, a substantial gravity pressure difference would exist between this assembly and other colder assemblies in the core. This condition would give rise to natural circulation flow boiling accompanied by pressure and flow oscillations. It is possible that such oscillations could prevent or delay dryout and provide substantial post-voiding heat removal. The tests described in this report were conceived with the objective of obtaining basic information and data relating to this possibility.

To accomplish this objective a natural circulation test loop was designed to simulate LMFBR geometry and flow conditions predicted to exist at the time boiling is initiated in a LOPI accident. The test loop included: (1) a vertical tube test section, (2) upper and lower plenum tanks, (3) an external down-commer, (4) sight flow indicators and (5) instrumentation. The test section was an electrically heated tube designed with a hydraulic diameter and length similar to current LMFBR (FTR) design. The upper and lower plenum tanks were provided with means for controlling liquid subcooling above and below the test section. The down-commer was large enough to eliminate down-commer hydraulics. Water at a pressure of 1 atmosphere was used to simulate sodium. Sight flow indicators were provided to observe flow conditions at the test section inlet and exit. Instrumentation was provided to measure test section pressures, inlet and exit temperatures, tube wall temperatures, heat flux and oscillation frequencies.

Steady state tests were conducted for subcooled flow boiling, saturated flow boiling, CHF and post CHF conditions. Subcooled flow boiling was observed for heat fluxes below 1×10^4 BTU/hr ft^2. For this condition, both pressure oscillations and temperature oscillations at the heated surface were observed; but the pressure oscillations were not observed continuously. Saturated flow boiling was observed for heat fluxes between 3×10^4 BTU/hr ft^2 and CHF. For this condition, pressure oscillations were observed continuously. As the CHF condition was approached, a periodic downward expansion of vapor from the heated section was observed at the bottom sight flow indicator and the flow regime appeared to be annular at the top sight flow indicator. CHF was observed at the top of the heated section when the heat flux reached 6.4×10^4 BTU/hr ft^2, but rewetting occurred after a few seconds. As the heat flux was increased further, the maximum surface temperature reached before rewetting increased; until, at a heat flux of 7.15×10^4 BTU/hr ft^2, the maximum temperature exceeded 900° F and rewetting no longer occurred.

A transient test was conducted for a post CHF condition. The heat flux was 7.3×10^4 BTU/hr ft^2. The oscillations observed under steady state conditions developed within a few seconds after the power was turned on. The equilibrium tube wall temperature upstream of the CHF location was reached in 10 seconds. The equilibrium tube wall temperature at the CHF location was reached in about 135 seconds.

A similarity analysis was done in order to scale the test results to LMFBR LOPI conditions. The results of this analysis indicate that the CHF for the LMFBR (FTR) would be at least 5×10^4 BTU/hr ft^2. This corresponds to a critical average linear power for the hot assembly of 1.06 kw/ft compared to an estimated 2.55 to 5.1 kw/ft being transferred to the coolant at the time boiling begins during a LOPI accident. On the basis of this analysis, the results of the water tests indicate that CHF would occur. But, this conclusion is conservative for a number of reasons and further experimental work on a more prototypical system is suggested.

ACKNOWLEDGEMENTS

The tests described herein were supported by the Union Carbide Corporation, Nuclear Division under Subcontract 4450 of Contract No. W-7405-eng-26 with the United States Energy Research and Development Administration.

Prof. P. Griffith initially suggested the tests and gave generously of his time to discuss their design and interpretation.

Shop facilities, laboratory space and miscellaneous parts of the experimental equipment were provided by the MIT Department of Mechanical Engineering.

Mr. J. Caloggero, Mr. F. Johnson and Mr. A. Crandall were most helpful in discussing the design of the test loop and were responsible for its fabrication and construction.

The draft report was reviewed by the ERDA LMFBR Loss of Pipe Integrity Working Group. Members of this group provided a number of constructive comments and suggestions that were incorporated into the final report.

Ms. Marsha Levine did an excellent job of typing both the draft and final reports.

I wish to express my thanks to all concerned.

TABLE OF CONTENTS

LIST OF FIGURES

LIST OF TABLES

I. INTRODUCTION

A. Background

In the Liquid Metal Cooled Fast Breeder Reactor (LMFBR), coolant voiding due to boiling causes a positive reactivity feedback and makes reactor control more difficult. In addition, post-voiding heat transfer in the LMFBR is thought to be ineffective; and it is presently assumed that coolant boiling would result in melting of the fuel rod cladding. For these reasons LMFBR's are currently designed so that the maximum coolant temperature during normal operation is about 600°F below the saturation temperature. Nevertheless, even with this large margin, reactor safety analyses must consider the possibility of unanticipated transients or postulated accidents that would lead to coolant temperature excursions and boiling.

The most serious of the postulated accidents considered is the Loss of Pipe Integrity (LOPI) accident. This accident is postulated to occur as a result of a double-ended guillotine break of a reactor coolant pipe at the inlet to the core. Calculations (1) indicate that, as a result of such a break, reactor flow would decrease to about 20 to 30 percent of its initial value within 0.5 seconds and then remain approximately at this level over the next several seconds. The pressure in the reactor core is calculated to change similarly; decreasing from its initial, full flow value to about 25 psia within 0.5 seconds and then remaining approximately constant at that level. Since the reactor protection system scrams the control rods upon sensing the accident condition, the reactor power also decreases quickly. However, because of the stored energy in the fuel rods and the thermal inertia associated with the properties and dimensions of the fuel rods, the core heat flux drops more slowly;

and calculations indicate that it only decreases to about 25 to 50 percent of its initial, full power value during the first 1 - 2 seconds. Therefore, the sodium coolant in the highest power power fuel assembly rapidly increases in temperature and is calculated to begin boiling in about 1 second. As soon as boiling begins, the flow is assumed to stagnate, resulting in "dryout" and an increase in clad temperature to its melting point within about 1 second after the start of boiling or 2 seconds after the start of the accident.

It should be recognized, however, that the severe temperature excursion just described is based on present calculational models that assume flow stagnation and dryout almost simultaneously with boiling. This assumption results from the fact that analysis and experiments show that, before boiling begins at the fuel clad surface during a LOPI accident, the bulk temperature of the sodium would increase to about 30 to 50°F above the saturation temperature. Under these circumstances, once a vapor bubble is formed in the superheated liquid its growth rate would be very rapid and it would quickly fill the coolant channel cross section. This rapid formation of vapor would be accompanied by a sharp local increase in static pressure that could stop or even reverse the flow in the upstream section of the coolant channel. Although a liquid film would probably initially remain between the vapor bubble and the wall, the concern is that because of the flow stagnation, this film would be quickly evaporated, resulting in overheating of the fuel clad.

The assumption that film dryout occurs as a result of rapid vapor bubble growth and consequent flow stoppage or reversal when boiling is initiated during a LOPI accident may be valid. However, this assumption has never been put to any real test; and, if it could be shown that film dryout does not occur immediately after boiling is

initiated and that substantial heat can be removed under post voiding conditions, it may be possible to show that clad melting does not occur.

A possible mechanism for prevention or delay of dryout and substantial post-voiding heat removal has been suggested by Griffith (2). This mechanism is described in the following paragraphs from Reference (2):

> "The cold regions of the core never will boil. As the flow coasts down, boiling can occur in the hot assembly, however, giving rise to a substantial gravity pressure difference between the hot and cold channels. This pressure difference is about 1 ft. of liquid per foot. This pressure head can be used to overcome the friction and momentum pressure drops for the evolved vapor in the hot channel. Making the assumptions of steady flow, no entrainment, and saturated vapor out, it is calculated that about 2 kw can be removed in this way...More, or less, is possible.
>
> A combination of hot rods and two phase flow similar to that which we have after first voiding in a LMFBR occurs in the FLECHT-SET experiments (3). In the FLECHT-SET experiments we find flow oscillations, much carry over, better cooling with carry over, superheating of the evolved vapor and a host of other phenomena that are not yet adequately described. It is not evident which of these will occur in an LMFBR and whether indeed, they will help or hinder the heat transfer."

The tests described in this report were conceived with the purpose of obtaining basic information and data relating to this suggestion.

B. Objective

The objective of the tests was to obtain data and information concerning the nature and effect of flow oscillations on heat transfer in a low-pressure natural circulation system similar to the LMFBR under conditions approximating those predicted to exist during a LOPI accident at the time boiling begins (about 1 second after the start of the accident). It was expected that this data and information would help to answer some important questions relating to such conditions and, therefore, would be of value in designing and interpreting more

prototypical experiments to be conducted with sodium cooled rod bundles at the Oak Ridge National Laboratory. These questions are the following:

1) What types of oscillations occur? What appears to be the cause of these oscillations? How do they affect post-voiding, pre-CHF heat transfer?

2) Under what conditions does CHF occur? What is the mechanism? What is the role of the observed oscillations? How is rewetting and post-CHF heat transfer related to the oscillations? How does the power corresponding to CHF compare to the power it takes to completely vaporize a steady homogeneous flow driven by the hydrostatic pressure difference between the inlet and outlet of the test section (or the appropriate length)?

3) To what extent are the answers to the previous questions applicable to the LMFBR during the first few seconds of a LOPI accident?

II. APPARATUS

A. Design Basis

In order to accomplish the objective given in Section I.B, a test loop was designed to simulate natural circulation boiling in the LMFBR under conditions approximating those predicted to exist during a LOPI accident at the time boiling begins. This design was based on several simplifying assumptions concerning LMFBR geometry and the flow conditions that would exist during such an accident. These assumptions were the following:

1) Although, as discussed in Section I.A, there would still be some pump induced flow through the core when boiling begins, it was conservatively assumed that this flow is negligible. Under this condition, the only flow would be due to the buoyancy force resulting from the density difference between the boiling sodium in the hot assembly and the liquid sodium in the colder assemblies. The reactor vessel would then become a natural circulation "loop" as shown in Figure II-1a. The test loop was therefore designed to simulate this reactor vessel "loop." This test loop consisted of a vertical tube test section and a down-commer pipe connected to upper and lower plenum tanks as shown in Figure II-1b.

2) As mentioned in Section I.A the sodium coolant pressure is approximately 25 psia at the time boiling begins and does not change much over the next several seconds. Because of the similarity between the liquid and vapor densities of water at 14.7 psia and sodium at 25 psia (and the expectation that these properties would be of major importance in determining post voiding hydraulics and heat transfer under natural circulation conditions), the test loop was therefore designed to operate with water at a constant pressure of 14.7 psia.

3) During the first several seconds of a LOPI accident the bulk liquid sodium temperatures in the upper and lower plenum would remain at approximately the same temperature as before the accident. Therefore the test loop was designed so that the bulk water temperatures in the upper and lower plenum tanks could be held constant. (The temperatures selected were such that the negative quality or subcooling in each plenum tank was the same as for the sodium in each plenum of the reactor vessel, as will be discussed in Section III.)

4) Although the heat flux would be changing (decreasing) at the time boiling begins, the rate of change is sufficiently small so that the transient natural circulation condition

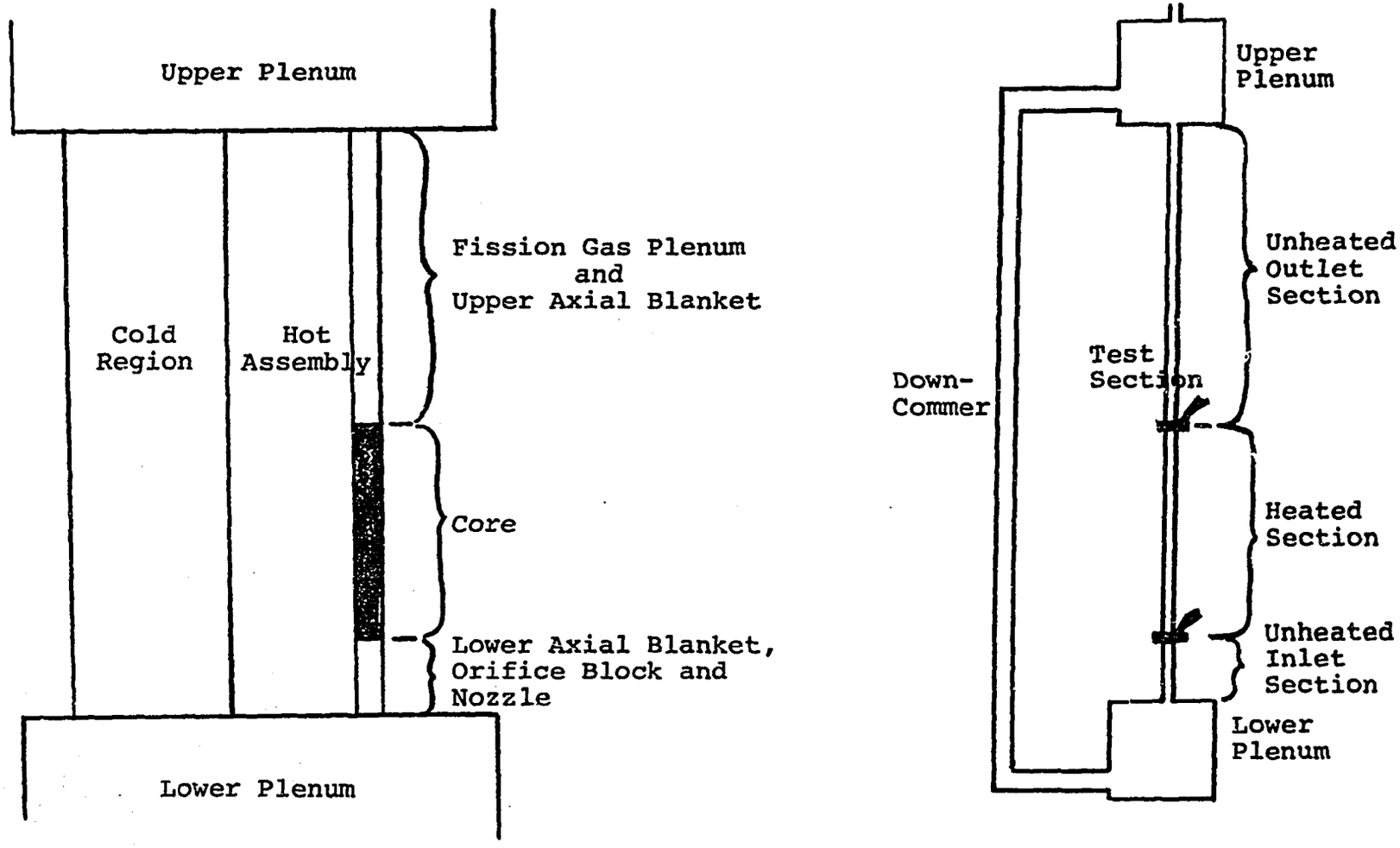

a) LMFBR Vessel "Loop"

b) Natural Circulation Test Loop

Figure II-1

Assumed Reactor/Test Loop Geometry

at a particular heat flux should be approximately the same as the corresponding steady state condition at the same heat flux. Therefore, it was assumed that the test loop could be operated at constant heat flux using the test procedure outlined in Section III.B. (However in order to provide a check on this assumption, a transient test was run as described in Section III.C.)

5) The CHF mechanism under LOPI accident conditions would probably be liquid film "dryout" as discussed in Section I.A. For this mechanism, CHF generally occurs at the end of the heated channel or tube and is primarily a function of channel power rather than local heat flux. Therefore it was assumed that non-uniform heat flux effects would not be of major importance, and the vertical tube test section was designed to operate with a uniform axial heat flux distribution over its heated length.

As stated in Section I.B, the objective of the tests was to obtain data and information concerning the nature and effect of pressure and flow oscillations on CHF and post-CHF heat transfer. Therefore the test loop was designed (and operated) to have flow rate - pressure drop characteristics similar to the LMFBR vessel "loop" shown in Figure II-1a. The analysis that was done to identify the key geometry parameters and fluid conditions that need to be matched in order to obtain this similarity, as well as similarity in other respects, is described in Section II.B which follows.

B. Similarity Analysis

Consider the active section of the reactor hot fuel assembly (Figure II-1a) or the heated section of the test loop (Figure II-1b). Assume that the liquid and vapor are flowing upwards in one-dimensional, homogeneous flow as shown schematically for the heated section of the test loop in Figure II-2. For this flow condition, the conservation laws for mass, momentum and energy applied to the control volume shown in Figure II-2 give the following equations:*

*For symbols not defined in the text or in Figure II-2, refer to NOMENCLATURE section at end of report.

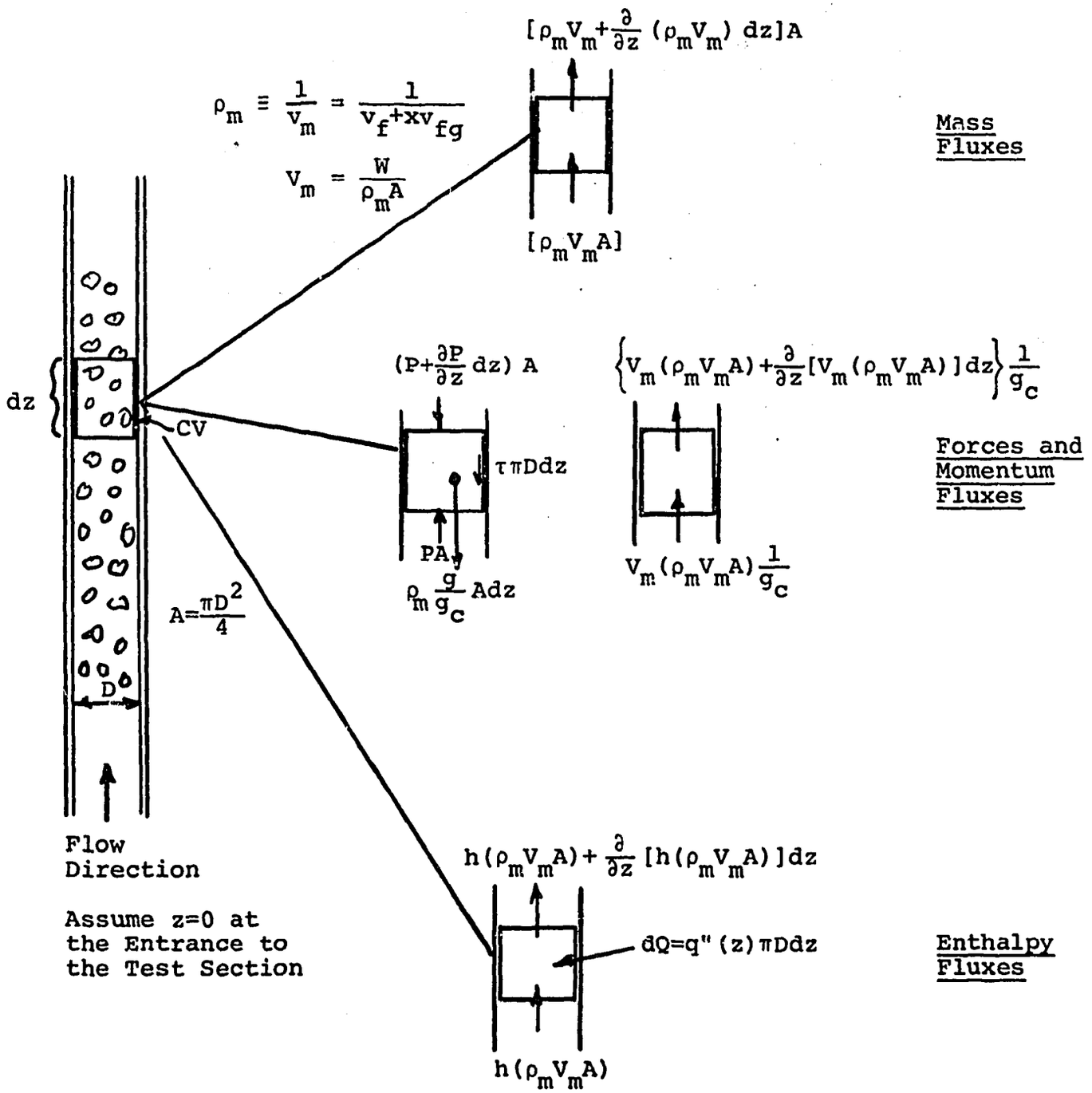

Figure II-2

Control Volume Used for Similarity Analysis (Section II.A.2)

$$\frac{\partial \rho_m}{\partial t} = -\frac{\partial}{\partial z}(\rho_m V_m) \qquad \text{(II-1)}$$

$$-\frac{\partial P}{\partial z} - \frac{4\tau}{D} - \rho_m \frac{g}{g_c} = \left[\frac{\partial}{\partial t}(\rho_m V_m) + \frac{\partial}{\partial z}(\rho_m V_m^2)\right]\frac{1}{g_c} \qquad \text{(II-2)}$$

$$dQ = \frac{\partial}{\partial t}(u\rho_m)Adz + \frac{\partial}{\partial z}[h(\rho_m V_m)]Adz \qquad \text{(II-3)}$$

where

ρ_m is the density of the liquid-vapor mixture

V_m is the velocity of the liquid-vapor mixture, $W/\rho_m A$

Equation (II-1) can be combined with Equations (II-2) and (II-3) to give the following equations for conservation of mass/momentum and mass/energy:

$$-\frac{\partial P}{\partial z} - \frac{4\tau}{D} - \rho_m \frac{g}{g_c} = \left[\rho_m \frac{\partial V_m}{\partial t} + \rho_m V_m \frac{\partial V_m}{\partial z}\right]\frac{1}{g_c} \qquad \text{(II-4)}$$

$$dQ = \left\{\left(\rho_m \frac{\partial h}{\partial t} - \frac{1}{J}\frac{\partial P}{\partial t}\right) + \rho_m V_m \frac{\partial h}{\partial z}\right\} A dz \qquad \text{(II-5)}$$

Equations (II-4) and (II-5) can also be applied to single phase liquid flow in other sections of the reactor or test loop providing that:

ρ_m is replaced by ρ_L

V_m is replaced by $V_L = \frac{W}{\rho_L A}$

z is defined more generally as the distance along the flow direction rather than just the vertical distance

Then, Equations (II-4) and (II-5) can be integrated around the loop to obtain the following integral equations:

$$\underbrace{\int_0^L \frac{1}{g_c}\left(\rho_m \frac{\partial V_m}{\partial t}\right) dz}_{\text{INERTIA}} = \underbrace{-\int_0^L \frac{4\tau}{D} dz}_{\text{FRICTION}} \underbrace{- \int_0^L (\rho_m - \rho_f)\frac{g}{g_c} dz}_{\text{GRAVITY}} \underbrace{- \int_0^L \frac{1}{g_c}\left[\rho_m V_m \frac{\partial V_m}{\partial z}\right] dz}_{\text{ACCELERATION}} \qquad \text{(II-6)}$$

$$\frac{Q}{A} = \int_0^L \rho_m \frac{\partial h}{\partial t} dz + \int_0^L \rho_m V_m \frac{\partial h}{\partial z} dz \qquad \text{(II-7)}$$

where L is the length of the reactor fuel assembly or test section in Figure II-1. Implicit in these equations are the following assumptions:

1) During pressure and flow oscillations, energy storage and inertia effects external to the reactor fuel assembly or test section are assumed to be negligible compared to those within the reactor fuel assembly or test section.

2) The friction and acceleration effects external to the test section are negligible compared to those within and entering or leaving the test section. (The friction and acceleration effects associated with entering or leaving the fuel assembly or test section are assumed to be included in the first and third terms on the right hand side of Equation [II-6]).

3) The liquid density, ρ_L is approximately equal to the density of saturated liquid, ρ_f.

4) In Equation (II-5) the part of the energy storage term associated with changes in pressure is assumed to be neglible compared to the part associated with changes in enthalpy (i.e.,

$$\int_0^L \left[\frac{1}{J}\frac{\partial P}{\partial t}\right]dz \ll \int_0^L \left[\rho_m \frac{\partial h}{\partial t}\right]dz).$$

5) The heat capacity of the part of the loop external to the test section is such that

$$\int_{external} (\rho_m \frac{\partial h}{\partial t})\,dz = \int_0^L (\rho_m V_m)\frac{\partial h}{\partial z}\,dz$$

with essentially no change in the upper and lower plenum temperatures (as would be the case for the reactor); or an external heat removal system is provided such that

$$Q_{external} = -\int_0^L (\rho_m V_m)\frac{\partial h}{\partial z} A dz$$

Equations (II-6) and (II-7) can be further simplified by using the following additional approximations and relationships:

$$\int_0^L \frac{1}{g_c}\rho_m\left(\frac{\partial V_m}{\partial t}\right)dz \simeq \frac{L}{Ag_c}\left\{\frac{dW}{dt} + \frac{W}{\rho_f L_{1\phi} + \bar{\rho}_m L_{2\phi}}\left[(\rho_f - \bar{\rho}_m)\frac{dL_{2\phi}}{dt} - L_{2\phi}\frac{d\bar{\rho}_m}{dt}\right]\right\}$$

$$\int_0^L \frac{4\tau}{D}dz \simeq \left[4f\left(\frac{L'_{1\phi}}{D} + \bar{R}\frac{L'_{2\phi}}{D}\right)\right]\frac{W^2}{2\rho_f A^2 g_c}$$

$$\bar{R} \simeq \frac{1}{L_{2\phi}}\int_{L_{1\phi}}^{L_{1\phi}+L'_{2\phi}}\left(\frac{\rho_f}{\rho_m}\right)dz$$

$$\int_0^L \frac{1}{g_c}\left[\rho_m V_m \frac{\partial V_m}{\partial z}\right]dz = 0$$

$$\int_0^L (\rho_m - \rho_f)\frac{g}{g_c}dz = (\bar{\rho}_m - \rho_f)\frac{g}{g_c}L_{2\phi}$$

$$\bar{\rho}_m = \frac{1}{L_{2\phi}}\int_{L_{1\phi}}^{L_{1\phi}+L_{2\phi}}\rho_m dz$$

$$\rho_m \simeq \frac{\rho_f}{1+x\left(\frac{\rho_f}{\rho_g}\right)}$$

$$\int_0^L \rho_m \frac{\partial h}{\partial t}dz \simeq h_{fg}\rho_g \frac{\left[(\rho_f - \bar{\rho}_m)\frac{dL_{2\phi}}{dt} + L_{2\phi}\frac{d\bar{\rho}_m}{dt}\right]}{\frac{\rho_f L_{1\phi} + \bar{\rho}_m L_{2\phi}}{L}}$$

$$\int_0^L (\rho_m V_m)\frac{\partial h}{\partial z}dz \simeq \frac{W}{A}h_{fg}(x_{out} - x_1)$$

where

$L_{1\phi}$ is the length of the single phase liquid region within the reactor fuel assembly or test section.

$L'_{1\phi}$ is the equivalent length of the single phase region, including the effect of inlet contraction and orifice.

$L_{2\phi}$ is the length of the two phase region within the reactor fuel assembly or test section.

$L'_{2\phi}$ is the equivalent length of the two phase region, including the effect of outlet expansion.

f is the Fanning friction factor.

$x_{out}-x_1$ is the quality change along the test section, where x_1 is equal to $\frac{C_f(T_1-T_{sat})}{h_{fg}}$ and T_1 is the inlet plenum temperature.*

Thus

$$\frac{L}{Ag_c}\left\{\frac{dW}{dt}+\frac{W}{\rho_f L_{1\phi}+\bar{\rho}_m L_{2\phi}}\left[(\rho_f-\bar{\rho}_m)\frac{dL_{2\phi}}{dt}-L_{2\phi}\frac{d\bar{\rho}_m}{dt}\right]\right\}$$

$$=(\rho_f-\bar{\rho}_m)\frac{g}{g_c}L_{2\phi}-\left[4f\left(\frac{L'_{1\phi}}{D}+\bar{R}\frac{L'_{2\phi}}{D}\right)\frac{W^2}{2\rho_f A^2 g_c}\right] \qquad \text{(II-8)}$$

and

$$Q=h_{fg}\rho_g A\frac{\left[(\rho_f-\bar{\rho}_m)\frac{dL_{2\phi}}{dt}+L_{2\phi}\frac{d\bar{\rho}_m}{dt}\right]}{\frac{\rho_f L_{1\phi}+\bar{\rho}_m L_{2\phi}}{L}}+Wh_{fg}(x_{out}-x_1) \qquad \text{(II-9)}$$

Now, for steady flow, the $\frac{dW}{dt}$, $\frac{dL_{2\phi}}{dt}$ and $\frac{d\bar{\rho}_m}{dt}$ terms in Equations (II-8) and (II-9) are equal to zero and these equations become:

$$0=(\rho_f-\bar{\rho}_m)\frac{g}{g_c}L_{2\phi}-\left[4f\left(\frac{L'_{1\phi}}{D}+\bar{R}\frac{L'_{2\phi}}{D}\right)\right]\frac{W^2}{2\rho_f A^2 g_c} \qquad \text{(II-10)}$$

and

$$Q=Wh_{fg}(x_{out}-x_1) \qquad \text{(II-11)}$$

Also, $L_{1\phi}$, $L'_{1\phi}$, $L_{2\phi}$, and $L'_{2\phi}$ can be expressed in terms of L_1, L'_1 (the equivalent length of the unheated inlet section), L_2, L'_2 (the equivalent length of the unheated outlet section), L_H (the heated length) and L_B (a "boiling" length) for the test section or reactor assembly by the expressions:**

$$\left.\begin{aligned} L_{1\phi} &= L_1+(L_H-L_B)\\ L'_{1\phi} &= L'_1+(L_H-L_B)\\ L_{2\phi} &= L_B+L_2\\ L'_{2\phi} &= L_B+L'_2 \end{aligned}\right\} \qquad \text{(II-12)}$$

*Note that $x_{out}\neq x_2=\frac{C_f(T_2-T_{sat})}{h_{fg}}$ where T_2 is the upper plenum temperature.

**See Figure II-3.

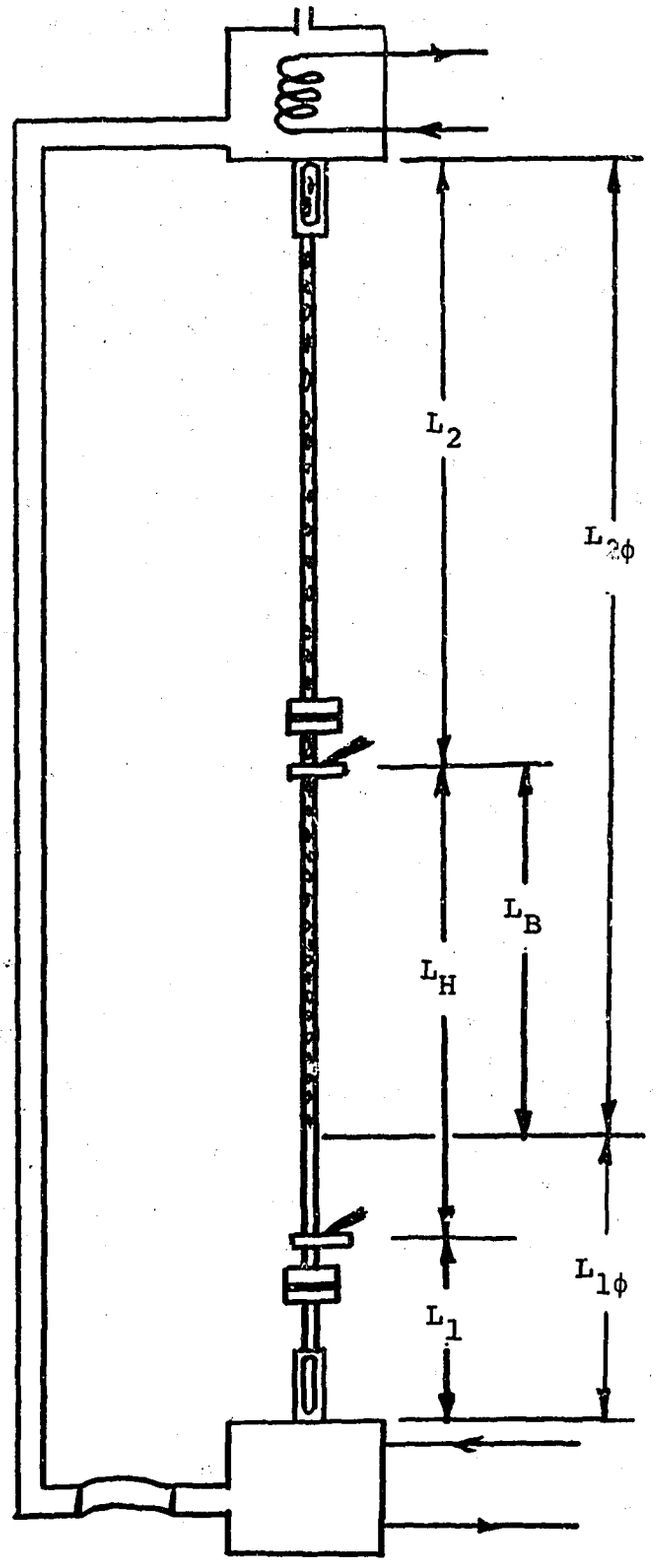

Figure II-3

Schematic Diagram Relating $L_{1\phi}$ and $L_{2\phi}$ to L_1, L_2, L_H and L_B

where L_B is defined in terms of mass flow rate, inlet quality, power, heat flux distribution and L_H by:

$$\frac{\int_{L_1}^{L_1+L_H-L_B} q''(z)\,dz}{\int_{L_1}^{L_1+L_H} q''(z)\,dz} = \frac{-Wx_1}{Q/h_{fg}} \qquad \text{(II-13)}$$

which, for a uniform heat flux distribution would become:

$$\frac{L_H-L_B}{L_H} = \frac{-Wx_1}{(Q/h_{fg})} \qquad \text{(II-14)}$$

Therefore, for steady flow conditions and uniform heat flux distribution, one can conclude from Equations II-10, II-11, II-12 and II-14 that:

$$W = W\left(\rho_f, \rho_g, x_1, \frac{Q}{h_{fg}}, f \text{ or } \mu_f \text{ and wall roughness}, L_1, L_1', L_H, L_2, L_2', A, D\right) \qquad \text{(II-15)}$$

or

$$x_{out} = x_{out} \text{ (same parameters as for W)} \qquad \text{(II-16)}$$

This means that, for steady flow conditions and neglecting effects of non-uniform axial heat flux distribution, W and x_{out} will be the same for the test loop and the reactor providing the following parameters are the same for the two systems:

ρ_f, ρ_g

x_1 or $C_f \dfrac{(T_1-T_{sat})}{h_{fg}}$

$\dfrac{Q}{h_{fg}}$

μ_f and wall roughness

$L_1, L_1', L_H, L_2, L_2'$

A

D

For unsteady flow conditions, such as would result from oscillations between two possible steady flow conditions, the above result (along with consideration of Equations [II-8] and [II-9]) indicates that $\frac{dW}{dt}$, $\frac{dL_{2\phi}}{dt}$, and $\frac{d\bar{\rho}_m}{dt}$ (and therefore W[t] and x_{out}[t]) would also be the same for the test loop and the reactor if the above parameters are the same. However, Equations (II-8) and (II-9) were derived for upflow; and, since flow oscillations might cause momentary downflow of liquid from the upper plenum, the following additional parameter should probably also be included if W(t) and $x_{out}(t)$ are to be the same for the two systems:

$$x_2 \text{ or } \frac{C_f(T_2-T_{sat})}{h_{fg}}$$

For both the test loop and the reactor, it is expected (as discussed previously in Section II.A) that CHF would be due to "dryout" of the liquid film under annular flow conditions. Under such conditions, CHF would occur at the top of the heated length when (Q/h_{fg}) is sufficiently high so that the exit quality exceeds some critical value. If one assumes that <u>any</u> liquid present at the CHF location would wet the heated surface, this critical quality would be 1.0; and the critical value of Q/h_{fg} corresponding to CHF could be determined from Equation (II-16) by setting $x_{out} = 1.0$. Moreover, this critical $\frac{Q}{h_{fg}}$ would be the same for the reactor and the test loop providing the parameters listed previously are the same for the two systems.

However, it is probable that some of the liquid at the CHF location would be entrained by the vapor and would not be able to wet the heated surface. In this event, the quality at the CHF location would be less than 1.0 and the critical (Q/h_{fg}) would also be a function of any parameters that would affect the amount of liquid entrainment. Such parameters would include the liquid surface tension in addition to the

parameters listed previously. Therefore, the liquid surface tension should be the same for the reactor and the test loop if the critical (Q/h_{fg}) is to be the same. (Of course, this condition could not be even approximately satisfied, since water was the fluid used for the test loop and the surface tension for water is substantially less than for sodium. Nevertheless, because of this difference, sodium would be expected to have less entrainment for an otherwise identical flow condition. Therefore, the water tests should indicate a conservatively low exit quality or $[Q/h_{fg}]$ at CHF.)

If the flow is oscillating when CHF occurs, the liquid film flow rate at the CHF location would also oscillate and could be very small or essentially zero for short periods of time. Under such conditions, the critical (Q/h_{fg}) would probably be influenced by the conductivity of the liquid film, in addition to the previous listed parameters. (As for the surface tension, it was not possible to satisfy this condition, since the conductivity of water is much less than for sodium. However, this is again conservative in that a lower liquid conductivity should result in a lower critical value of Q/h_{fg}.)

Post CHF hydrodynamics and heat transfer would be a function of parameters that influence the Liedenfrost temperature. But, such parameters would include only the liquid surface tension and those parameters previously listed as determining the mass flow rate and exit quality. The surface tension (along with the surface material and roughness) would determine the contact angle and therefore the wetting characteristics of the fluid-surface combination. (See parenthetical comment regarding surface tension in previous paragraph.)

For post CHF conditions where the heated surface oscillates as a result of periodic dryout followed by rewetting, the initial rate

of temperature rise subsequent to dryout (and therefore the time available for rewetting before the Liedenfrost temperature is exceeded) would depend upon geometry and thermal properties of the tube wall or clad. This is shown by the following approximate equation derived from an energy balance on a differential length of the tube wall or clad, assuming negligible heat transfer to the coolant:

$$\frac{dT_s}{dt} \simeq \frac{q''}{\rho_s C_s \delta} \qquad \text{(II-17)}$$

where ρ_s, C_s and δ are, respectively, the density, specific heat and thickness of the tube wall or cladding. Therefore, if $\frac{dT_s}{dt}$ is to be the same for the test loop and the reactor for a given post CHF q", ρ_s, C_s and δ for the tube wall and clad would have to be the same; and these parameters should also be added to those listed previously. (Since stainless steel was used for the test section and is also the reactor clad material, ρ_s and C_s were about the same. However, it was not possible to match δ; and therefore δ for the test section tube was about a factor of three greater than for the reactor clad. Also, because of the difference in h_{fg} between water and sodium, the value of q" corresponding to a given post CHF value of (Q/h_{fg}) would be lower for the test loop than for the reactor by about a factor of 2. Therefore $\frac{dT_s}{dt}$ for the test loop under post CHF conditions was about a factor of 6 lower than would be expected for the reactor for the same (Q/h_{fg}). This, of course, is not in the conservative direction; since the lower $\frac{dT_s}{dt}$ would allow more time to rewet the heated surface before the Liedenfrost temperature is exceeded.

C. Description of Test Loop

1. General

A schematic diagram of the test loop is shown in Figure II-4. Tables II-1A and II-1B compare values of the parameters identified from

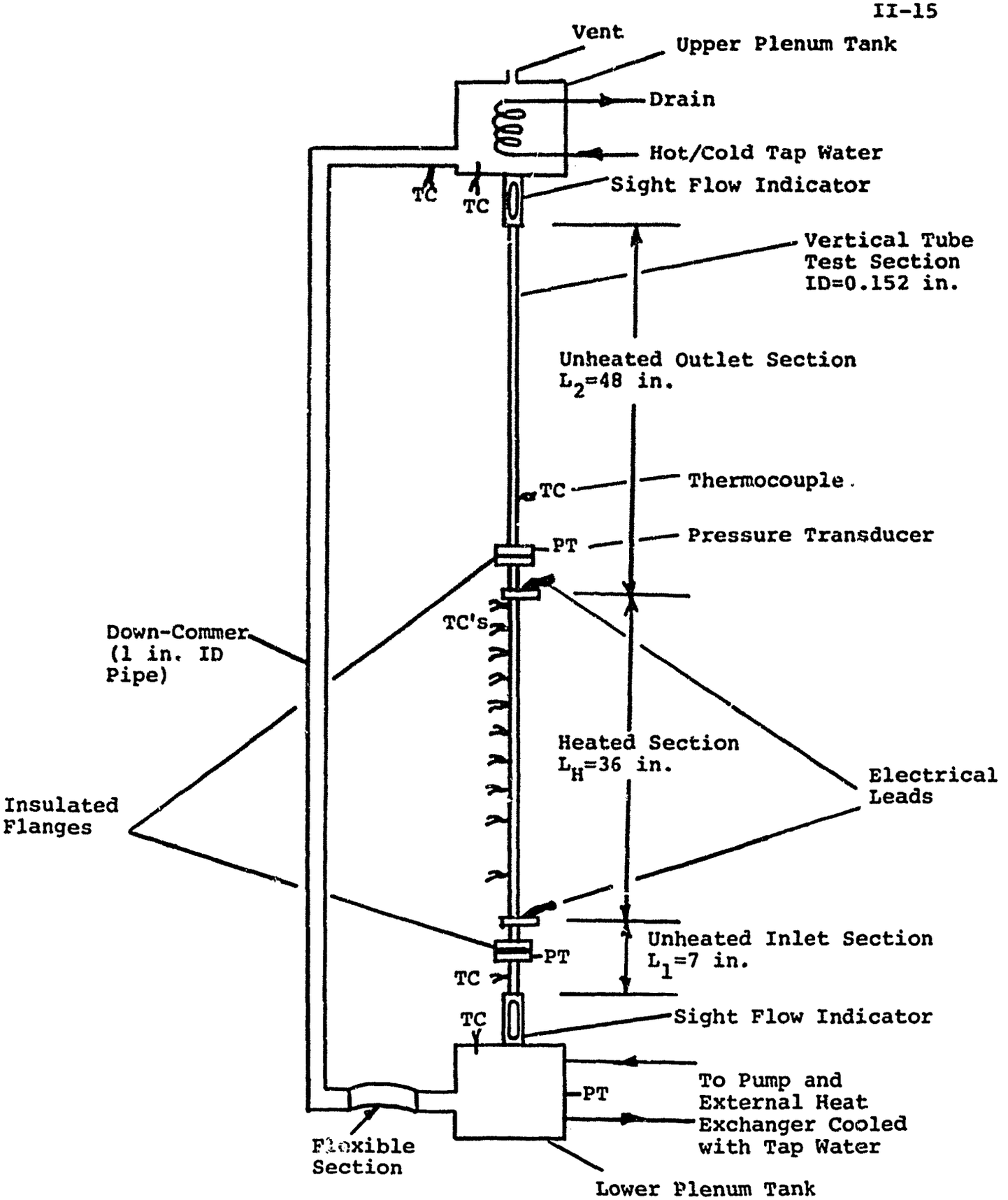

Figure II-4

Schematic of Water Test Apparatus

Table II-1A

Comparison of Test Section Parameters with Current LMFBR Fuel Assemblies

Parameter	Test Apparatus	FTR	CRBR
Heated Surface Material & Geometry	Electrically Heated Tube	316 ss Clad Fuel Rod Bundle	316 ss Clad Fuel Rod Bundle
L_1	7 in.	7 in.	14 in.
L_1'	10.5 in.**	131 in.***	
L_H	36 in.	36 in.	36 in.
L_2	48 in.	48 in.	62 in.
L_2'	55 in.**	57 in.***	
D	0.152 in.	0.128 in.*** for average subchannel	
L	91 in.	91 in.	112 in.
A	0.0181 in^2	0.0154 $in.^2$*** for average subchannel	
Surface Roughness	Commercial Tubing	Approximately Same as Commercial Tubing	
ρ	494 lb_m/ft^3	498 $lb_m ft^3$	498 lb_m/ft^3
C_f	0.12 BTU/lb_m°F	0.12 BTU/lb_m°F	0.12 BTU/lb_m°F
δ	0.049 in.	0.015 in.	0.015 in.

*See Figure II-1 and NOMENCLATURE for definition of symbols

**See discussion in Section II.C.2

***See discussion in Section V.B.1

Table II-1B

Comparison of Fluid Conditions for Water Tests at 14.7 psia with Those for LMFBR at Inception of Boiling During LOPI Accident*

Fluid Condition**	Water Tests	FTR	CRBR
P	14.7 psia	25 psia	25 psia
T_{sat}	212°F	1670°F	1670°F
ρ_f	59.8 lb_m/ft^3	46.4 lb_m/ft^3	46.4 lb_m/ft^3
ρ_g	0.0373 lb_m/ft^3	0.025 lb_m/ft^3	0.025 lb_m/ft^3
(ρ_f/ρ_g)	1603	1865	1865
h_{fg}	970.3 BTU/lb_m	1650 BTU/lb_m	1650 BTU/lb_m
C_f	1.0 BTU/lb_m°F	0.31 BTU/lb_m°F	0.31 BTU/lb_m°F
T_1	70°F	792°F	725°F
x_1 or $\frac{C_f(T_1-T_{sat})}{h_{fg}}$	-0.146	-0.165	-0.173
T_2	110°F	1100°F	995°F
x_2 or $\frac{C_f(T_1-T_{sat})}{h_{fg}}$	-0.105	-0.107	-0.126
μ_f	0.687 $lb_m/ft\ hr$	0.363 $lb_m/ft\ hr$	0.363 $lb_m/ft\ hr$
σ_f	0.004 lb_f/ft	Approximately 0.012 lb_f/ft	Approximately 0.012 lb_f/ft
k_f	0.394 BTU/hr ft°F	31.5 BTU/hr ft°F	31.5 BTU/hr ft°F

*In accordance with assumptions outlined in Section II.A.1

**See NOMENCLATURE for definition of symbols

the similarity analysis in Section II.A.2 with corresponding values of these parameters for current LMFBR designs (FTR, CRBR).

The principal components of the test loop included: (1) a vertical tube test section, (2) two sight flow indicators, (3) upper and lower plenum tanks, (4) an external down-commer, (5) a power supply and (6) instrumentation. A description of each of these components is given in the subsections that follow.

2. Test Section

The vertical tube test section was made from commercial, Type 304 stainless steel tubing with an inside diameter of 0.152 in. and a wall thickness of 0.049 in. It consisted of three sections: (a) an unheated inlet section that was 7 in. long, (b) a heated section that was 36 in. long, and (c) an unheated outlet section that was 48 in. long. The total length was therefore 91 in.

The equivalent length of the unheated inlet section (including the effect of the inlet contraction) was 10.5 in. The equivalent length of the unheated outlet section (including the effect of the outlet expansion) was 54 in. (See Table II-1A.) These equivalent lengths were obtained from the following equations:

$$L_1' = 7 + \frac{K_1 D}{4f} \qquad \text{(II-18)}$$

and

$$L_2' = 48 + \frac{K_2 D}{4f} \qquad \text{(II-19)}$$

where K_1, K_2 and f were assumed to have values appropriate to single phase flow regardless of the flow condition. These values (based on information from Reference (4) were the following:

$$K_1 = 0.5$$

$$K_2 = 1.0$$

$$f = 0.0055$$

The test section was connected at each end to a sight flow indicator by means of a Swagelok fitting. The sight flow indicators were in turn connected to the upper and lower plenum tanks by means of a bushing and a coupling welded to the tank covers. All of these fittings were stainless steel. The test section, sight flow indicators and plenum tanks were supported by a Dexion frame, bolted to the floor and ceiling of the laboratory room. The test section was vertically aligned by means of adjustable clamps made of aluminum.

3. Sight Flow Indicators

The sight flow indicators also were obtained from a commercial supplier (Ernst Model No. EEP 4000-S). Each of these indicators consisted basically of a glass tube with an inside diameter of 7/8 in. and a length of 4 7/8 in. The glass tube was partially enclosed within a bronze support structure with 1/4 pipe fittings at each end. See Figure III-5.

4. Plenum Tanks

The upper and lower plenum tanks were made from 8 in. stainless steel pipe and 1/4 in. stainless steel plates as shown in Figure III-6. Stainless steel couplings were welded to each tank to make connections to the test section and external down commer as indicated.

The upper plenum tank was provided with additional couplings and fittings for: (a) a vent to the atmosphere, (b) hot and/or cold tap water to flow through a coil of copper tubing located inside, (c) a sight glass to allow viewing of the water level, and (d) a thermocouple well. The lower plenum tank was provided with additional fittings for: (a) allowing direct flow of cooling water to and from an external pump and heat exchanger and (b) a thermocouple well.

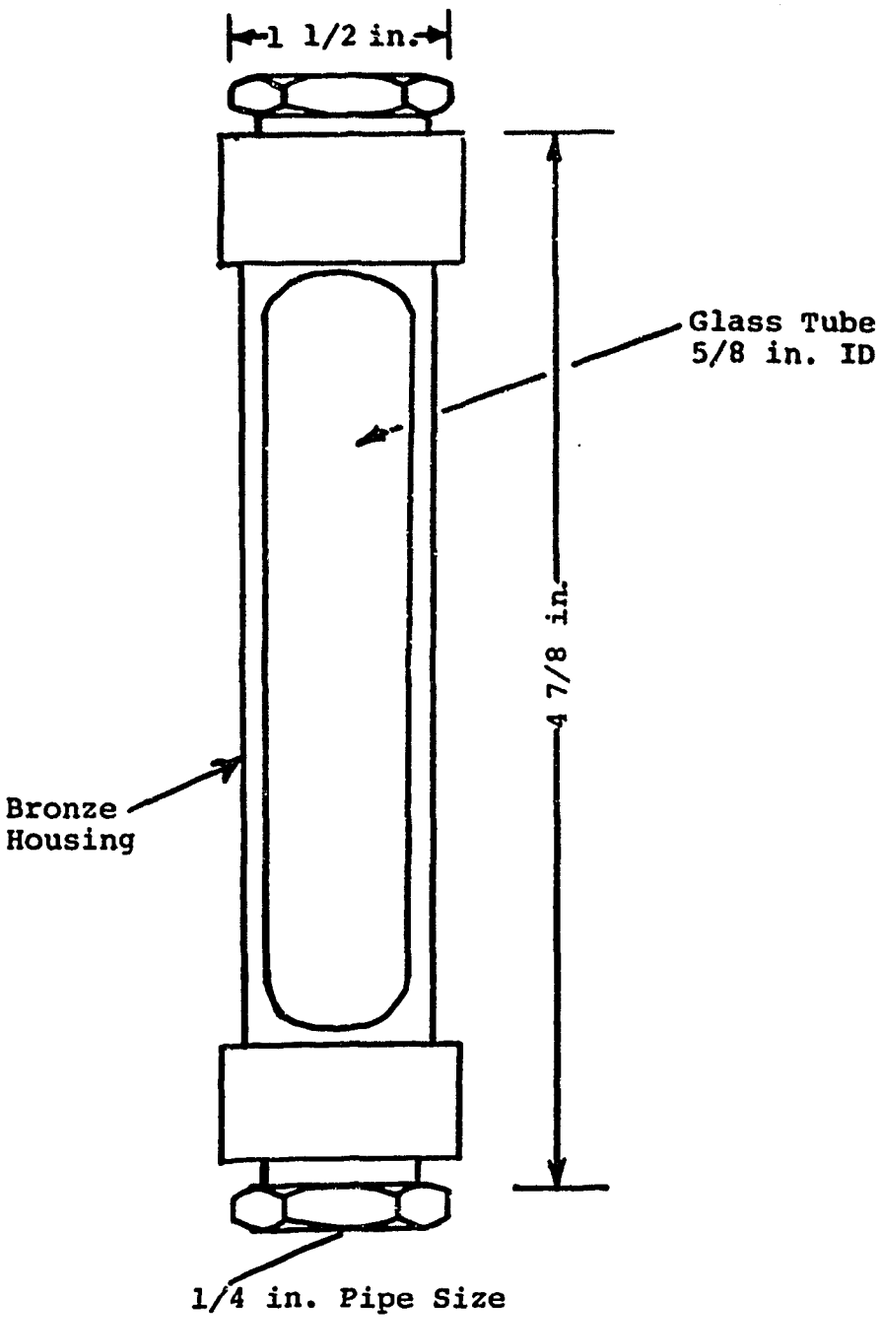

Figure II-5

Sight Flow Indicator

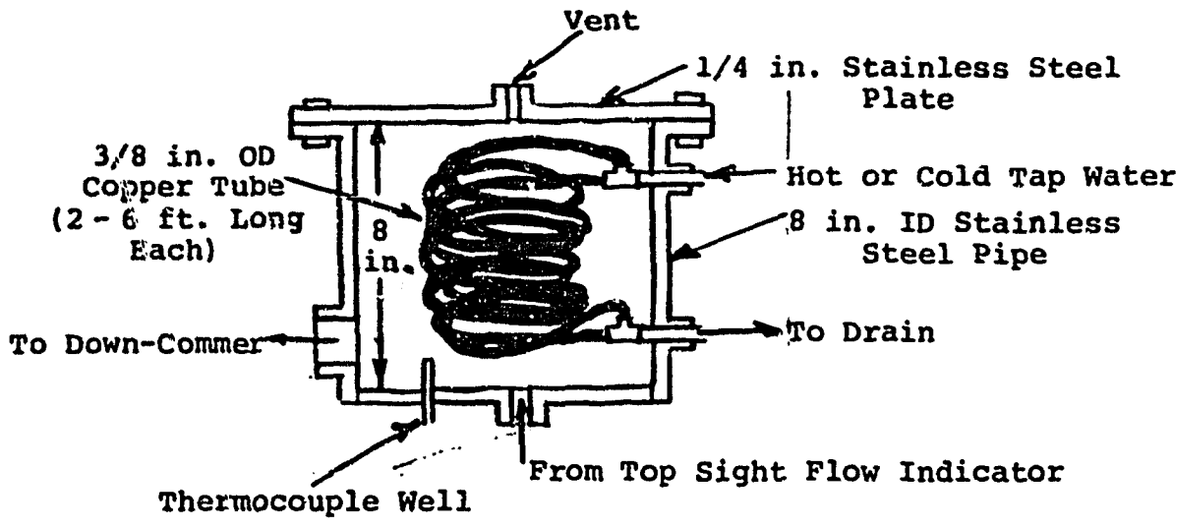

a) Upper Plenum Tank

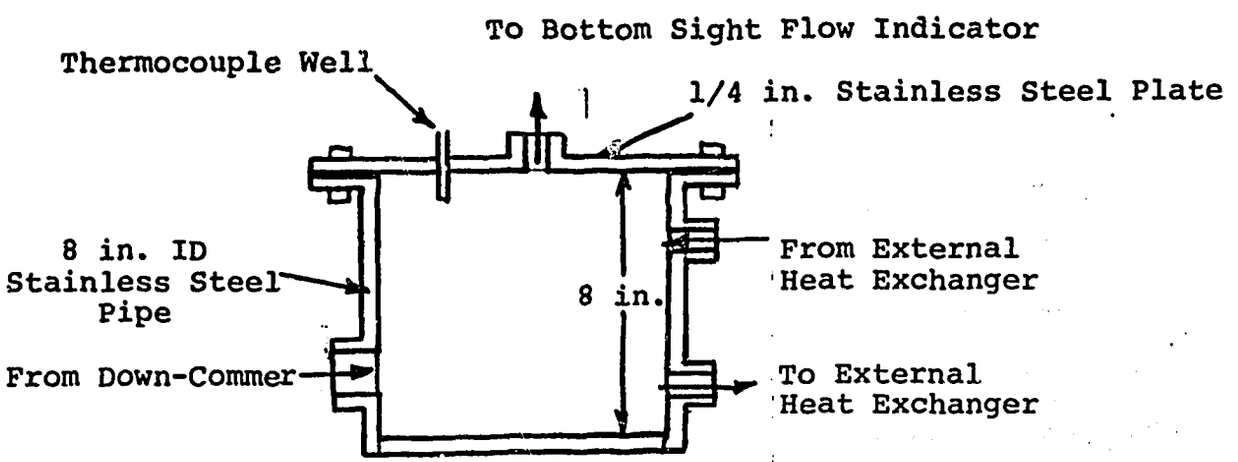

b) Lower Plenum Tank

Figure II-6

Upper and Lower Plenum Tanks

A schematic diagram is shown in Figure II-7 of the hydraulic system and heat exchanger used to control the fluid temperatures in each of the plenum tanks. The heat exchanger for the upper plenum was located within the tank and consisted of two 6 ft. long coils of 3/8 in. O.D. copper tubing. Hot and/or cold tap water was circulated through the coils to a drain. The heat exchanger for the lower plenum was a couterflow, shell and tube heat exchanger and was located external to the tank. Cold tap water was supplied to the shell and water from the lower plenum tank was circulated through the heat exchanger tubes by means of a small centrifugal pump. Flow rates were controlled with globe valves located as shown in Figure II-6. The heat exchangers and all piping and valves were made of copper and bronze.

5. Down-commer

The down-commer was made from 1 in. I.D. stainless steel pipe and fittings except for the flexible section included to allow for thermal expansion of the test section. The flexible section was made from 1 in. I.D. braided brass pipe. The 1 in. pipe size was chosen on the basis that it was sufficiently large compared to the test section diameter of 0.152 in. so that down-commer hydraulics had essentially no effect on the loop flow-pressure drop characteristics.

6. Power Supply

Power to the test section was supplied by a 15 kw DC generator, rated at 15 volts and 1000 amperes. The generator was driven by a 220 volt, 3 phase AC motor. A portable control console was provided to regulate the generator power from zero to the maximum as required. This regulation was accomplished by a set of coarse and fine rheostats. A knife switch located on the portable console could be used to quickly

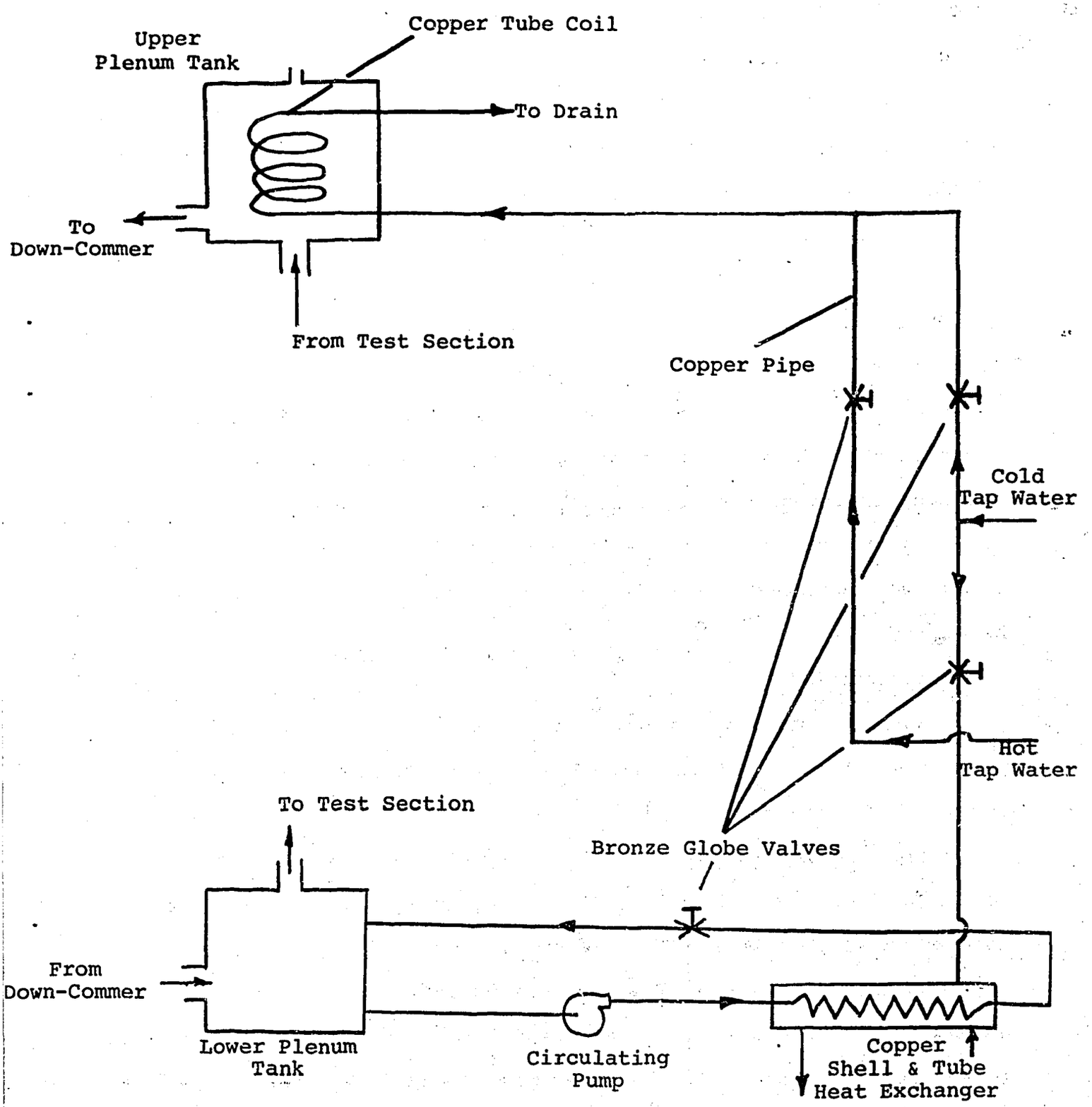

Figure II-7

Schematic of Hydraulic System and Heat Exchangers Used to Control Upper and Lower Plenum Temperatures

stop (or start) the flow of current from the generator without stopping it or changing the rheostat settings.

Current from the generator was supplied to the test section through four flexible neoprene welding cables connected to each end of the heated section. The cables were clamped to an aluminum lug which was in turn clamped to the test section, as shown in Figure II-8.

The heated section of the test section was electrically insulated from the rest of the loop by two flanges located about 3 in. upstream and downstream of the heated section. The flanges were designed in a way such that the continuity of stainless steel along the test section was interrupted by a small teflon insert that, in effect, replaced the tube wall at the location of the flange. The design of the flange was such that the effect on flow through the test section would be negligible.

7. Instrumentation

Instrumentation was provided to measure loop temperatures and pressures and power to the heated section of the test section. A schematic diagram is shown in Figure II-9.

Temperatures were measured by thermocouples located to provide measurements at 15 locations. Thermocouples T_1 through T_{10} were located at 10 positions along the outside wall of the heated section as shown in Figure II-10. T_{11} was located on the outside wall of the unheated inlet section. T_{12} was inside the thermocouple well located in the top cover plate of the lower plenum tank. T_{13} was located on the outside wall of the unheated outlet section. T_{14} was inside a thermocouple well located in the lower cover plate of the upper plenum tank.

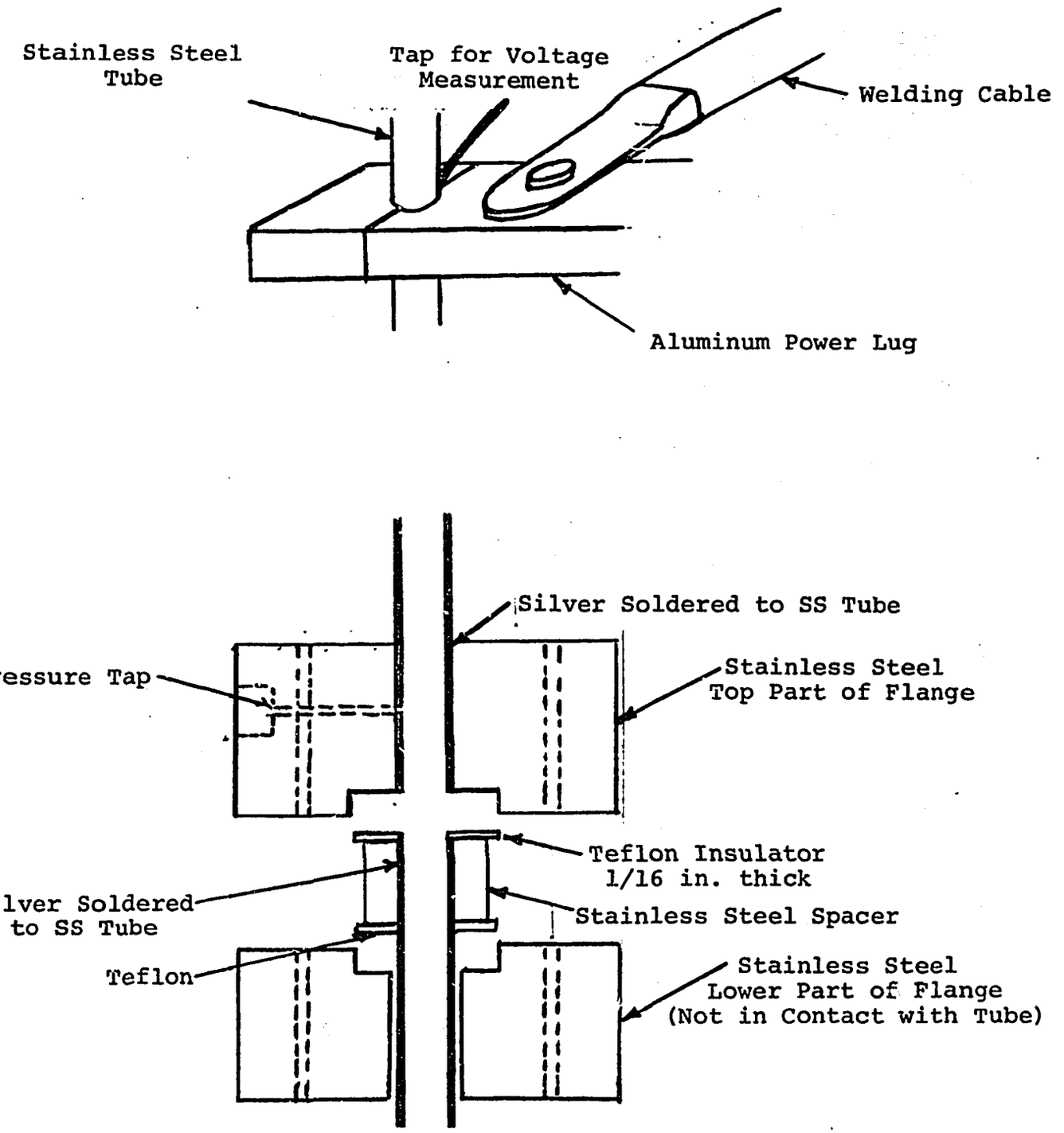

Figure II-8

Detail of Test Section Showing Power Lug Connection and Insulated Flange

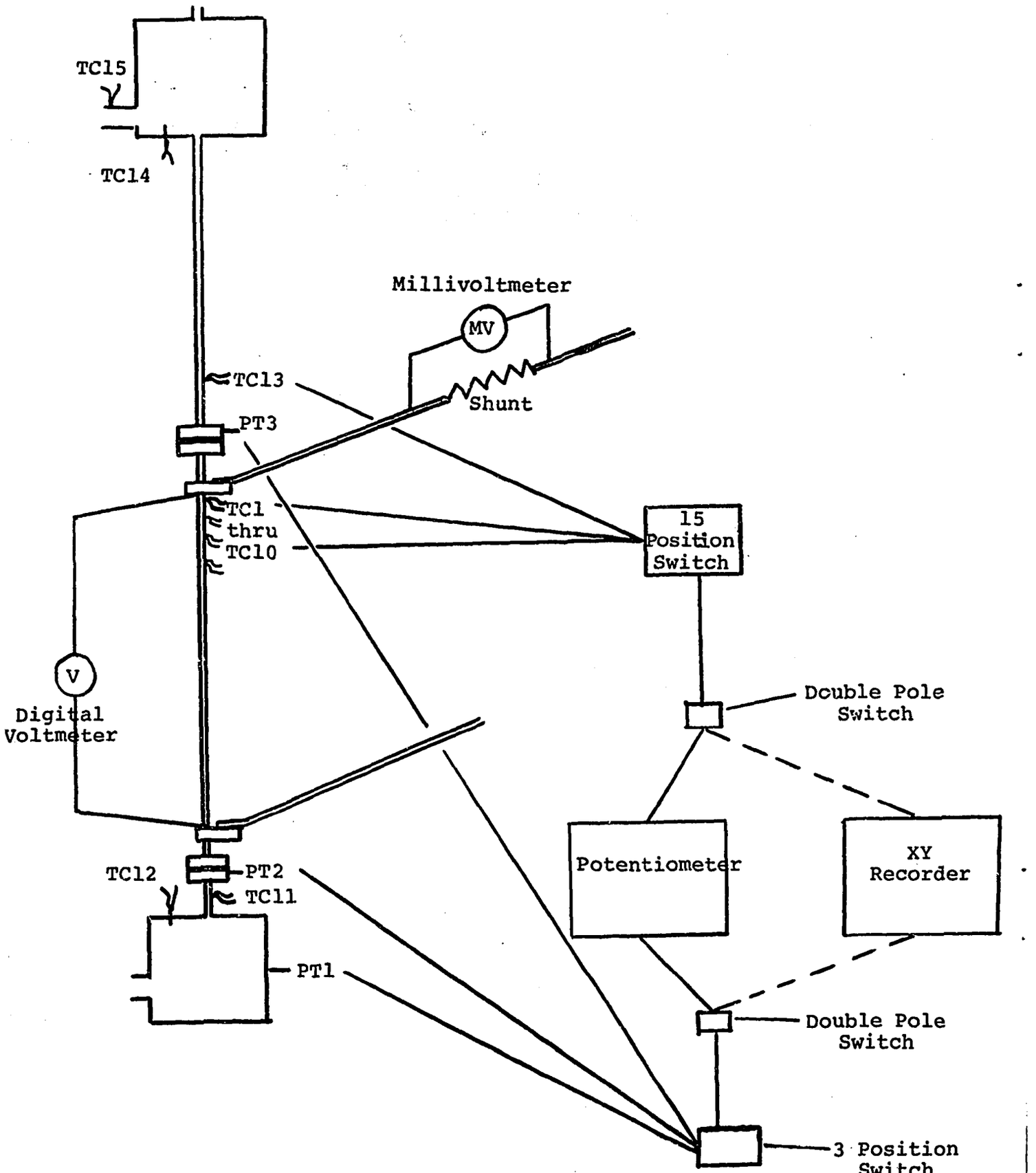

Figure II-9
Schematic of Loop Instrumentation

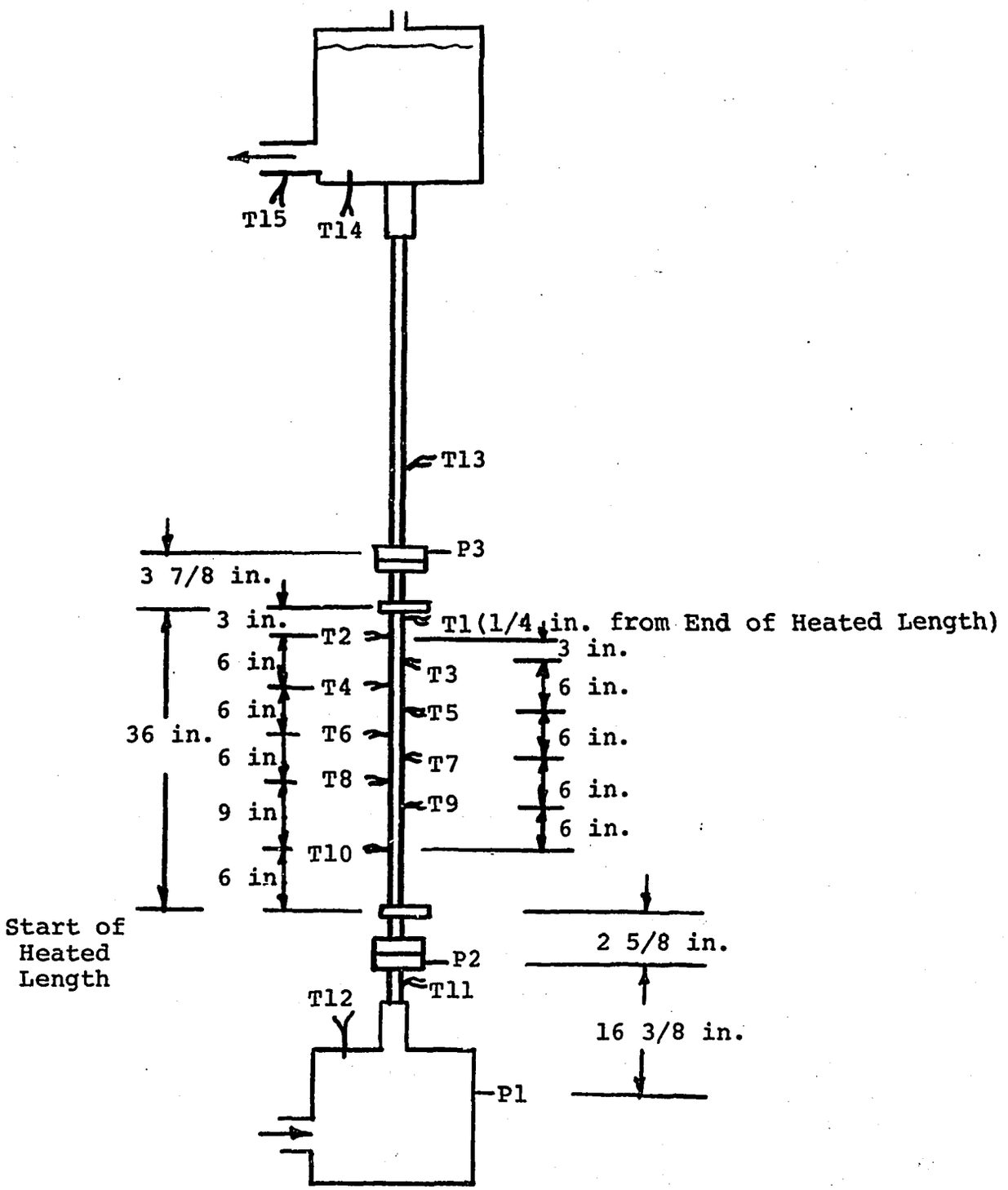

Figure II-10

Location of Pressure and Temperature Measurements

All thermocouples were made of 30 ga. chromel-alumel thermocouple wire. The thermocouples attached to the test section were electrically insulated by a 0.002 to .003 in. thick layer of mica. They were held against the tape by means of asbestos string wrapped several times around the thermocouple and mica.

Thermocouple output could be measured by either a potentiometer or an XY recorder. This was made possible by connecting each of the 15 thermocouples to a 16 position switch which was in turn connected to a double pole switch connected to the potentiometer and recorder. See Figure II-9.

Pressures were measured by three Tyco Type AB pressure transducers with a range of 0 - 6 psig. Excitation was provided by 6 volt dry cell batteries. The calibrated full scale output of each transducer at 6 volts excitation was 120 mv $\pm$ 1%. The transducers were located as shown in Figure II-9. P_1 was mounted in the wall of the lower plenum tank. P_3 was mounted in the lower half of the insulating flange below the heated section. P_3 was mounted in the upper half of the insulating flange above the heated section.

As for the thermocouples, the output of the pressure transducers could be measured by either a potentiometer or an XY recorder. This was accomplished by connecting each transducer to a three position switch which was in turn connected to the potentiometer and recorder. See Figure II-9.

Power to the test section was obtained by measuring the current and voltage drop. The current was determined by measuring the voltage drop across a standard shunt using a Model 322 No. 396 millivoltmeter with a 0 - 18 mv range. The shunt was calibrated to give a voltage drop of 50 mv at 1000 amperes. The voltage across the test section was measured

directly with a Triplett Model 4235-F multirange digital voltmeter. The voltage taps were clamped between the test section wall and the aluminum power lug shown previously in Figure II-8.

BLANK PAGE

III. TEST PROCEDURES

A. General

The test procedures were designed to simulate heat transfer and flow conditions approximating those predicted to occur at various times during the first few seconds of a LMFBR LOPI accident. The choice of these procedures was based on consideration of the LOPI accident sequence described in Section I.A and the assumptions outlined in Section II.A.

Three types of tests were conducted. The first was a steady state test in which the test section power was slowly increased to the desired test condition and then held constant while data was taken. The second was a transient test in which the test section power was increased almost instantaneously to the level corresponding to the desired condition. The third was a transient cooling test to determine the Liedenfrost temperature. The detailed procedures used for each of these tests are outlined in the subsections that follow.

B. Steady State Tests

During a LOPI accident, the coolant in the hot fuel assembly goes through a succession of flow conditions ranging from forced convection of subcooled liquid to natural convection flow boiling and CHF. The procedure used for the steady state tests was designed to produce this same sequence of conditions, except that for each condition the only flow was due to natural circulation. The procedure was the following:

1) The water temperatures in the upper and lower plenum tanks were adjusted by controlling the flow of hot and/or cold tap water to the heat exchangers described in Section II.C.3. The upper plenum temperature was adjusted to 110°F. The lower plenum temperature was adjusted as nearly as possible to 70°F. These temperatures were selected to produce upper and lower plenum qualities approximately equivalent to those that would be expected in the FTR during the first few seconds of a LOPI accident (see Table II-1A).

2) The power to the test section was then slowly increased until the heat flux was at the desired level; and the water flows to the upper and lower plenum heat exchangers were adjusted as required to maintain the temperatures set in Step 1.

3) Once the desired flow condition was established, data was recorded and conditions observed at the sight flow indicators. Data taken included: (a) test section power (voltage and current) and (b) test section and plenum temperatures and pressures (potentiometer readings and XY recorder traces). Observation of conditions at the sight flow indicators were made with the following questions in mind: What is the flow regime entering or leaving each end of the test section? If the regime is two-phase, what is the spatial configuration of vapor and liquid? Is the observed flow regime steady? If not, what is the nature of the observed oscillations? How do these oscillations appear to correlate with data taken with the XY recorder?

4) During a particular run, while data was being taken as described in Step 3, the upper and lower plenum tank temperatures were periodically checked and adjustments were made to the water flows to the upper and lower plenum heat exchangers as necessary to maintain the conditions initially established in Step 1. (For some of the runs, problems with the pump used to circulate water to the lower plenum heat exchanger made this step difficult, as noted in Tables IV-1, IV-2, and IV-3 of Section IV.A.)

5) Three test runs were conducted as outlined in Steps 1 through 4. The first was at a heat flux of 1×10^4 BTU/hr ft^2 (approximately the onset of subcooled boiling). The second was at a heat flux of 1.75×10^4 BTU/hr ft^2 (subcooled boiling). The third was at a heat flux of 3.83×10^4 BTU/hr ft^2 (bulk boiling). The fourth was at a sequence of heat fluxes ranging from 1.3×10^4 to 7.3×10^4 BTU/hr ft^2 (beyond CHF).

C. Transient Tests

After completion of the steady state tests, two transient tests were conducted using the following procedures:

1) After the steady state test at 7.3×10^4 BTU/hr ft^2 (beyond CHF) was completed, the power to the test section was decreased to zero by opening a knife switch in the power supply circuit. Then, after waiting for the test section temperatures to decrease to their equilibrium, zero heat flux levels, the test section heat flux was increased almost instantaneously to its initial value by closing the knife switch. During the initial part of the resulting transient the test section wall temperature at location T_6 (near the center of the heated length) was followed using the XY recorder. Later in the transient the temperature at location

T_1 (near the top of the heated length) was followed. Observations of the conditions at the sight flow indicators were also made during the transient to see how fast the original flow condition appeared to be reestablished.

3) Next, a transient cooling test was run to determine the Liedenfrost temperature. This test was initiated from a zero heat flux condition. First the test section power was slowly but steadily increased until the heat flux was about 8×10^4 BTU/hr ft^2. The tube wall temperature at the top of the heated section was allowed to increase to a temperature beyond 1500°F (well above the Liedenfrost temperature expected on the basis of previous steady state tests beyond CHF). When the temperature had exceeded 1500°F the power was quickly decreased to well below the power required for CHF. During the resulting transient, the temperature at location T_1 was followed using the XY recorder in order to determine the tube wall temperature at which the cooldown rate increased significantly (Liedenfrost temperature).

D. Data Reduction

1. Thermocouple Data

The thermocouple data was obtained as mv readings from the potentiometer and the XY recorder traces. The Y scale on the recorder traces was converted to mv by setting the pen at zero for the zero mv condition and then using the Y scale setting (mv/division). This conversion was periodically cross checked by comparison with the potentiometer reading of the same thermocouple.

The fluid temperatures were relatively steady at Locations T_{11}, T_{13} (inlet and exit of the heated section) and T_{12}, T_{14}, T_{15} (plenum tanks). Therefore the mv readings corresponding to these temperatures were obtained from the potentiometer readings. On the other hand, temperatures at Locations T_1 through T_{10} (along the outside wall of the heated section) were observed to change with time as a result of oscillations of the test section pressure and flow. Therefore, mv readings corresponding to temperatures at these locations were obtained from the XY recorder traces by estimating the average reading over several minutes.

Millivolt readings obtained from the potentiometer and/or recorder were converted to °F by means of standard calibration tables for chromel-alumel thermocouples. The fluid temperatures obtained from this conversion are the values listed in the data tables given in Section IV. The test section outside wall temperatures along the heated length (obtained from conversion of the average readings estimated from the XY recorder traces) were, however, first corrected for the temperature drop across the tube wall. This was done using the following equation from Reference (12):

$$T_i = T_o + \frac{q''R_1}{2k}\left(1 - \frac{2R_2^2}{R_2^2-R_1^2}\ln\frac{R_2}{R_1}\right) \qquad \text{(III-1)}$$

where

T_i, T_o are the inside and outside tube wall temperatures

R_1, R_2 are the inside and outside tube radii

k is the thermal conductivity for stainless steel
110 BTU/hr ft °F at 212°F
150 BTU/hr ft °F at 950°F

q" is the inside surface heat flux

The resulting inside tube wall temperatures are the values listed for locations T_1 through T_{10} in the data tables given in Section IV.

Errors in the temperature data would be due to thermocouple and and measurement error. This error should be within ± 1°F for those temperatures which were not oscillating and were obtained directly from the potentiometer readings. On the other hand, for those temperatures that were oscillating and therefore were averaged, the error could be as much as ± 5°F.

2. Pressure Transducer Data

The pressure transducer data was obtained as mv readings from the potentiometer and XY recorder traces in the same manner as described

for the thermocouples. However, because of the large pressure oscillations observed for most of the test conditions, the potentiometer was only useful as a check on the recorder Y scale conversion (mv/division).

Millvolt readings from the XY recorder (or the potentiometer when such readings could be made) were converted to psig. using the following equation based on information provided by the manufacturer:

$$P(\text{psig}) = \frac{\text{mv. reading}}{\text{excitation voltage}} \times 0.3 \qquad \text{(III-2)}$$

(The excitation voltage provided by the dry cell batteries was measured before each run by the digital voltmeter described in Section II.C.7.)

According to the manufacturer, the full scale accuracy of the transducers used for the pressure measurements was $\pm$ 1 percent of the full scale reading of 6 psig. This was checked by comparing measured and calculated static pressures at zero power and found to be a little low. Differences of up to $\pm$ 3 percent were observed in these comparisons.

3. Test Section Power Measurement

Test section power was obtained from the measurements of test section current and voltage using the following equation:

$$Q(\text{kw}) = \frac{(\text{volts})\left(\frac{\text{mv}}{50} \times 1000\right)}{1000} \qquad \text{(III-3)}$$

where $\left(\frac{\text{mv}}{50} \times 1000\right)$ is the test section current in amperes based on the millivoltmeter readings and the shunt calibration.

The test section heat flux was obtained from the power measurement by means of the equation:

$$q'' = \frac{Q(3413)}{\pi D L_H}$$

or

$$q''(\text{BTU/hr ft}^2) = Q(\text{kw})(2.859 \times 10^4) \qquad \text{(III-4)}$$

Errors in the power measurement and therefore in the heat flux would be due to instrument error and unsteadiness during a test run. Error in the heat flux would also be due to heat loss to the atmosphere. (For the initial runs at lower heat flux [Runs 1, 2 and 3] the test section was not insulated. But, for the later runs up to and beyond CHF, about 1/4 in. of asbestos tape was wrapped around the heated section.) Considering both sources of error, the error in the calculated heat flux values is estimated to be less than $\pm$ 5 percent.

4. Calculation of Flow from Energy Balance

For those test conditions for which the test section exit fluid temperature was less than the saturation temperature , the average flow through the test section was obtained from an energy balance on the heated section. The equation used was the following:

$$W(\text{lb/sec}) = \frac{Q(\text{kw})(3413)}{C_f(T_{13}-T_{12})(3600)} \qquad \text{(III-5)}$$

5. Calculation of Heat Transfer Coefficients

The heat tranfer coefficient at the top of the heated section was calculated using an average of the inside tube wall temperatures at Locations T_1 and T_2. The equation used was the following:

$$\bar{h}_{1,2} = \frac{q''}{\left(\frac{T_1+T_2}{2}\right) - T_{13}} \qquad \text{(III-6)}$$

The values of W and h_{12} are also included in the data tables given in Section IV.

IV. DATA AND OBSERVATIONS

A. Steady State Tests

1. Onset of Subcooled Boiling (Run #1)

Steam bubbles resulting from subcooled boiling were first observed at the top sight flow indicator when the heat flux was about 1×10^4 BTU/hr ft^2. Data for this test condition are given in Table IV-1 and Figures IV-1A and IV-1B. The corresponding observations at the sight flow indicators were the following:

> Top. Conditions changed periodically. Small bubbles were observed continuously at the top sight flow indicator. Periodically, the flow would appear to slow down momentarily followed by the appearance of much larger bubbles over the next several seconds.
>
> Bottom. Only liquid was observed.

2. Subcooled Boiling (Run #2)

Subcooled boiling was the heat transfer mechanism at the top of the heated section for heat fluxes between 1×10^4 and 3×10^4 BTU/hr ft^2. As the heat flux was increased within this range the following observations were made at the sight flow indicators:

> Top. Conditions continued to change periodically as observed for Run #1. However, the frequency of these changes increased as the heat flux was increased.
>
> Bottom. Single phase liquid flow continued to be observed until onset of saturated boiling at about 3×10^4 BTU/hr ft^2. At this heat flux, a spurt of small steam bubbles was observed every few seconds at the lower sight glass. However, these bubbles condensed within the first inch or two below the top of the glass.

Data corresponding to a heat flux of 1.75×10^4 BTU/hr ft^2 are given in Table IV-2 and Figures IV-2A, IV-2B, IV-2C, IV-2D, and IV-2E. The data in Table IV-2 are an average of results obtained on two successive days. Figures IV-2A and IV-2B show the pressure and temperature traces taken on the first day, immediately after completion of Run #1. Figure IV-2C shows pressure and temperature traces taken

Table IV-1

Data for Run #1 (Onset of Subcooled Boiling)

Power 0.363 kw

Heat Flux 1.04×10^{4} BTU/hr ft^2

Average Flow 3.74×10^{-3} lb_m/sec.

Heat Transfer Coefficient at 1,2 325 BTU/hr $ft^2 °F$

Average Tube Wall Temperatures	
Location	°F
T_1	206
T_2	
T_3	210
T_4	
T_5	189
T_6	
T_7	176
T_8	
T_9	169
T_{10}	147
T_{11}	78-85
T_{12}	77-85
T_{13}	174
T_{14}	109
T_{15}	107

Average Pressures (psig)		
Location	Without Heat	With Heat
P_1	4.01	3.92
P_2	3.66	3.65
P_3	2.30	2.21

NOTES

1) See Figure II-9 for locations of pressure and temperature measurements (T_1, P_1...etc.).
2) Circulating pump for lower plenum cooling was overheating. Therefore, it was necessary to turn it off during the run and T_{11} drifted from 78.5 to 85°F while other data was being taken.

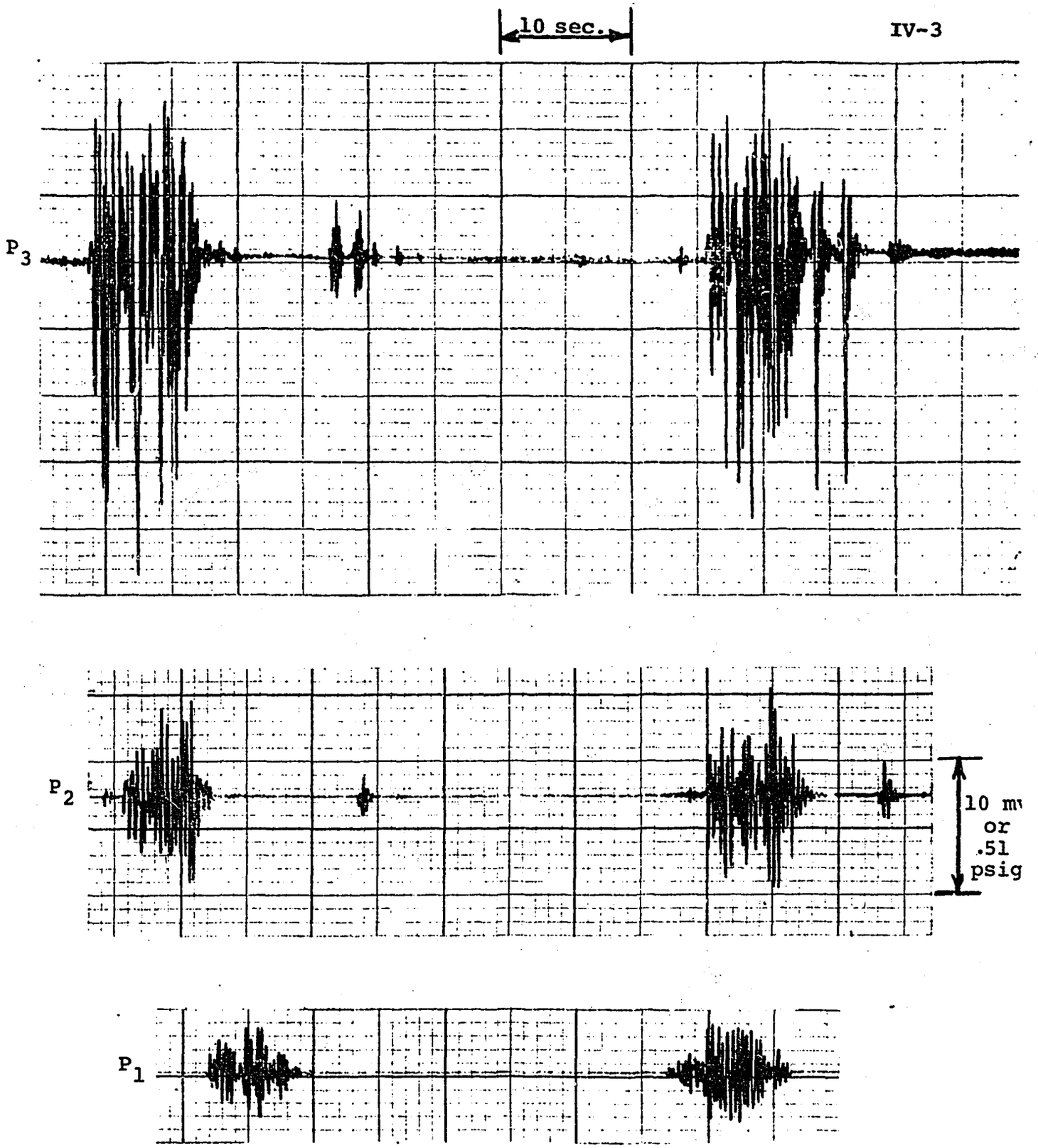

Note: These traces were taken sequentially and not simultaneously.

Figure IV-1A

Pressure Traces from XY Recorder for Run #1
(Onset of Subcooled Boiling)

Figure IV-1B

Temperature Traces from XY Recorder for
Run #1 (Onset of Subcooled Boiling)

Note: These traces were taken sequentially and not simultaneously.

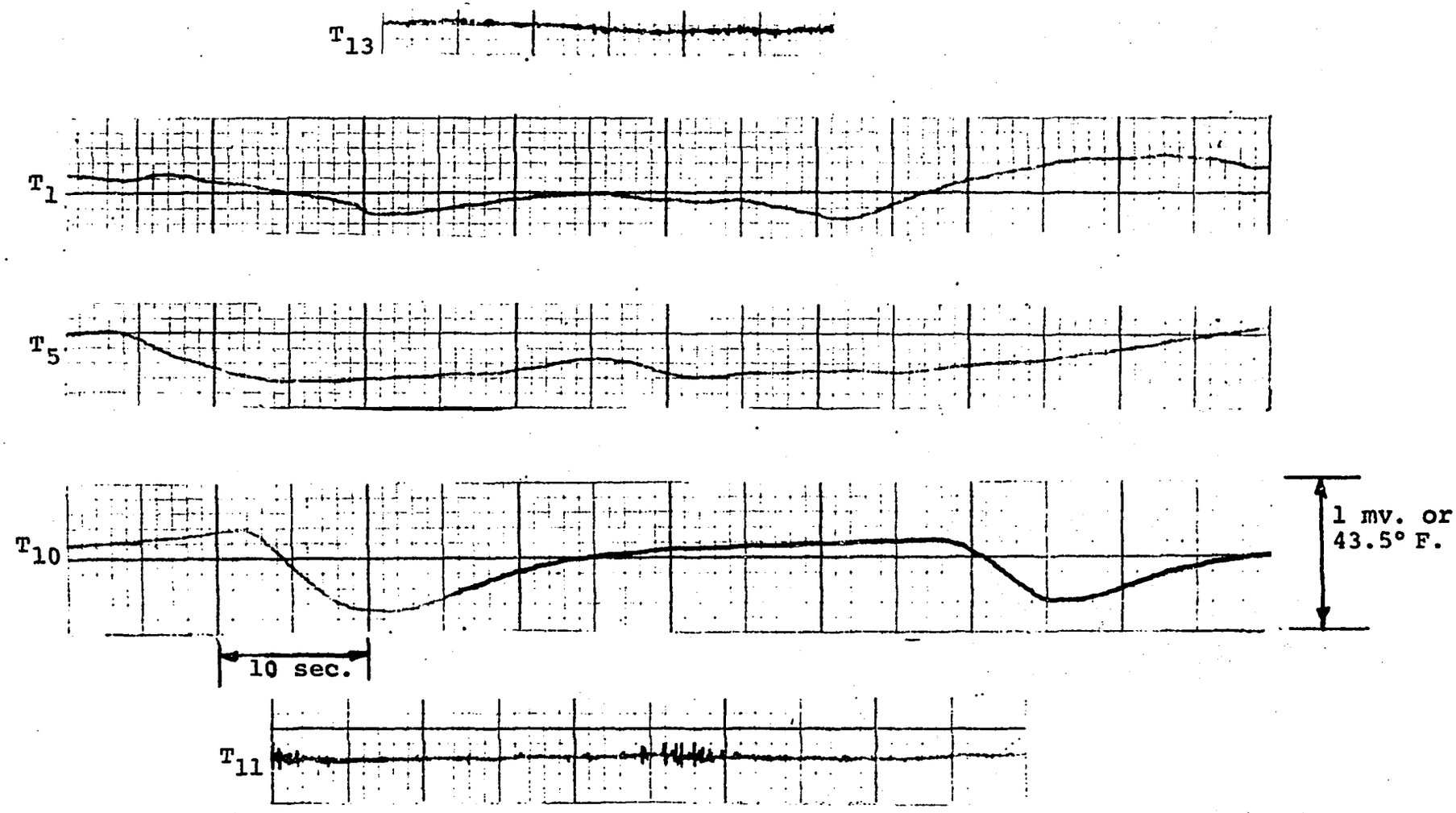

Table IV-2

Data for Run #2 (Subcooled Boiling)

Power 0.606 kw

Heat Flux 1.73×10^{4} BTU/hr ft^2

Average Flow 4.73×10^{-3} lb_m/sec.

Heat Transfer Coefficient at 1,2 865 BTU/hr ft^2°F

Average Tube Wall Temperatures	
Location	°F
T_1	215.5
T_2	
T_3	218.5
T_4	
T_5	
T_6	189.5
T_7	183
T_8	
T_9	175.5
T_{10}	176.5
T_{11}	77±2
T_{12}	74±1
T_{13}	195.5
T_{14}	110.5±2
T_{15}	107

Average Pressures (psig)		
Location	Without Heat	With Heat
P_1	4.01	3.88
P_2	3.66	3.41
P_3	2.30	2.18

NOTES

1) See Figure II-9 for locations of pressure and temperature measurements (T_1, P_1...etc.).
2) Instead of leaving circulating pump off as was done for Run #1, it was turned off and on periodically. In this manner it was possible to maintain T_{11} and T_{14} constant to within about ± 2°F.
3) Start and stopping the circulating pump and varying the flow to the external heat exchanger was found to have no effect on the pressure traces.

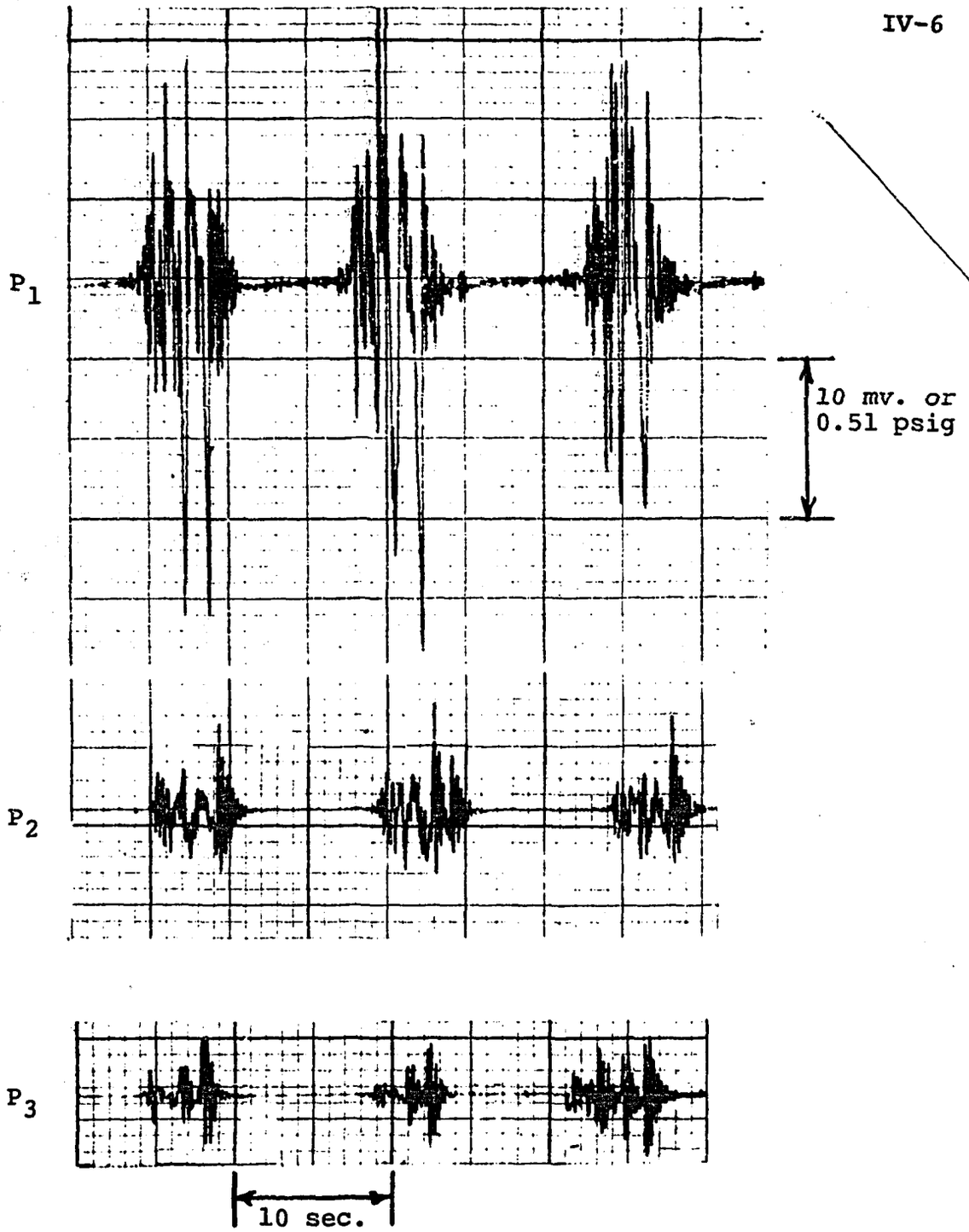

Note: These traces were taken sequentially and not simultaneously.

Figure IV-2A

Pressure Traces from XY Recorder for Run #2 (Subcooled Boiling - Taken on First Day Just After Completing Run #1)

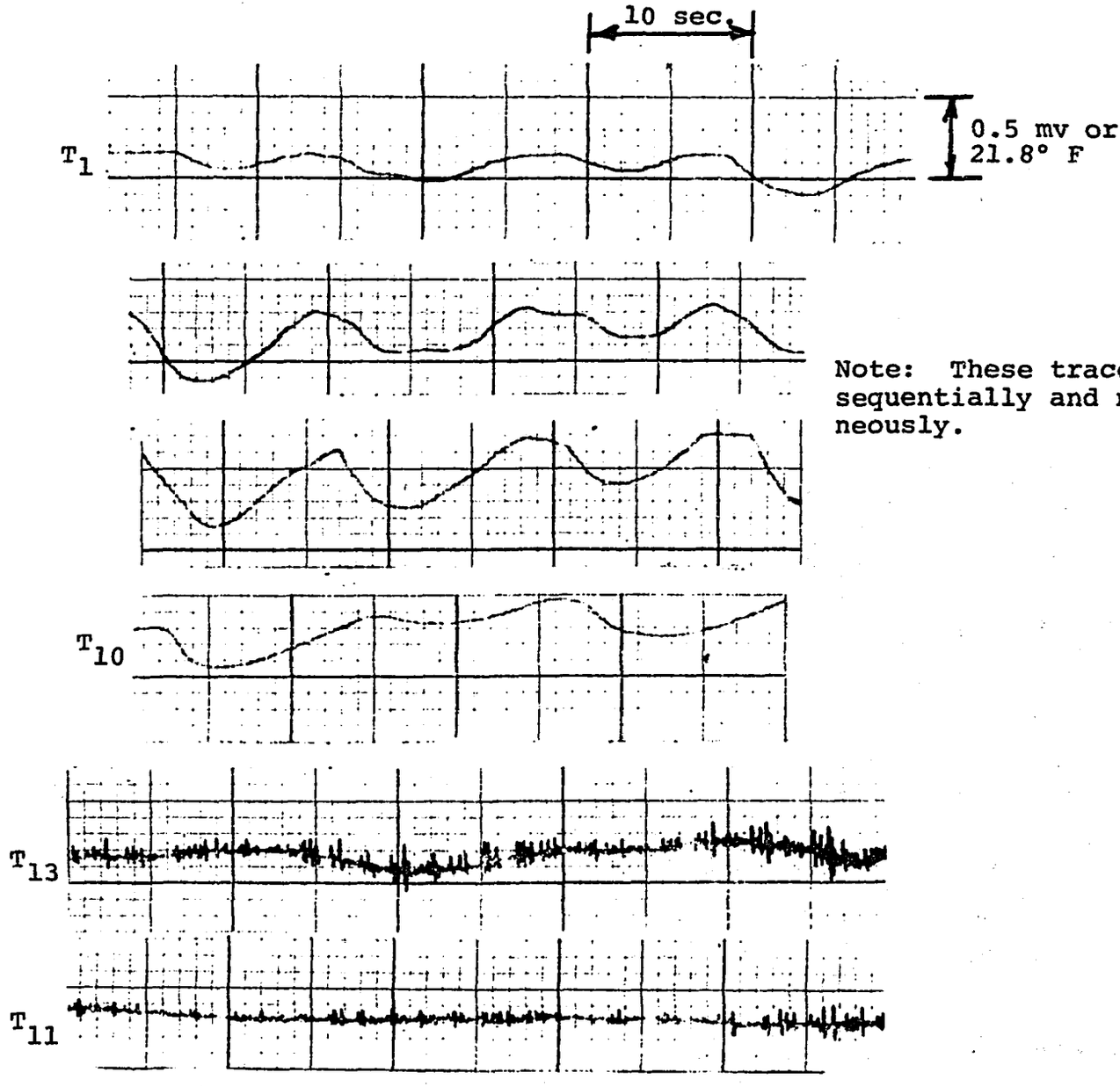

Note: These traces were taken sequentially and not simultaneously.

Figure IV-2B

Temperature Traces from XY Recorder for Run #2 (Subcooled Boiling - Taken on First Day Just After Completing Run #1

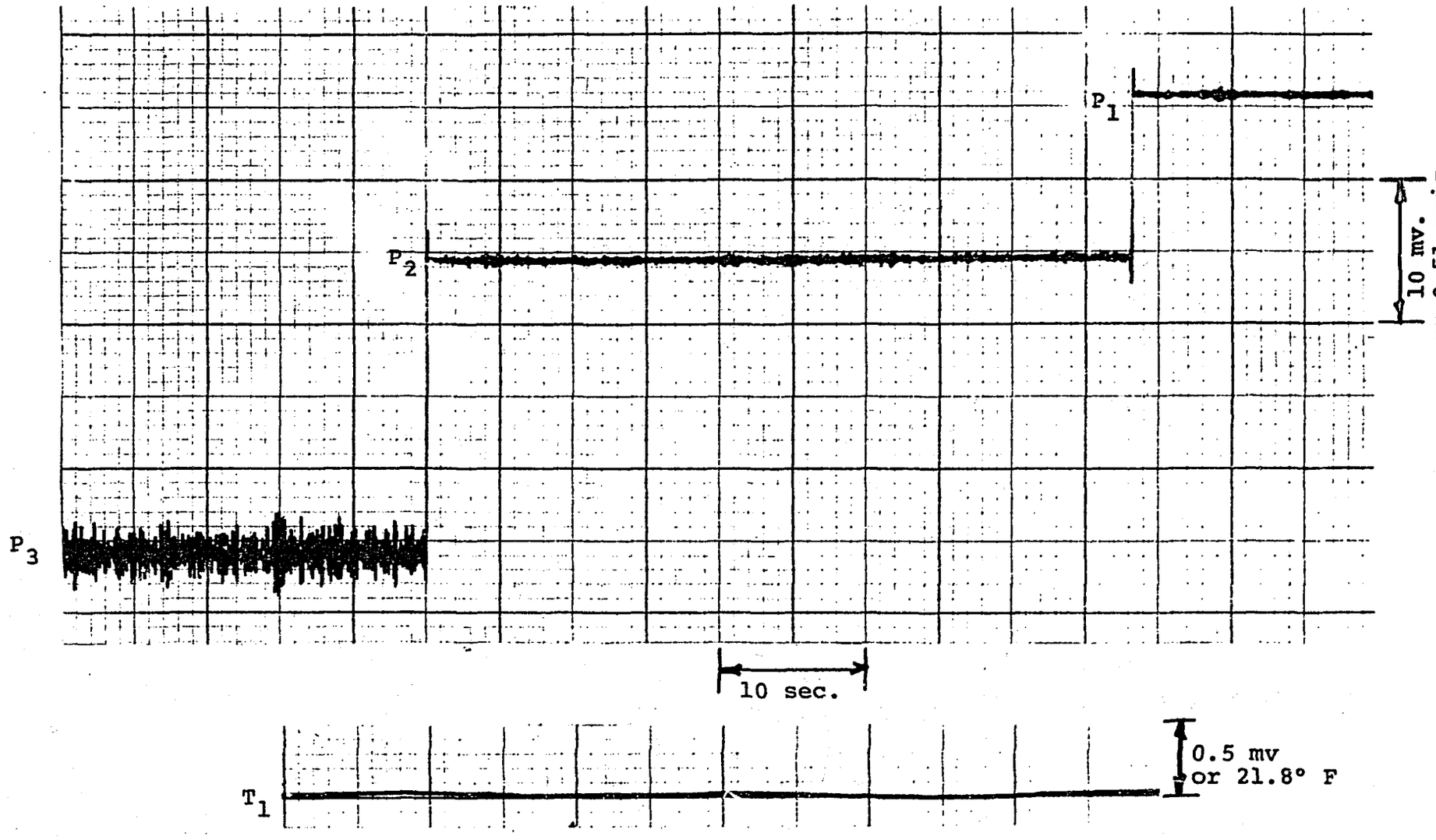

Figure IV-2C

Pressure and Temperature Traces from XY Recorder for Run #2 (Subcooled Boiling - Taken on Second Day Less Than 10 Minutes After Heating Up Test Section)

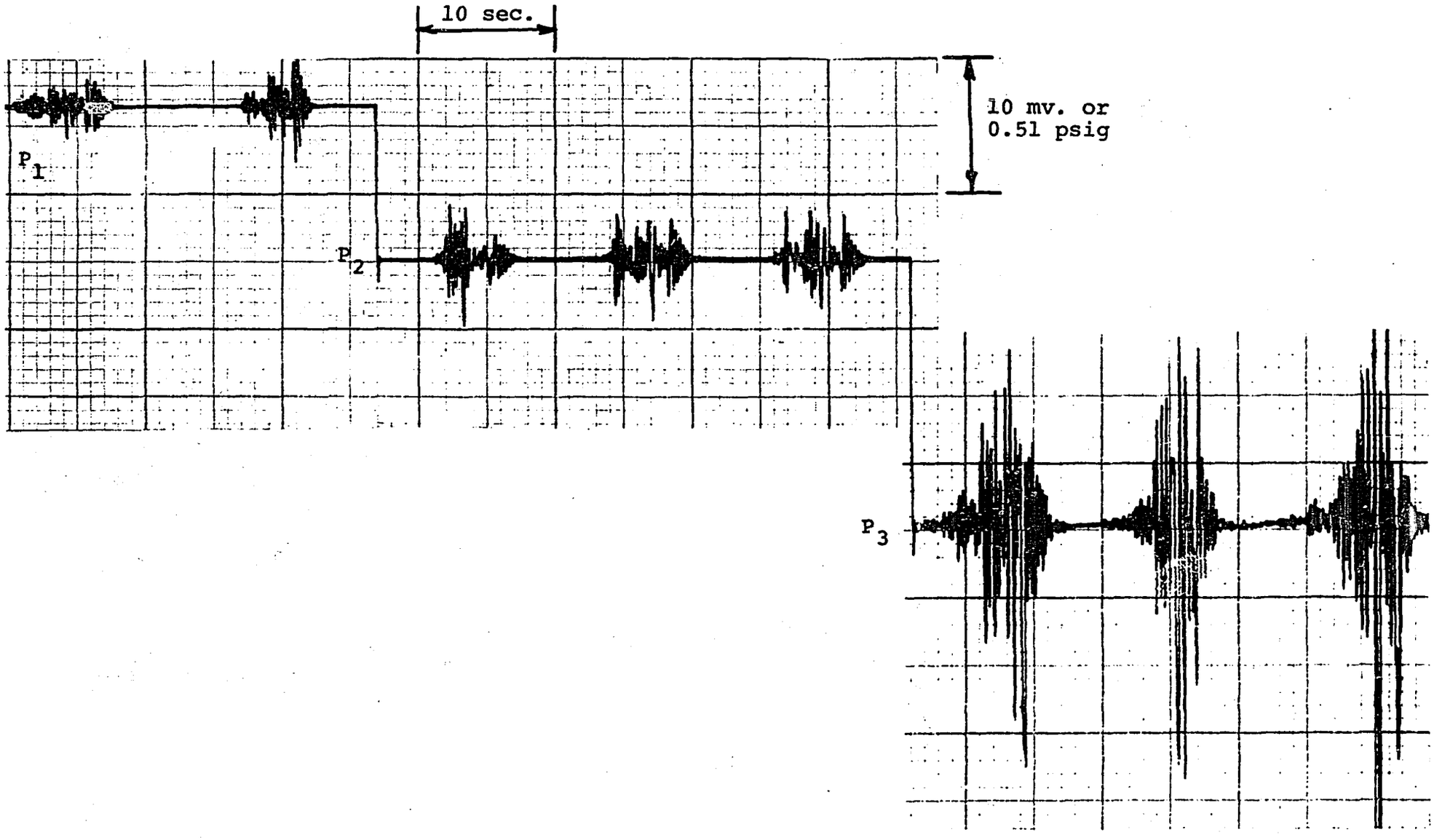

Figure IV-2D

Pressure Traces from XY Recorder for Run #2
(Subcooled Boiling - Taken on Second Day
20-40 Minutes After Heating Up Test Section)

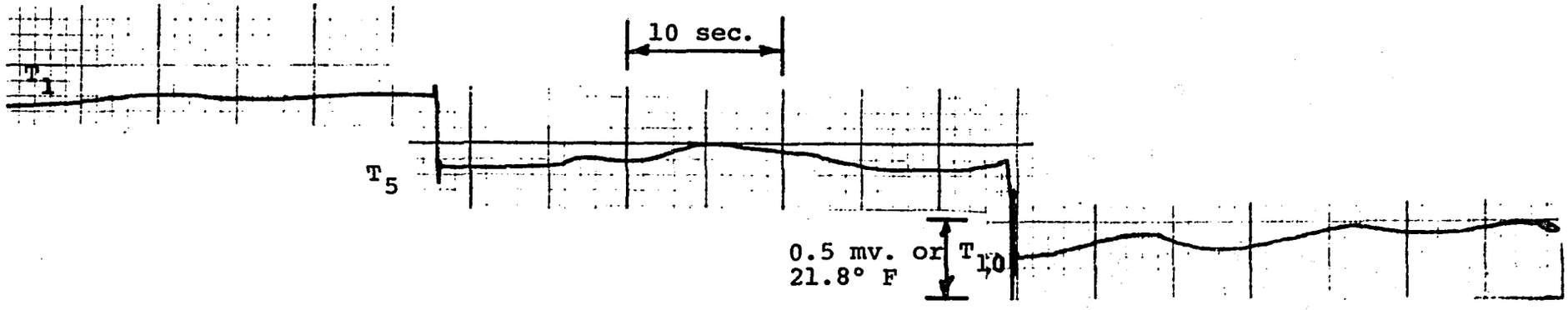

Figure IV-2E

Temperature Traces from XY Recorder for Run #2
(Subcooled Boiling - Taken on Second Day 20-40
Minutes After Heating Up Test Section)

on the second day within 10 minutes after heating up the test section. Figures IV-2D and IV-2E show pressure and temperature traces taken the second day between 20 and 40 minutes after heating up the test section. A comparison of these figures shows that the pressure and temperature oscillations observed for Run #1 (and for Run #2 on the first day) did not develop until sometime beyond 10 minutes after initially heating up the test section on the second day. Figure IV-2D indicates that the high frequency pressure oscillations occur at locations P_1, P_2 and P_3 at about the same time. Figure IV-2E shows that the peak in the temperature oscillations occurs at locations T_1, T_5 and T_{10} at about the same time. Thus the pressure (and temperature) oscillations at various locations were approximately in phase with each other.

3. Saturated Boiling (Run #3)

Saturated boiling was the heat transfer mechanism at the top of the heated section for heat fluxes between 3×10^4 BTU/hr ft^2 and the CHF condition. As the heat flux was increased within this range, the following observations were made at the sight flow indicators:

> Top. Above 3×10^4 BTU/hr ft^2 bubbles became larger and were observed continuously. Above 4×10^4 BTU/hr ft^2 these bubbles appeared to have agglomerated and the flow configuration appeared more annular or semi-annular than bubbly.
>
> Bottom. As the heat flux was increased, the spurts of bubbles into the lower sight glass became more noticeable and more frequent. Also these bubbles became larger. Above 5×10^4 BTU/hr ft^2 only one large bubble was observed pushing its way down toward the lower plenum every few seconds. It was possible at this point to hear the oscillations going on within the heated section.

Data corresponding to a heat flux of 3.83×10^4 BTU/hr ft^2 are given in Table IV-3 and Figures IV-3A, IV-3B, IV-3C, IV-3D, IV-3E. The first four of the figures are pressure traces taken with various

Table IV-3

Data for Run #3 (Bulk Boiling)

Power 1.34 kw

Heat Flux 3.83×10^4 BTU/hr ft^2

Average Flow _____ lb_m/sec.

Heat Transfer Coefficient at 1,2 1741 BTU/hr $ft^2 °F$

Average Tube Wall Temperatures	
Location	°F
T_1	235
T_2	235
T_3	235
T_4	236
T_5	231
T_6	237
T_7	234
T_8	
T_9	232
T_{10}	227
T_{11}	188
T_{12}	73±2
T_{13}	213
T_{14}	110-111
T_{15}	105

Average Pressures (psig)		
Location	Without Heat	With Heat
P_1		
P_2		
P_3		

NOTES

1) See Figure II-9 for locations of pressure and temperature measurements (T_1, P_1...etc.).
2) Temperature oscillations were much higher frequency and less in amplitude than observed for Runs 1 and 2. (See Figure IV-3E.) Therefore average temperatures were estimated by adjusting the potentiometer until galvanometer deflections were approximately equal to either side of the zero.
3) Circulating pump for lower plenum cooling was turned off and on periodically as was done in Run #2.
4) T_8 was not operable.
5) No determination of average flow could be made for this run, since the exit quality was greater than zero.

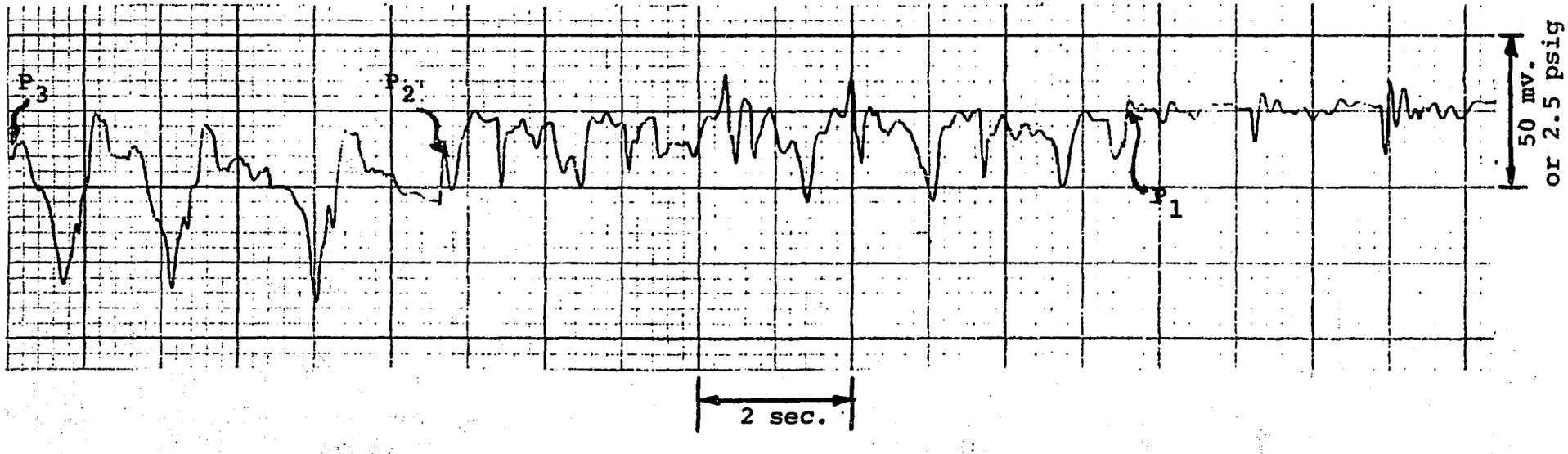

Figure IV-3A

Pressure Traces from XY Recorder for Run #3
(Bulk Boiling)

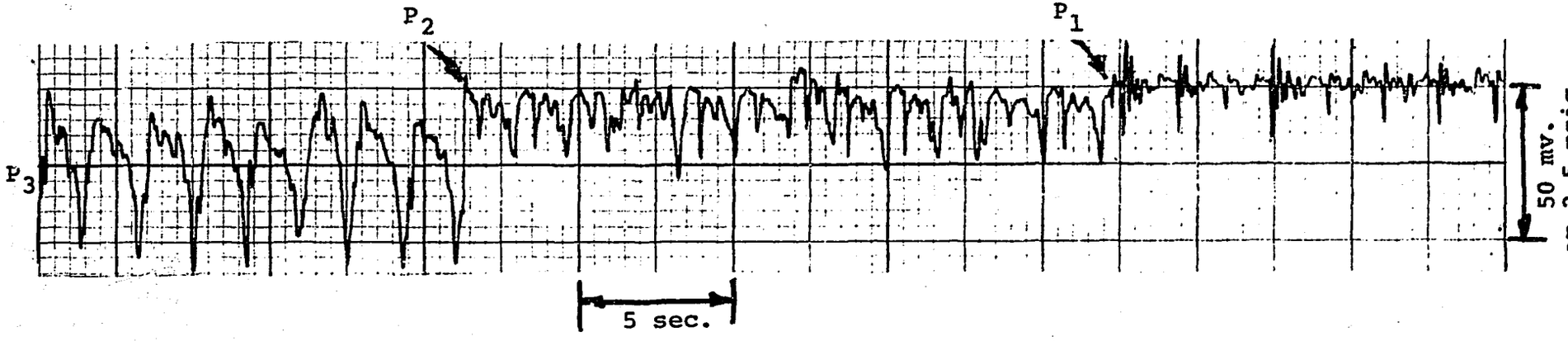

Figure IV-3B

Pressure Traces from XY Recorder for Run #3
(Bulk Boiling)

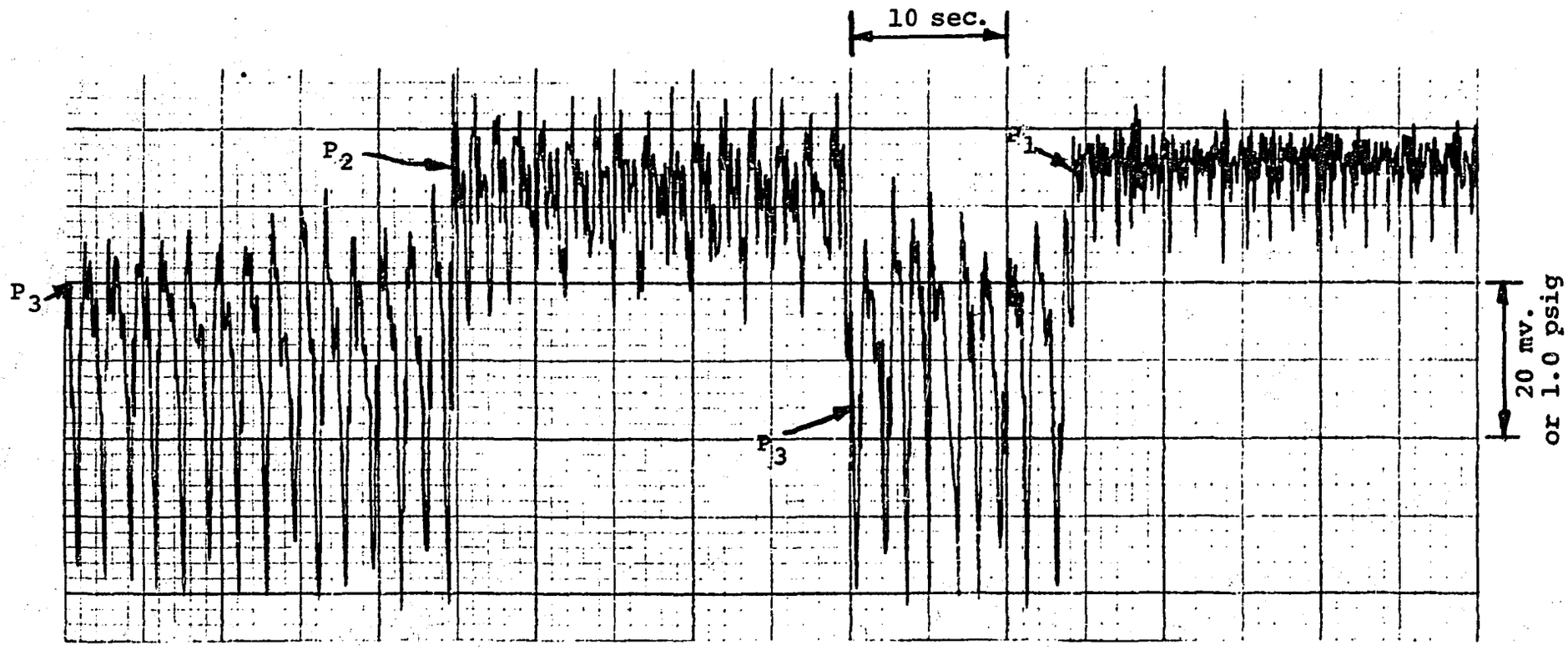

Figure IV-3C

Pressure Traces from XY Recorder for Run #3
(Bulk Boiling)

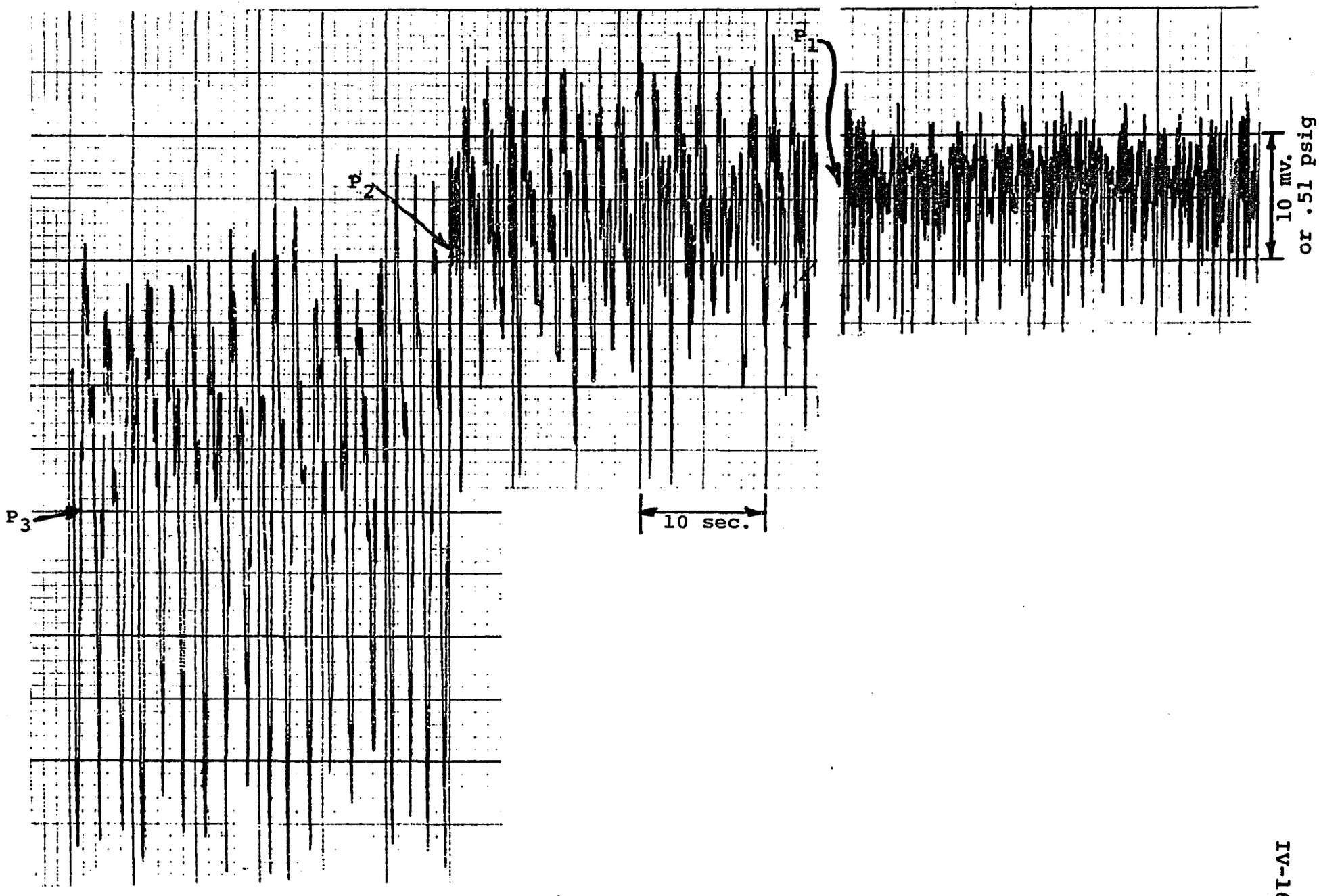

Figure IV-3D

Pressure Traces from XY Recorder for Run #3
(Bulk Boiling)

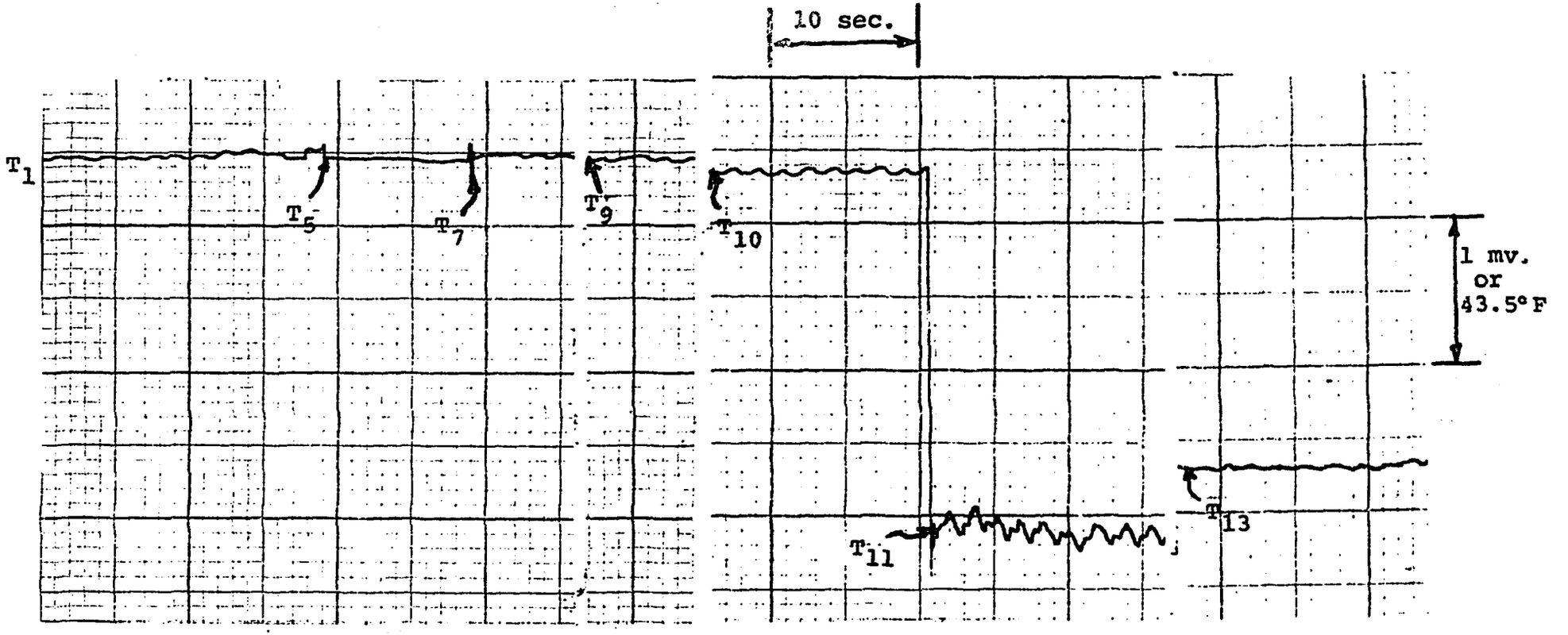

Figure IV-3E

Temperature Traces from XY Recorder for Run #3 (Bulk Boiling)

settings of the horizontal traversing speed. Thus it was possible to observe the details of the high frequency pressure oscillations. Figure IV-3A shows that the period of these oscillations was 1 to 2 seconds. Also the oscillations at locations P_1, P_2 and P_3 appear to be in phase with each other. Figure IV-3E shows XY temperature traces for locations T_1, T_5, T_7, T_9, T_{10}, T_{11} and T_{13}. These traces show that the low frequency, high amplitude oscillations observed for subcooled conditions were not present at this condition. Only high frequency low amplitude oscillations, probably related to the high frequency pressure oscillations, were observed. It should also be noted (from Table IV-3 and Figure IV-3E) that T_{11}, the fluid temperature upstream of the inlet to the heated section was substantially greater than the lower plenum temperature due to condensation of steam from the bubble pushing downward from the heated section.

4. Onset of CHF (Run #4)

The onset of CHF at the top of the heated section was observed at a heat flux of about 6.4×10^4 BTU/hr ft^2. Data taken as this condition was approached and exceeded are given in Table IV-4 and Figure IV-4. These data show that, for heat fluxes above 6.4×10^4 BTU/hr ft^2, T_1 oscillated over a temperature range that became increasingly greater; until, at a heat flux of about 7.15×10^4 BTU/hr ft^2, the upper end of this range exceeds 900°F. For higher heat fluxes T_1 no longer oscillated and at 7.3×10^4 BTU/hr ft^2 was fairly steady at 1180°F. Table IV-4 shows that at 7.3×10^4 BTU/hr ft^2, even though T_1 has gone through CHF, the temperature of the fluid leaving the top of the test section is still the saturation temperature. Visual observations at the sight flow indicators were the following:

Table IV-4

Data for Run #4 (Onset of CHF)

Power kw	Heat Flux BTU/hr ft^2°F	Average Tube Wall Temperatures of (°F)			Heat Transfer Coefficient at the Top of Heated Section BTU/hr ft^2°F	Average Fluid Temperatures of (°F)	
		T_1	T_2	T_3		T_{11}	T_{13}
0.45	1.29×10^4	208	214.5	213	337	69	173
1.07	3.07×10^4	217.5	224.5		2362		208
1.37	3.91×10^4	227	237	239	2058	168	213
1.73	4.95×10^4	242	250	251	1500	195	213
2.07	5.93×10^4	277	267	262	1005	191	213
2.23	6.37×10^4	281			937		213
2.28	6.51×10^4	295-340	268		794-513		213
2.32	6.63×10^4	318-430			632-306		213
2.50	7.14×10^4	518-904			234-103		213
2.55	7.29×10^4	1179			75		213

T_{12} 69-76°F

T_{14} 107-112°F

Table IV-4
(Continued)

NOTES

1) See Figure II-9 for locations of pressure and temperature measurements (T_1, P_1...etc.).

2) The tube wall temperatures given for power levels below 2.28 kw are time average values obtained from XY recorder traces as for Runs 1 and 2.

3) The tube wall temperature at location T_1 oscillated over a range of from 50 to 400°F for power levels of 2.28, 2.32 and 2.50 kw. Therefore, for these power levels the range of oscillation rather than the average temperature is given.

4) At 2.55 kw, the tube wall temperature at T_1 was stable at the time average temperature given.

5) Circulating pump for lower plenum cooling was operable for this run. Therefore it was not necessary to turn the pump on and off as was done for Runs 1, 2 and 3.

6) The heat transfer coefficients at the top of the heated section were based on the average of T_1 and T_2 for power levels below 2.23 kw. For power levels above 2.23 kw, only T_1 was used.

7) The heated section was insulated with approximately 1/8 in. of asbestos tape during the run.

Figure IV-4

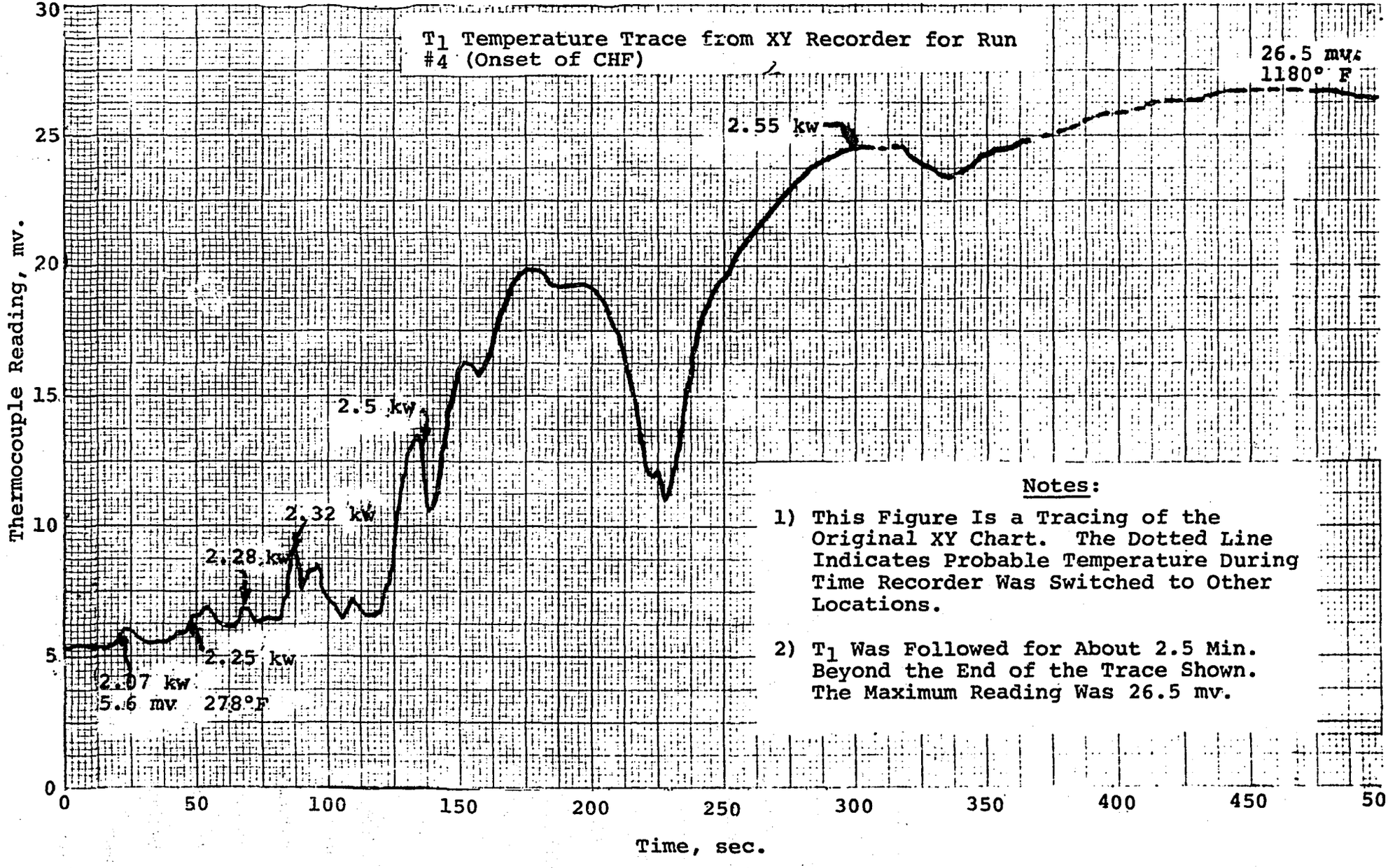

Notes:

1) This Figure Is a Tracing of the Original XY Chart. The Dotted Line Indicates Probable Temperature During Time Recorder Was Switched to Other Locations.

2) T_1 Was Followed for About 2.5 Min. Beyond the End of the Trace Shown. The Maximum Reading Was 26.5 mv.

Top. Water was clearly present in the steam leaving the test section.

Bottom. The large bubble observed pushing toward the lower plenum in previous runs was now periodically disappearing below the lower end of the sight glass.

B. Transient Tests

1. Step Increase in Heat Flux to Beyond CHF (Run #5)

After taking the temperature trace shown in Figure IV-4 the power was decreased to zero using a knife switch in the power supply circuit; and test section temperatures were allowed to decrease to their equilibrium, zero heat flux levels. Then the power was almost instantaneously brought back to the initial condition, again using the knife switch. A complete temperature trace was not obtained. However, the partial trace is shown in Figure IV-5. This figure shows the temperature at location T_6 as the power was first decreased and then increased. T_6 is shown to reach its original level of about 5.3 mv (264°F) in about 10 seconds. (At the same time it was visually observed at the sight flow indicators that the original flow conditions were reestablished almost immediately.) After about 135 seconds the recorder was switched to T_1 which was observed to be approaching its original value as shown in the figure. The power was then decreased to zero to end the run.

2. Liedenfrost Temperature (Run #6)

One test was run in which CHF was approached and exceeded in a manner similar to Run #4. However, in this case the heat flux was increased to about 8×10^4 BTU/hr ft^2 rather than 7.3 BTU/hr ft^2 as in Run 4. The temperature at T_1 was allowed to increase to above 1500°F before the power was decreased. The resulting temperature transient is shown in Figure IV-6. This figure shows that the cool-down rate increased sharply when the tube wall temperature decreased

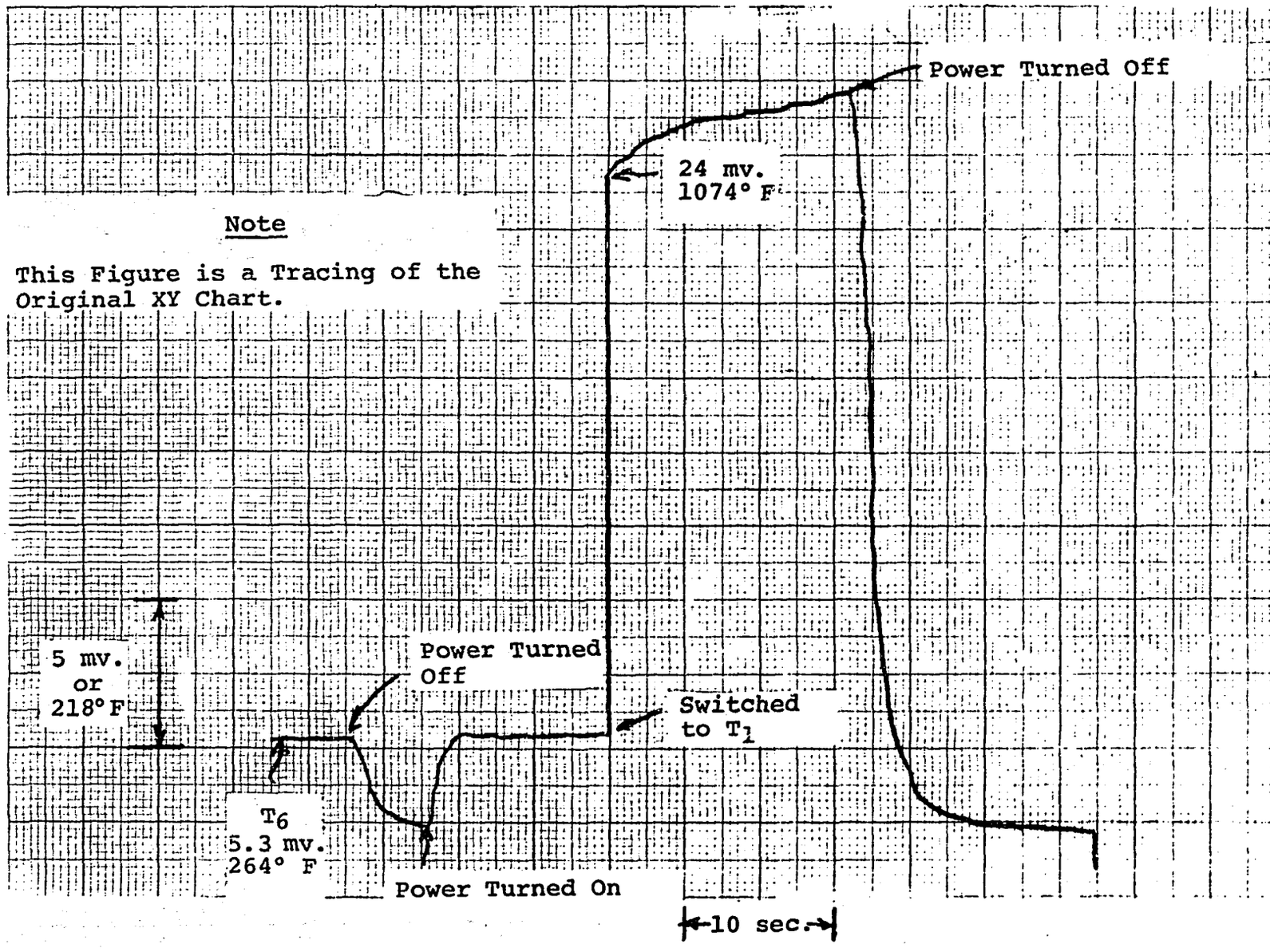

Figure IV-5

T_6 and T_1 Temperature Traces from XY Recorder for Run #5 (Step Increase in Heat Flux to

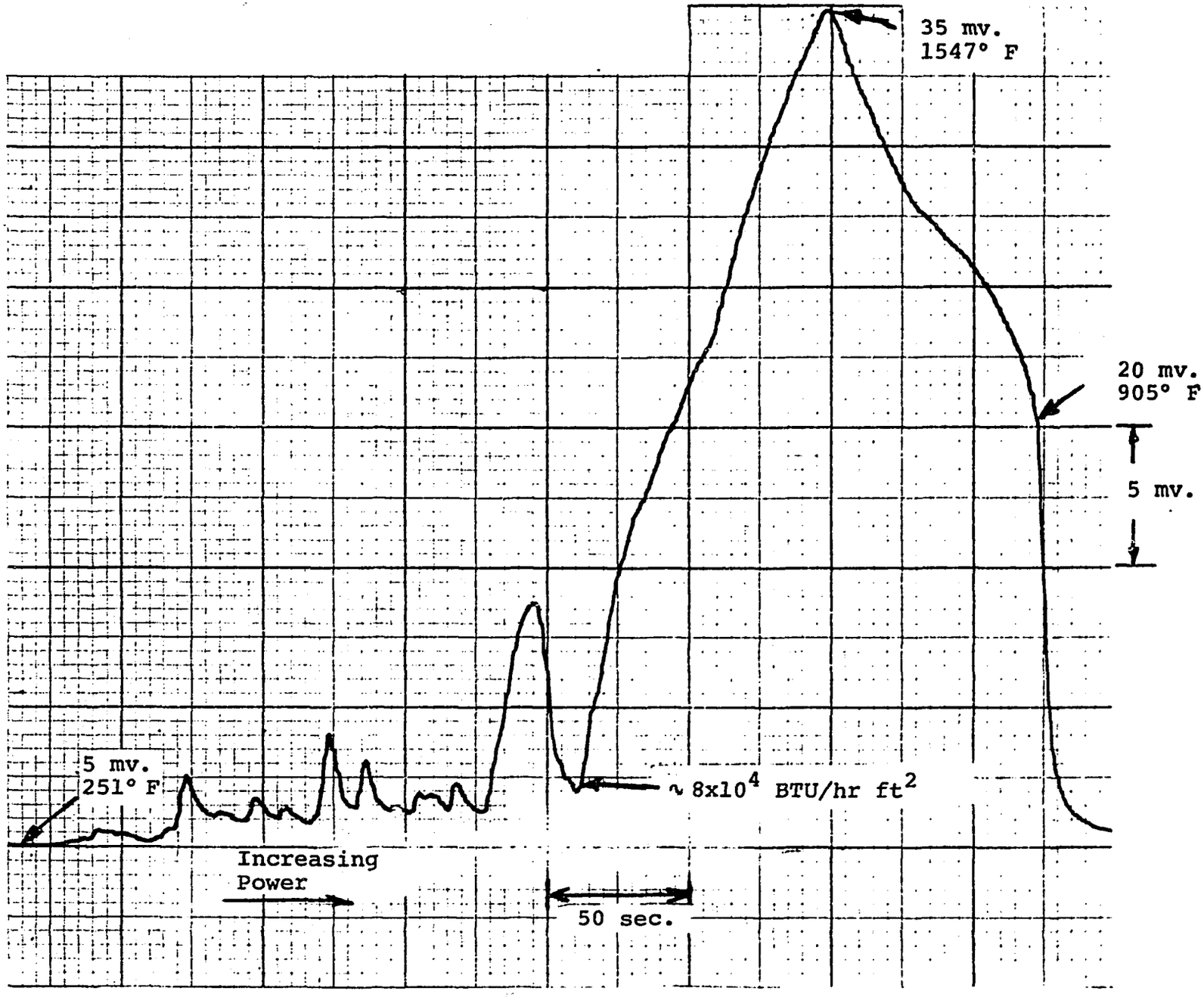

Figure IV-6

T_1 Temperature Trace from XY Recorder for Run #6 (Liedenfrost Temperature)

below about 900°F. This is apparently the temperature below which the wall can be rewetted. This is consistent with the results for Run #4 that indicated T_1 no longer oscillated once the temperature exceeded about 900°F.

V. ANALYSIS AND DISCUSSION

A. Analysis and Discussion of Tests

1. Flow-Pressure Drop Characteristics of Test Loop

In Section II.B, the following equations were derived from conservation of mass, momentum and energy, assuming one dimensional, homogeneous flow of liquid and vapor in the fuel assembly or test section:

$$\frac{L}{Ag_c}\left\{\frac{dW}{dt}+\frac{W}{\rho_f L_{1\phi}+\bar{\rho}_m L_{2\phi}}\left[(\rho_f-\bar{\rho}_m)\frac{dL_{2\phi}}{dt}-L_{2\phi}\frac{d\bar{\rho}_m}{dt}\right]\right\} \qquad \text{(II-8)}$$

$$=(\rho_f-\bar{\rho}_m)\frac{g}{g_c}L_{2\phi}-\left[4f\left(\frac{L'_{1\phi}}{D}+\bar{R}\frac{L'_{2\phi}}{D}\right)\frac{W^2}{2\rho_f A^2 g_c}\right.$$

$$Q=h_{fg}\rho_g A\frac{(\rho_f-\bar{\rho}_m)\frac{dL_{2\phi}}{dt}+L_{2\phi}\frac{d\bar{\rho}_m}{dt}}{\frac{\rho_f L_{1\phi}+\bar{\rho}_m L_{2\phi}}{L}}+\dot{W}h_{fg}(x_{out}-x_1) \qquad \text{(II-9)}$$

where

$$\bar{\rho}_m=\frac{1}{L_{2\phi}}\int_{L_{1\phi}}^{L_{1\phi}+L_{2\phi}}\rho_m\,dz$$

$$\bar{R}=\frac{1}{L'_{2\phi}}\int_{L_{1\phi}}^{L_{1\phi}+L'_{2\phi}}\left(\frac{\rho_f}{\rho_m}\right)dz$$

$$\rho_m\simeq\frac{\rho_f}{1+x\left(\frac{\rho_f}{\rho_g}\right)}$$

and

$L_{1\phi}$, $L_{2\phi}$ are lengths of the single and two-phase regions

$L'_{1\phi}$, $L'_{2\phi}$ are the equivalent lengths of the single and two phase regions including effects of inlet contraction and outlet expansion

BLANK PAGE

It was further shown in Section II.B that, for steady flow and uniform axial heat flux distribution, Equations (II-8) and (II-9) become:

$$0 = (\rho_f - \bar{\rho}_m)\frac{g}{g_c}L_{2\phi} - \left[4f\left(\frac{L'_{1\phi}}{D} + \bar{R}\frac{L'_{2\phi}}{D}\right)\right]\frac{W^2}{2\rho_f A^2 g_c} \qquad \text{(II-10)}$$

$$Q = Wh_{fg}(x_{out} - x_1) \qquad \text{(II-11)}$$

where $L_{1\phi}$, $L'_{1\phi}$, $L_{2\phi}$ and $L'_{2\phi}$ are related to the boiling length, L_B, and L_1, L'_1, L_H, L_2 and L'_2 by the expressions:

$$\left.\begin{aligned} L_{1\phi} &= L_1 + (L_H - L_B) \\ L'_{1\phi} &= L'_1 + (L_H - L_B) \\ L_{2\phi} &= L_B + L_2 \\ L'_{2\phi} &= L_B + L'_2 \end{aligned}\right\} \qquad \text{(II-12)}$$

and L_B is defined in terms of mass flow rate, inlet quality, power, heat flux distribution and L_H by:

$$\frac{L_B}{L_H} = 1 + \frac{Wx_1}{Q/h_{fg}} \qquad \text{(II-14)}$$

Equations (II-10), (II-11), (II-12) and (II-14) can thus be used to determine the steady state flow-pressure drop characteristics of the test loop. This is done by first performing the integrations required by the definitions of $\bar{\rho}_m$ and $\bar{R}$ using the previously given approximation for ρ_m and the following expressions relating quality to axial position, z, under uniform heat flux conditions:

$$x = \frac{Q/h_{fg}}{W}\,\frac{(z - L_{1\phi})}{L_H} \qquad L_{1\phi} < z < L_1 + L_H \qquad \text{(V-1a)}$$

$$x = \frac{Q/h_{fg}}{W} + x_1 \qquad L_1 + L_H < z < L_{1\phi} + L_{2\phi} \qquad \text{(V-1b)}$$

Then, substituting the results of these integrations and Equations (II-11), (II-12) and (II-14) into Equation (II-10), and rearranging gives:

$$\rho_f \frac{g}{g_c}(L_H+L_2) = \rho_f \frac{g}{g_c}(L_H+L_2) \left\{ \left[(1-\frac{L_B}{L_H}) + \frac{L_B}{L_H} \frac{\ell n(1+\phi)}{\phi} \right] \frac{L_H}{L_H+L_2} + \left[\frac{1}{1+\phi}\right] \frac{L_2}{L_H+L_2} \right\} + \frac{4f}{D} (L_H+L_2) \frac{W^2}{2\rho_f A^2 g_c}$$

$$\left\{ \left[\frac{L_1'}{L_H} + (1-\frac{L_B}{L_H}) + (1+\frac{\phi}{2}) \frac{L_B}{L_H} \right] \frac{L_H}{L_H+L_2} + [1+\phi] \frac{L_2'}{L_H+L_2} \right\} \qquad \text{(V-2)}$$

where

$$\frac{L_B}{L_H} = \frac{x_{out}}{x_{out}-x_i}$$

$$\phi \equiv x_{out}(\frac{\rho_f}{\rho_g})$$

The left hand side of Equation (V-2) represents the constant external static head driving flow through (L_H+L_2'). The first term on the right hand side represents the test section static head loss; and the second term represents the test section frictional head loss. Thus, on a graph of ΔP vs. W, the left hand side of Equation (V-2) is

a single horizontal line. The right hand side is a set of parabolas for which the variable parameter is X_{out}. For a given value of X_{out}, the steady state solution of Equation (V-2) is then the value of W corresponding to the intersection of the parabola representing the right hand side and the horizontal line representing the left hand side. Solutions were obtained in this manner for the test loop conditions for values of X_{out} between 0 and 1.0, as shown in Figure V-1. The numerical values of the fixed parameters involving test section geometry and fluid properties were obtained from Table II-1A and II-1B. These values were the following:

$$\rho_f = 59.8 \text{ lb}_m/\text{ft}^3$$

$$x_1 = -.146$$

$$\frac{\rho_f}{\rho_g} = 1603$$

$$f = .0055$$

$$D = .152 \text{ in}$$

$$A = .0181 \text{ in}^2$$

$$L_1' = 10.5 \text{ in}$$

$$L_H = 36 \text{ in}$$

$$L_2 = 48 \text{ in}$$

$$L_2' = 55 \text{ in}$$

Since the test loop was operated at constant heat flux for most of the conditions studied, it is useful to convert Figure V-1 from a set of parabolas representing constant values of X_{out} to a set of curves representing constant q". This can be done by using the following equation derived from Equation (II-11) to determine for a

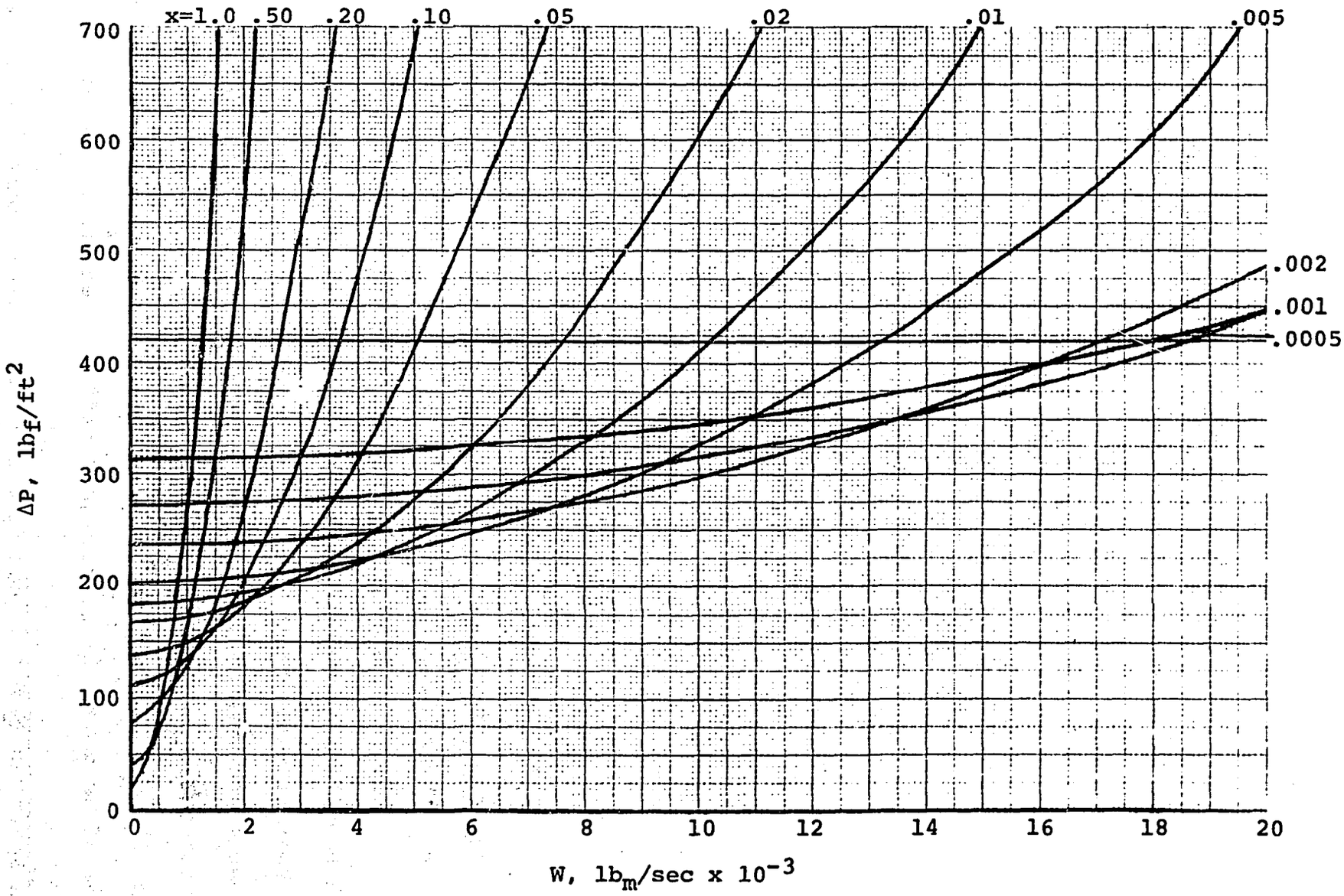

Figure V-1
Flow-Pressure Drop Characteristics of Test Loop with Exit Quality as a Parameter

given q" the values of W corresponding to the various values of represented X_{out} in Figure V-1:

$$q''\pi DL_H = Wh_{fg}(X_{out} - X_1) \qquad (V-3)$$

The result is shown in Figure V-2 for values of q" from 1×10^4 to 8×10^4 BTU/hr ft^2. From this figure one can observe the following:

1) For heat fluxes below 3×10^4 BTU/hr ft^2 there is only one steady state flow rate satisfying Equation (V-2). This flow rate corresponds to a value of $X_{out} < 0$ (subcooled) and is stable. (That is, a momentary decrease in flow rate at constant q" causes a decrease in ΔP which causes flow to return to its original value.)

2) At heat fluxes of 3×10^4 and 4×10^4 BTU/hr ft^2 there are three steady state flow rates satisfying Equation (V-2). These three flow rates correspond to values of X_{out} between zero and 1.0. However, only the flow rates corresponding to the lowest and highest X_{out} are stable. (At a flow rate of 5.4×10^{-3} lb_m/sec a momentary decrease in flow rate at constant q" causes an increase in ΔP which causes flow to decrease further until the lowest of the three stable flow rates is reached.*)

3) At heat fluxes of 5×10^4 BTU/hr ft^2 and above, there are still three steady state flow rates satisfying Equation (V-2). However, only two of these three flow rates correspond to values of X_{out} between 0 and 1.0. The third corresponds to $X_{out} > 1.0$ (superheated). Again, the intermediate flow rate (and X_{out}) is unstable.

2. Subcooled Boiling (Runs #1 and #2)

a. Summary of Principal Results

Steam bubbles due to subcooled boiling were first observed at a heat/flux of about 1×10^4 BTU/hr ft^2. Above 1×10^4 BTU/hr ft^2, the heat transfer mechanism at the top of the heated section appeared to oscillate between a condition approximating single phase convection and subcooled boiling. The onset of bulk boiling occurred at a heat flux of about 3×10^4 BTU/hr ft^2. Data and observations for this range of test conditions were presented in Sections IV.A.1 and IV.A.2.

*See Reference (5) for a good discussion of flow-pressure drop instabilities of the type indicated for this solution of Equation V-2.

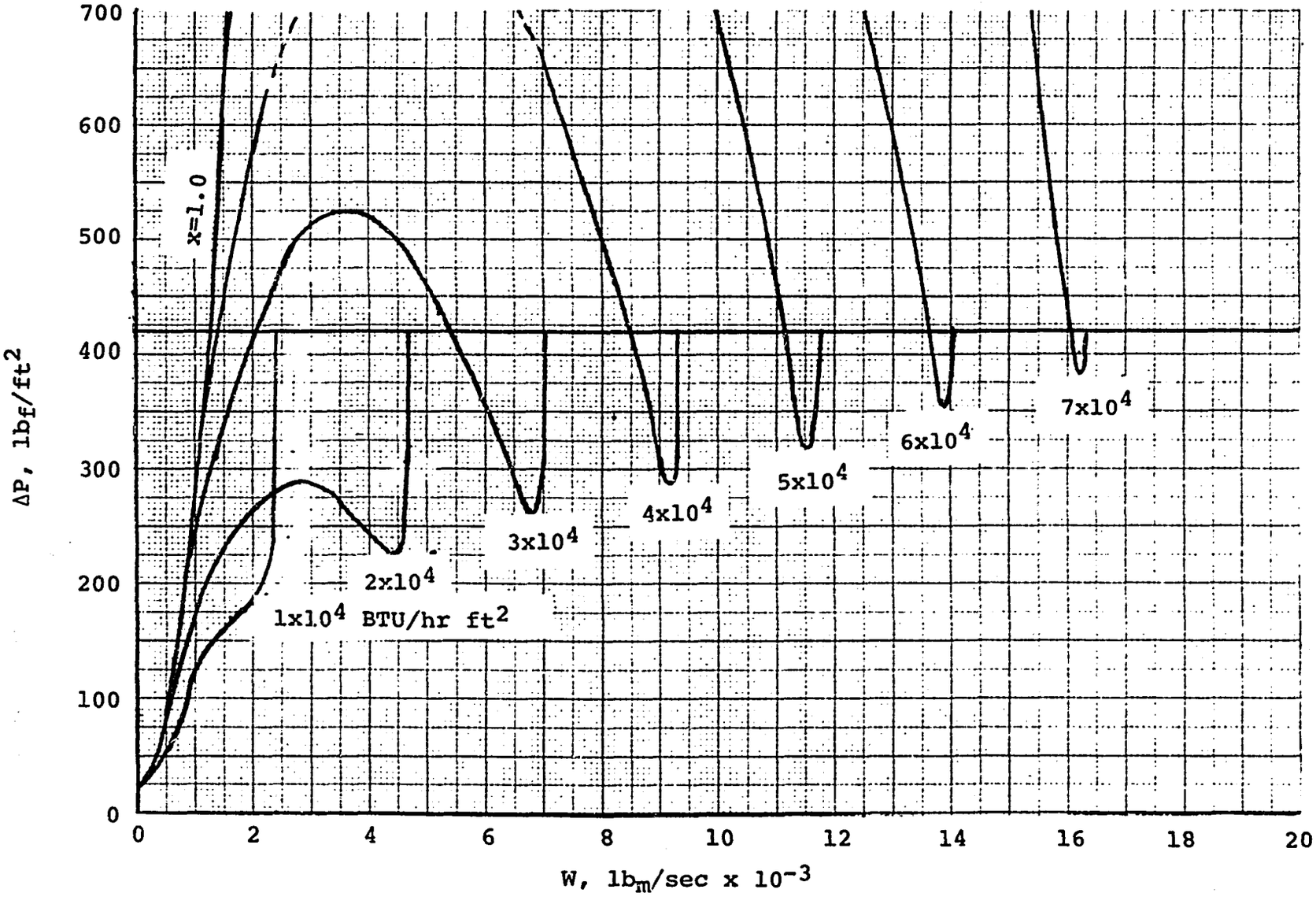

Figure V-2

Flow-Pressure Drop Characteristics of Test Loop with Heat Flux as a Parameter

The principal results are summarized below:

1) Small bubbles were continuously observed at the top sight flow indicator. However, these bubbles were probably largely due to noncondensable gases initially trapped in the test loop or dissolved in the water; since, as will be discussed later in this subsection, the tube wall temperature at the top of the heated section was only periodically high enough for subcooled boiling to occur. Periodically, the flow would appear to slow down momentarily followed by the appearance of much larger bubbles over the next several seconds. These larger bubbles were probably due to the onset of subcooled boiling. The time period between the appearance of the larger bubbles decreased as the heat flux was increased above 1×10^4 BTU/hr ft^2.

2) The test section pressures were steady except for high frequency oscillations that were observed for several seconds at regular intervals (see Figures IV-1A, IV-2A, and IV-2D). At a heat flux of 1.04×10^4 BTU/hr ft^2 the time period between occurrence of these oscillations was about 45 sec. and they lasted about 7.5 sec. At a heat flux of 1.75×10^4 BTU/hr ft^2 the time period between their occurrence was about 15 sec. and they lasted about 5 sec.

3) The tube wall temperatures within the heated section oscillated continuously as shown in Figures IV-1B and IV-2B. At a heat flux of 1.04×10^4 BTU/hr ft^2, the period of oscillation was about 45 seconds; at 1.75×10^4 BTU/hr ft^2, the period was between 10 and 15 seconds. Thus the period of the temperature oscillations at each heat flux was about the same as the time period between occurrence of the high frequency pressure oscillations.

4) When essentially the same test condition at 1.75×10^4 BTU/hr ft^2 was investigated on two different days, it was observed that periodic high frequency pressure oscillations and the corresponding temperature oscillations were not observed on the second day until the loop had been operating for about 20 minutes. Apparently a flow disturbance or some other initiating mechanism is required to start the cycle of periodic subcooled boiling; and, on the second day it took longer for this to occur.

5) At both 1.04×10^4 BTU/hr ft^2 and 1.75×10^4 BTU/hr ft^2, the average tube wall temperature increased with distance from the inlet to the heated section (see Tables IV-1 and IV-2). At 1.04×10^4 BTU/hr ft^2 the temperature at Locations T_1 and T_3 (near the top of the heated section) was 208° $\pm$ approximately 10°F. At 1.75×10^4 BTU/hr ft^2, the temperature at the same locations was 217°F $\pm$ approximately 6°F.

b. Analysis of Temperature Data

The variations of average tube wall temperature and fluid temperature with distance along the heated section for 1.04×10^4

BTU/hr ft^2 are shown graphically in Figure V-3. The same variations for 1.75×10^4 BTU/hr ft^2 are shown in Figure V-4. For each of the tube wall temperatures plotted on these figures, the maximum and minimum temperatures resulting from the temperature oscillations are also indicated.

In Figures IV-3 and V-4 a straight line is drawn between the inlet and outlet fluid temperatures. For a steady flow, uniform heat flux condition the fluid temperature variation would be linear. However, under oscillatory flow conditions such as observed in these tests where vapor generated within the heated section is periodically observed to force its way upstream, this may not be true. In the case of the tests described in this report, this is almost certainly the case for heat fluxes above 3×10^4 BTU/hr ft^2 since steam bubbles were periodically observed at the inlet sight flow indicator. However, for the subcooled boiling test conditions at heat fluxes of 1.04×10^4 BTU/hr ft^2 and 1.75×10^4 BTU/hr ft^2, the amount of vapor periodically generated and forced upstream was much smaller and probably had minimal effect on the fluid temperature variation along the tube. Thus the straight line variation shown is probably a good approximation for these conditions.

The fact that the average temperature at the upper end of the heated section was only 208°F for a heat flux of 1.04×10^4 BTU/hr ft^2 raises the question as to whether subcooled boiling really occurred at this heat flux. But, in considering this question, it should be noted that the temperature was about periodically 10°F higher than this. Thus the wall superheat was periodically as much as 6°F.

The amount of wall superheat required to initiate subcooled boiling can be predicted using a correlation such as the one developed by Rohsenow and Bergles (6). This correlation is based on experiments

Figure V-3

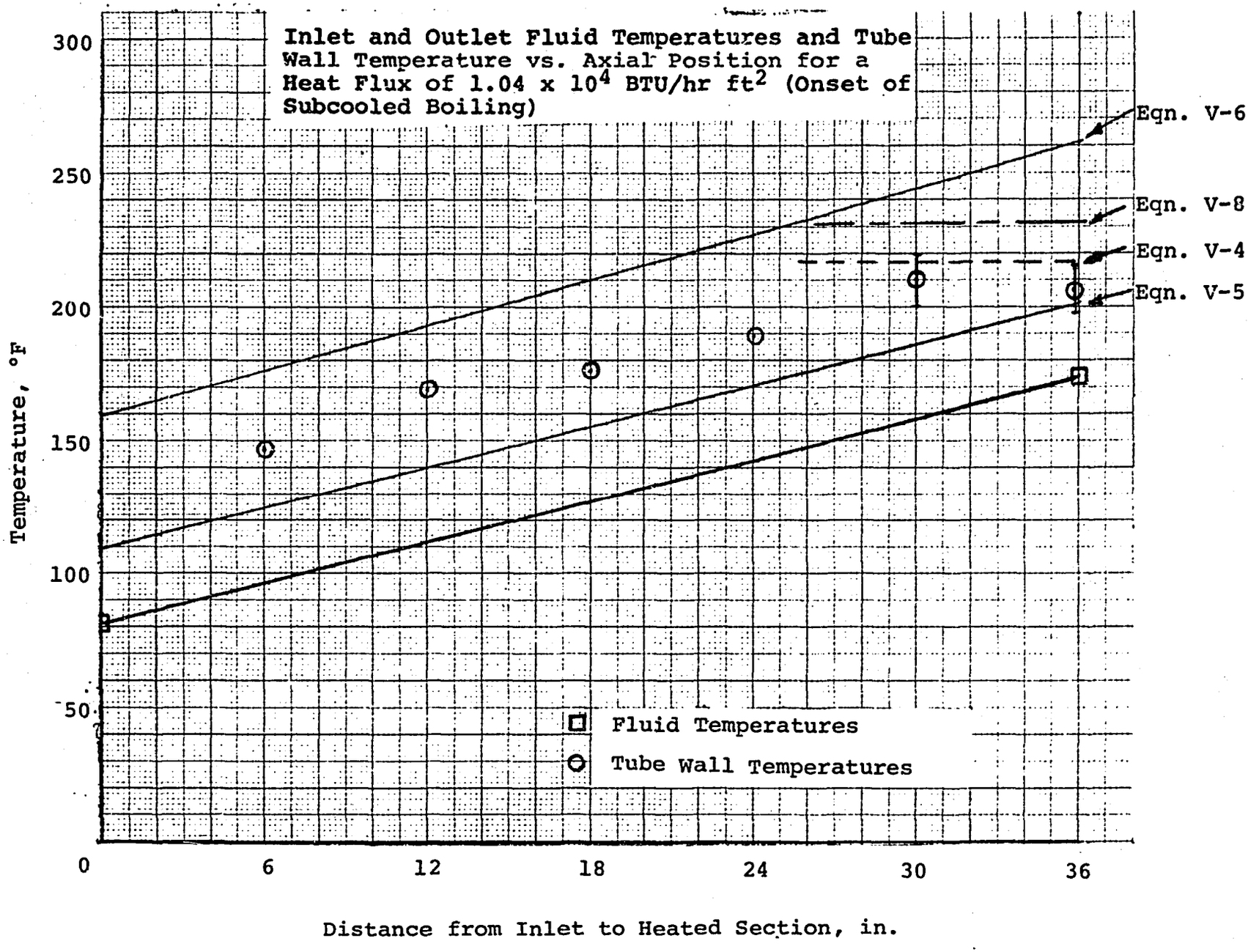
Inlet and Outlet Fluid Temperatures and Tube Wall Temperature vs. Axial Position for a Heat Flux of 1.04 x 10^4 BTU/hr ft^2 (Onset of Subcooled Boiling)
Eqn. V-6
Eqn. V-8
Eqn. V-4
Eqn. V-5
Fluid Temperatures
Tube Wall Temperatures
Temperature, °F
300
250
200
150
100
50
0
6
12
18
24
30
36
Distance from Inlet to Heated Section, in.

Figure V-4

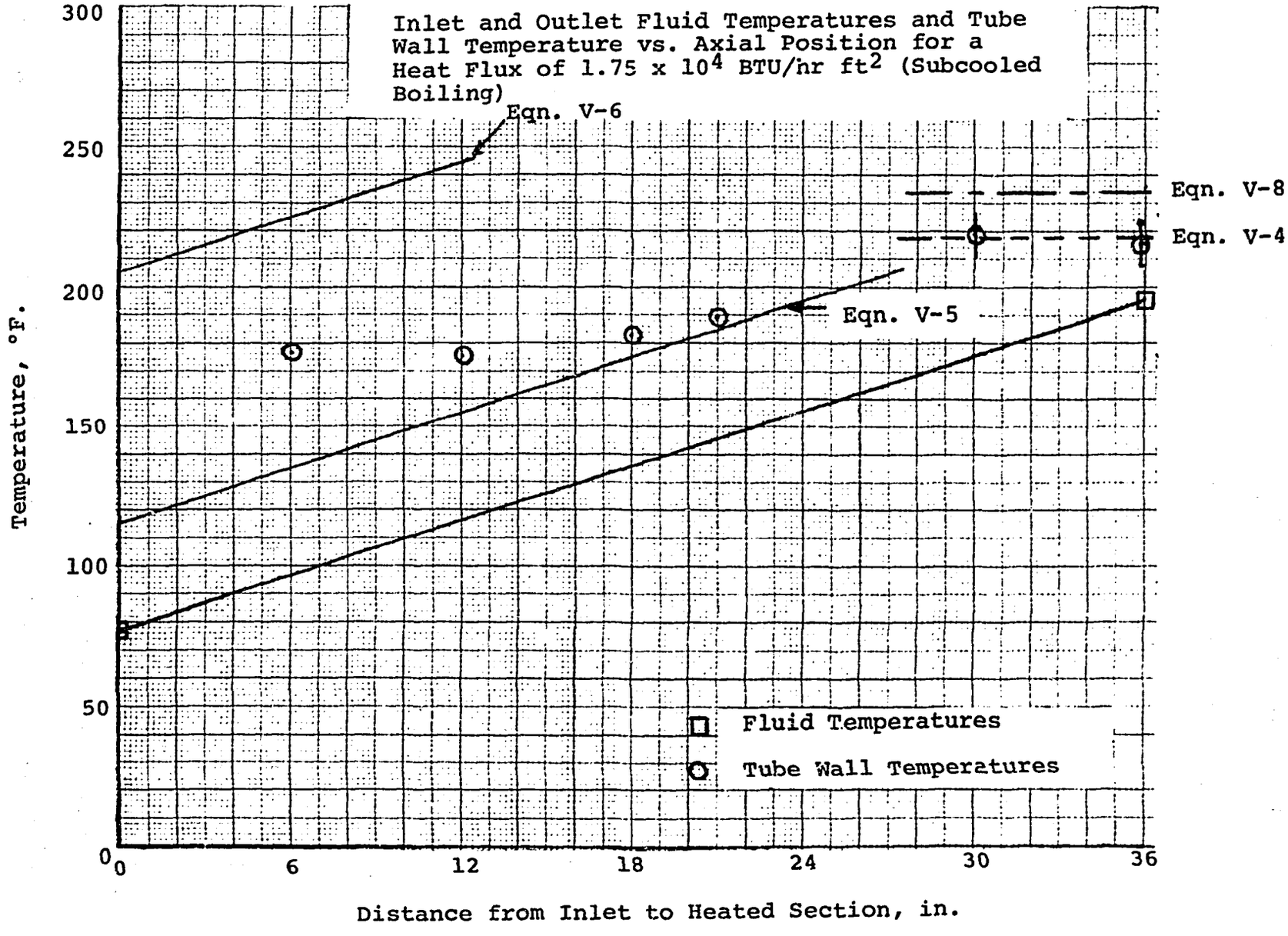
Inlet and Outlet Fluid Temperatures and Tube Wall Temperature vs. Axial Position for a Heat Flux of 1.75 x 10^4 BTU/hr ft^2 (Subcooled Boiling)
Eqn. V-6
Eqn. V-8
Eqn. V-4
Eqn. V-5
Fluid Temperatures
Tube Wall Temperatures
Temperature, °F.
300
250
200
150
100
50
0
0
6
12
18
24
30
36
Distance from Inlet to Heated Section, in.

set up to determine the onset of nucleate boiling for water over the pressure range 15-2000 psia. The correlation is given by the following equation:

$$q''_{ONB} = 15.6\ P^{1.156}(\Delta T_{sat})_{ONB}^{(2.30/P^{0.0234})} \qquad (V\text{-}4)$$

where

q''_{ONB} = the heat flux in BTU/hr ft^2 required for ONB (onset of nucleate boiling) at $(\Delta T_{sat})_{ONB}$

$(\Delta T_{sat})_{ONB}$ = the wall superheat in °F required for the onset of nucleate boiling at q''_{ONB}

P = pressure in psia

For a heat flux of 1.04 x 10^4 BTU/hr ft^2 and a pressure of 14.7 psia this equation gives:

$$(\Delta T_{sat})_{ONB} = 4.8°F$$

Thus the maximum temperature reached during the observed temperature oscillations was sufficient to initiate subcooled boiling. The value of T_{wall} corresponding to a ΔT_{sat} of 4.8°F is shown by a horizontal dotted line on Figure V-3.

For a heat flux of 1.75 x 10^4 BTU/hr ft^2, Equation (V-4) gives:

$$(\Delta T_{sat})_{ONB} = 6.1°F$$

The corresponding value of T_{wall} is shown by a horizontal dotted line in Figure V-4. As for the lower heat flux the tube wall temperatures near the top of the heated length were periodically high enough to initiate subcooled boiling. In this case, however, it appears that these temperatures were high enough for a greater portion of each cycle of oscillation.

Also shown on Figures V-3 and V-4 are two lines parallel to the assumed linearly varying fluid temperature. The line nearest to the

fluid temperature gives the wall temperature variation predicted, assuming a constant heat transfer coefficient along the heated length obtained using the Dittus Boelter correlation (7) and the mass flow rate obtained from an energy balance. This Dittus Boelter correlation applies to turbulent flow and is given by the following equation:

$$\frac{\bar{h}D}{k_f} = 0.023\ Re_f^{0.8} Pr_f^{0.4} \qquad \text{(V-5)}$$

where

$$Re_f = \frac{4W}{\pi D \mu_f}$$

$$Pr_f = \frac{\mu_f C_f}{k_f}$$

The line farthest above the fluid temperature gives the wall temperature variation predicted assuming a constant heat transfer coefficient along the heated length obtained using the following expression:

$$\frac{\bar{h}D}{k_f} = 4.36 \qquad \text{(V-6)}$$

which applies to laminar flow through a vertical uniformly heated tube (7).

Figure V-3 shows that, for a heat flux of 1.04×10^4 BTU/hr ft^2, the above correlations give tube wall temperatures that bracket the measured temperatures, indicating that at this heat flux the flow may be close to the laminar-turbulent transition. The average flow calculated from an energy balance on the heated section is 3.7×10^{-3} lb_m/sec (Table IV-1), which gives a Reynolds number, Re_f, of 1950. The range of Reynolds numbers corresponding to the laminar-turbulent transition is 2000-4000. Thus, the flow may have been laminar at least part of the time.

Figure V-4 shows for a heat flux of 1.75×10^4 BTU/hr ft^2, that the measured tube wall temperatures fall closer to the Dittus Boelter

equation, indicating that at this heat flux the flow was probably turbulent. For this test condition the average flow calculated from an energy balance on the heated section was 4.7×10^{-3} lb_m/sec which gives a Reynolds number of 2490. Thus the flow probably was turbulent most of the time for this test condition.

c. Analysis of Flow and Pressure Information

The average flow rates determined from an energy balance for both 1.04×10^4 BTU/hr ft^2 and 1.75×10^4 BTU/hr ft^2 were higher than predicted from the analysis in Section V.A.1. This can be seen from Figure V-5. This figure is a graph of the steady state solutions of Equation V-2 as determined in Figures V-1 and V-2. The stable and unstable solutions are shown in Figure V-5 as a function of heat flux and quality.

At 1.04×10^4 BTU/hr ft^2 the predicted flow from Figure V-5 is 2.4×10^{-3} lb_m/sec, compared to the 3.7×10^{-3} lb_m/sec obtained from an energy balance. However, the analysis in Section V.A.1 (which was used to obtain Figures V-3 and V-4 and therefore Figure V-5 and the predicted flow of 2.4×10^{-3} lb/sec) did not account for the effect of the periodic occurrence of subcooled boiling. When subcooled boiling occurs, the average flow would be expected to increase due to the increased density difference between the down-commer and the test section. As a first approximation, one could take the average flow during subcooled boiling to be approximately the same as the flow rate predicted for the onset of bulk boiling. Figure V-2 shows that this flow rate is approximately 7.2×10^{-3} lb_m/sec. Thus, if it is assumed that part of the time during each cycle of temperature oscillation is spent in subcooled boiling (with flow at about 7.2×10^{-3} lb/sec) and part of the time is spent in single phase convection (with

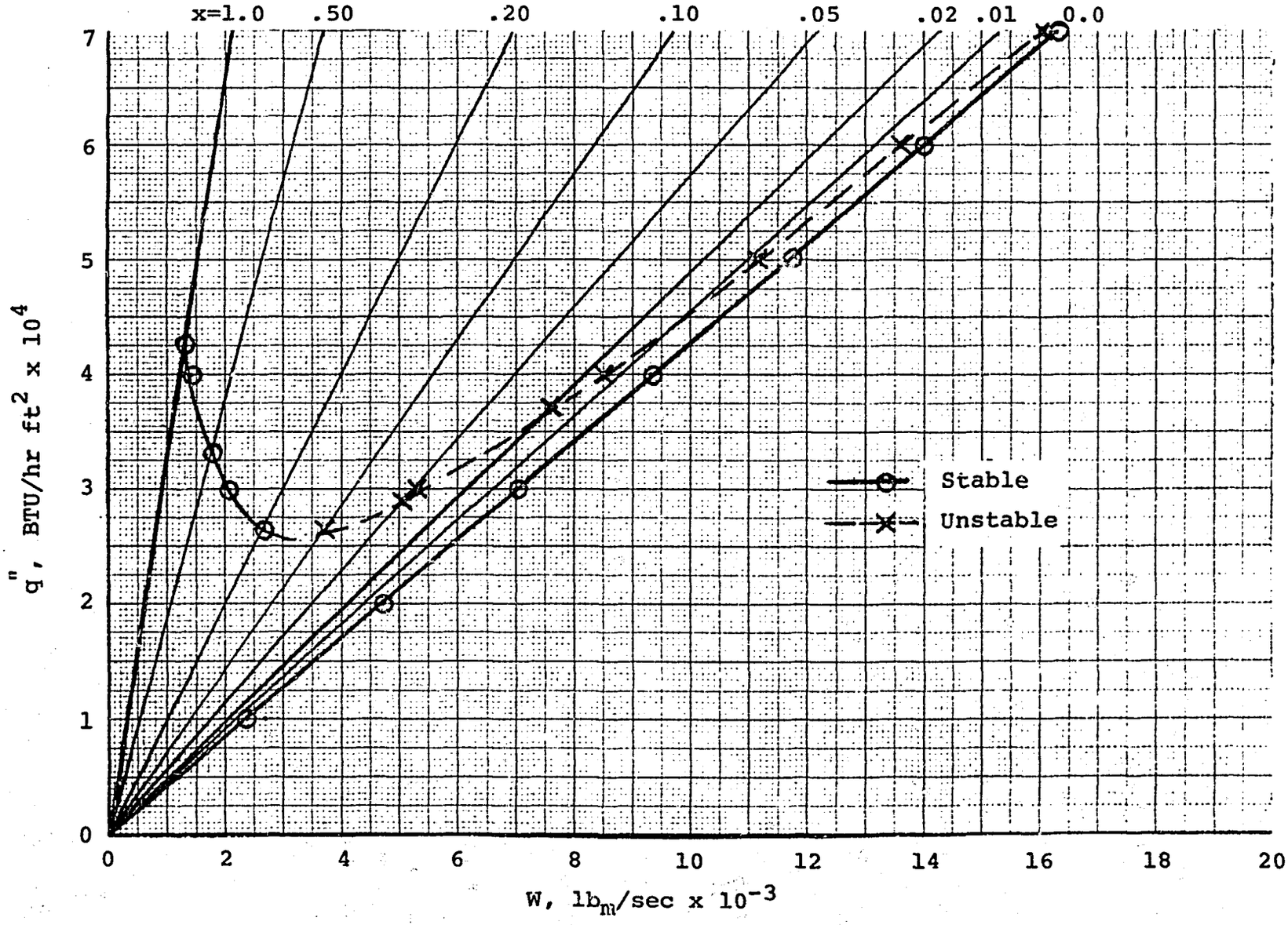

Figure V-5

Steady State Flow Conditions for Test Loop
Determined from Figures V-1 and V-2

flow at about 2.4×10^{-3} lb/sec), the expected average flow would be given by the following equation:

$$\bar{W} = F_1 W_1 + F_2 W_2 \qquad \text{(V-7)}$$

where

$\bar{W}$ = the expected average flow

F_1 = fraction of one cycle of temperature oscillation for which flow is single phase

W_1 = the predicted flow rate under single phase conditions (2.4×10^{-3} lb_m/sec for a heat flux of 1.04×10^4 BTU hr ft^2)

F_2 = fraction of one cycle of temperature oscillation for which subcooled boiling occurs

W_2 = predicted average rate for subcooled boiling (assume to be the same as for onset of bulk boiling or 7.2×10^{-3} lb_m/sec)

Then, if it is further assumed that the high frequency pressure oscillations shown in Figure IV-1A are associated with subcooled boiling and this information is used to obtain F_1 and F_2, this equation gives:

$$\bar{W} = \frac{7.5}{45} \times (7.2 \times 10^{-3}) + \frac{37.5}{45} (2.4 \times 10^{-3}) = 3.2 \times 10^{-3} \text{ lb}_m/\text{sec}$$

compared to the 3.7×10^{-3} lb_m/sec obtained from the energy balance.

For a heat flux of 1.75×10^{-3} BTU/hr ft^2 the expected average flow calculated in the same manner as above is:

$$\bar{W} = \frac{5}{15} (7.2 \times 10^{-3}) + \frac{10}{15} (4.1 \times 10^{-3}) = 5.1 \times 10^{-3} \text{ lb}_m/\text{sec}$$

compared to the 4.7×10^{-3} lb_m/sec calculated from an energy balance.

For a heat flux of 3.07×10^4 BTU/hr ft^2 (Run #4 - to be discussed in Section V.A.3), which corresponds approximately to the onset of bulk boiling, the expected average flow calculated from Equation (V-7) is:

$$\bar{W} = 7.2 \times 10^{-3} \text{ lb}_m/\text{sec}$$

compared to 7.3×10^{-3} lb_m/sec obtained from an energy balance.

The above results are shown in Figure V-6 as a graph of predicted average flow rate (from Equation [V-7] and data from pressure and temperature traces) and average flow rate obtained from an energy balance, both as a function of heat flux. Also shown on this figure is the flow rate obtained from an energy balance for a heat flux of 1.29×10^4 BTU/hr ft^2 (Run #4 to be discussed in Section V.A.4).

3. Bulk Boiling (Run #3)

a. Summary of Principal Results

At a heat flux of slightly above 3×10^4, the fluid temperature leaving the test section became equal to the saturation temperature. Thus this heat flux corresponded approximately to the onset of bulk boiling, in agreement with Figure V-2 and the analysis in Section V.A.1. Data and observations for heat fluxes above 3×10^4 BTU/hr ft^2 were presented in Section IV.A.3. The principal results are summarized below:

1) Above 3×10^4 BTU/hr ft^2, large bubbles were seen continuously at the top sight flow indicator. Above 4×10^4 BTU/hr ft^2, these bubbles appeared to have agglomerated and the flow configuration appeared more annular or semi-annular than bubbly.

2) At 3×10^4 BTU/hr ft^2, spurts of small bubbles were first seen at the lower sight flow indicator. As the heat flux was increased, these bubbles became larger and more frequent. Above 5×10^4 BTU/hr ft^2, only one large bubble was observed periodically pushing its way toward the lower plenum.

3) Above 3×10^4 BTU/hr ft^2, high frequency pressure oscillations were observed continuously. At 3.83×10^4 BTU/hr ft^2, XY recorder traces indicated that the period of these oscillations was 1 to 2 seconds. (See Figures IV-3A, IV-3B, IV-3C, and IV-3D.) Also these traces show the shape of the variation of pressure with time from cycle to cycle is quite similar.

4) At 3.83×10^4 BTU/hr ft^2, the tube wall temperatures were between 230°F and 240°F at all thermocouple locations along the heated length (Table IV-3). In addition, because vapor generated within the heated section was periodically forcing its way upstream and condensing, the average fluid temperature entering the heated section was 188°F (even though the inlet plenum temperature was 72°F.

Figure V-6

Comparison of Mass Flow Rates Predicted by Equation (V-7) with Mass Flow Rate Determined from Energy Balance (Subcooled Boiling)

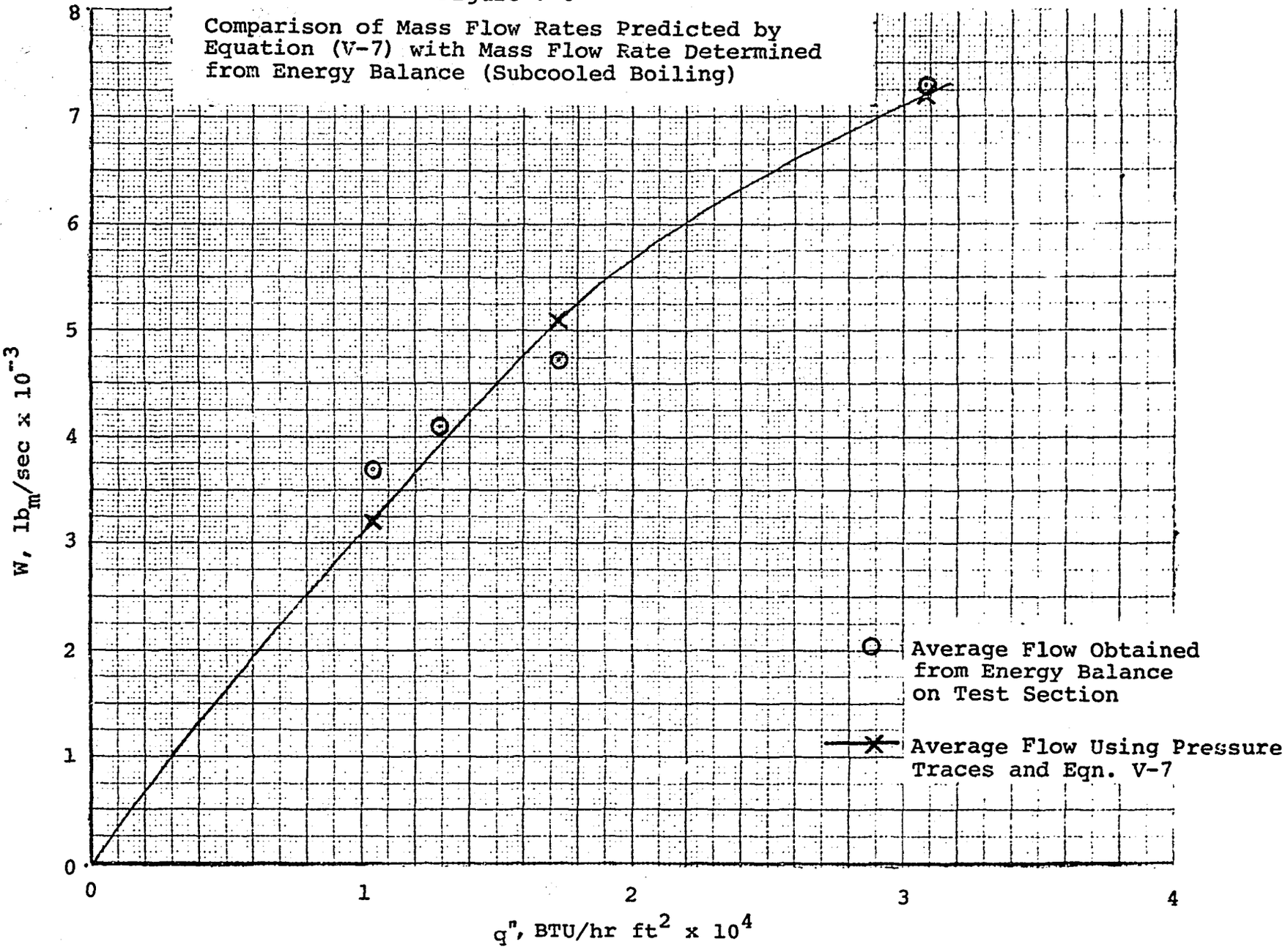

b. Analysis of Temperature Data

The average tube wall temperature measured at the various thermocouple locations along the heated section for a heat flux of 3.83×10^4 BTU/hr ft^2 are shown graphically in Figure V-7. Also shown are the inlet and exit fluid temperatures. The average tube wall temperatures range from 227 to 237°F corresponding to wall superheats of from 15 to 25°F. This compares with a $(\Delta T_{sat})_{ONB}$ of 8.8°F given by Equation (V-4). The tube wall temperature corresponding to this amount of wall superheat is about 221°F as indicated by the lower of the two dotted lines in Figure V-7. The upper dotted line shows the tube wall temperature predicted for fully developed nucleate boiling according to the Jens Lottes correlation (7):

$$\Delta T_{sat} = 1.9(q")^{1/4}\ e^{-P/900} \qquad \text{(V-8)}$$

where

$q"$ = heat flux in BTU/hr ft^2

P = pressure in psia

The tube wall temperature predicted from the Jens Lottes correlation is 238°F, in good agreement with the measured temperatures. Thus, fully developed bulk boiling appeared to exist at all thermocouple locations along the heated length except near the inlet.

The fact that, as the heat flux was increased above 3×10^4 BTU/hr ft^2, an increased amount of vapor was observed periodically forcing its way toward the lower plenum and condensing indicates that a substantial amount of the energy transferred to the fluid within the test section is periodically transported upstream and transferred in turn to the colder water upstream of the heated section. This is verified at a heat flux of 3.83×10^4 BTU/hr ft^2 by the fact that the water temperature leaving the unheated inlet section was 188°F compared to 72°F at its entrance.

Figure V-7

Tube Wall Temperatures vs. Axial Position for a Heat Flux of 3.83×10^4 BTU/hr ft^2 (Bulk Boiling)

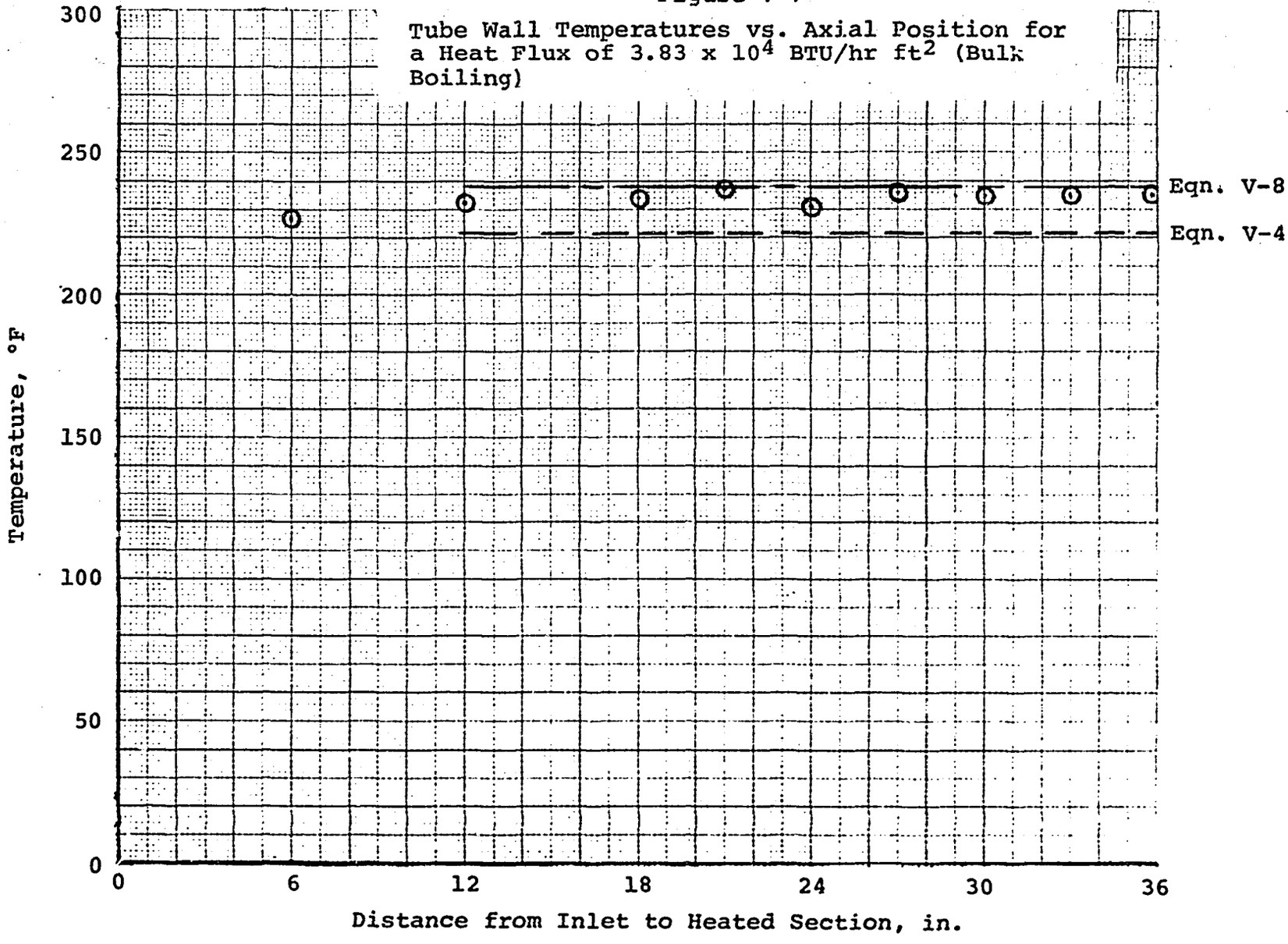

c. Discussion of Pressure Oscillation Data and Observations

The pressure oscillations shown in Figures IV-3A, IV-3B, IV-3C, and IV-3D were observed to occur at about the same frequency as the appearance of steam bubbles at the lower sight flow indicator (every few seconds). Thus, the two were probably related. In addition, these occurrences were probably accompanied by oscillations in flow through the test section. A possible explanation of these oscillations, based on consideration of Figures V-5 and V-2, is given in the following paragraphs.

At each heat flux above 3×10^4 BTU/hr ft^2, Figure V-5 indicates that there are two stable flow rates corresponding to each heat flux. The highest of these flow rates corresponds to a low quality exit condition and the lowest flow rate corresponds to a high quality exit condition. Figure V-2 shows further that the range of stability near to the highest of these two flow rates is very narrow. For example, at 4×10^4 BTU/hr ft^2, a momentary decrease in flow from the higher stable flow rate of 9.4×10^{-3} lb_m/sec to below 8.5×10^{-3} lb_m/sec would result in an unstable flow condition and a further decrease in flow toward the lower of the two stable flow rates or 1.4×10^{-3} lb/sec. Figure V-5 indicates that the corresponding change in exit quality would be from less than .01 to between 0.8 and 0.9.

However, the periodic appearance of vapor upstream of the heated section and the continuous oscillations in pressure suggests a somewhat different and more complex sequence than this. Specifically, the appearance of vapor upstream of the test section inlet indicates that an increased average void fraction corresponding to the low flow, high exit quality condition is achieved by steam pushing its way upstream in counterflow, rather than by an increase in exit quality while maintaining cocurrent upflow. Also, the continuous pressure

oscillations indicate that, whatever the sequence resulting in a decreased flow and increased void fraction, the situation is quickly reversed, resulting in a return toward the original high flow, lower void fraction condition.

Therefore, it is clear that a strict quantitative interpretation of Figures V-5 and V-2 such as done above for the case of 4×10^4 BTU/hr ft^2 is not correct. Nevertheless the following qualitative facts derived from these figures still appear valid:

1) For a given heat flux in the bulk boiling range, there are two stable flow conditions. One of these conditions is a high flow, low quality condition and the other is a low flow, high quality condition.

2) The high flow, low quality condition tends to be unstable since only a relatively small, momentary decrease in flow creates an unstable situation resulting in a further decrease in flow.

Starting with these facts and considering again the example of 4×10^4 BTU/hr ft^2, one can then return to the part of the previous discussion where the flow is assumed to decrease momentarily below 8.5×10^{-3} lb_m/sec. When this condition is reached and the flow begins to decrease further, the amount of vapor generated within the test section increases. Apparently, however, a condition quickly develops where the rate of vapor generation is greater than the rate at which it can flow out the top of the heated section. Thus the local pressure builds up and the excess vapor pushes downward through the heated section. At the same time, the liquid flow into the test section decreases and the void fraction within the test section increases. Eventually, enough of the test section is voided so that the steam being generated can flow out the top of the heated section as fast as it is being generated. However, this flow condition is not in thermal equilibrium in the upstream half of the test section due to the presence of a substantial amount of subcooled water. As a result the steam

in this part of the test section begins to condense and the water flow into the test section increases, causing still further condensation and a return toward the original high flow, lower void fraction condition from which the transient initially started. Then, since this flow condition tends to be unstable the sequence begins again.

Assuming that the two flow conditions between which the system oscillated at a given heat flux are approximated by the two stable flow conditions indicated in Figure V-5, the average flow was probably somewhere between the flow corresponding to these two conditions. However, because of the way in which the low flow, higher void fraction condition is achieved, the exit quality corresponding to this condition is probably significantly lower than predicted from Figure V-5. Thus, for a given heat flux there is probably more water present at the top of the heated length than predicted from the homogeneous model.

4. Onset of CHF (Run #4)

a. Summary of Principal Results

The onset of CHF occurred at a heat flux of 6.4×10^4 BTU/hr. This corresponded to a test section power of about 2.25 kw. Data and observations for this test condition are presented in Section IV.A.4. The principal results are summarized below:

1) Flow conditions at the sight flow indicators were substantially the same for all heat fluxes above 4×10^4 BTU/hr ft^2. As CHF was approached, the large steam bubble observed at the lower sight flow indicator appeared to be periodically pushing its way into the lower plenum.

2) The temperature at location T_1 at the top of the heated section was first observed to oscillate at a heat flux of 6.4×10^4 BTU/hr ft^2. Above this heat flux, T_1 oscillated over a temperature range that became increasingly greater; until, at a heat flux of about 7.15×10^4 BTU/hr ft^2, the upper end of the range of oscillation exceeded 900°F. For higher heat fluxes T_1 no longer oscillated. At 7.3×10^4 BTU/hr ft^2, T_1 was fairly steady at 1180°F (see Table IV-4).

3) As the CHF condition was approached and exceeded, the fluid temperature leaving the top of the heated section remained at the saturation temperature (see Table IV-4). Also, water was observed to be present at the top sight flow indicator.

b. Analysis and Discussion of Temperature Data

Temperature data from Table IV-4 is shown graphically in Figure V-8 as a function of heat flux. The temperatures shown include the tube wall temperatures at locations T_1, T_2, and T_3 (near the top of the heated section) and the fluid temperatures at T_{11} and T_{13} (inlet and exit of the test section). For the temperatures that were observed to oscillate (Location T_1 at heat fluxes above 6.4×10^4 BTU/hr ft^2) the range of these oscillations is also shown.

Figure V-8 indicates that, just beyond the CHF (defined as the heat flux at which large temperature oscillations were first observed) of 6.4×10^4 BTU/hr ft^2, dryout of the tube wall occurs. However, rewetting occurs periodically; and, at 6.5×10^4 BTU/hr ft^2, the maximum tube wall temperature is only about 60°F above its pre-CHF temperature of 280°F. Apparently this is due to the water periodically entering the test section as a result of the pressure and flow oscillations discussed in Section V.A.3. As the heat flux is increased further, the maximum tube wall temperature reached during each temperature excursion becomes greater; until, at a heat flux of 7.15×10^4 BTU/hr ft^2, this temperature is about 900°F. Above this heat flux, rewetting was no longer observed; and, at 7.3×10^4 BTU/hr ft^2, the tube wall temperature was relatively stable at 1180°F. This result indicates that the maximum tube wall temperature at which rewetting can occur (Liedenfrost temperature) is 900°F. Independent verification of this is discussed in Section V.A.5.

Figure V-8 also shows that, above a heat flux of about 3×10^4 BTU/hr ft^2, the fluid temperature at the inlet to the heated section

Figure V-8

Inlet and Outlet Fluid Temperatures and Tube Wall Temperatures at T_1, T_2 and T_3 as a Function of Heat Flux for Run #4 (Onset of CHF)

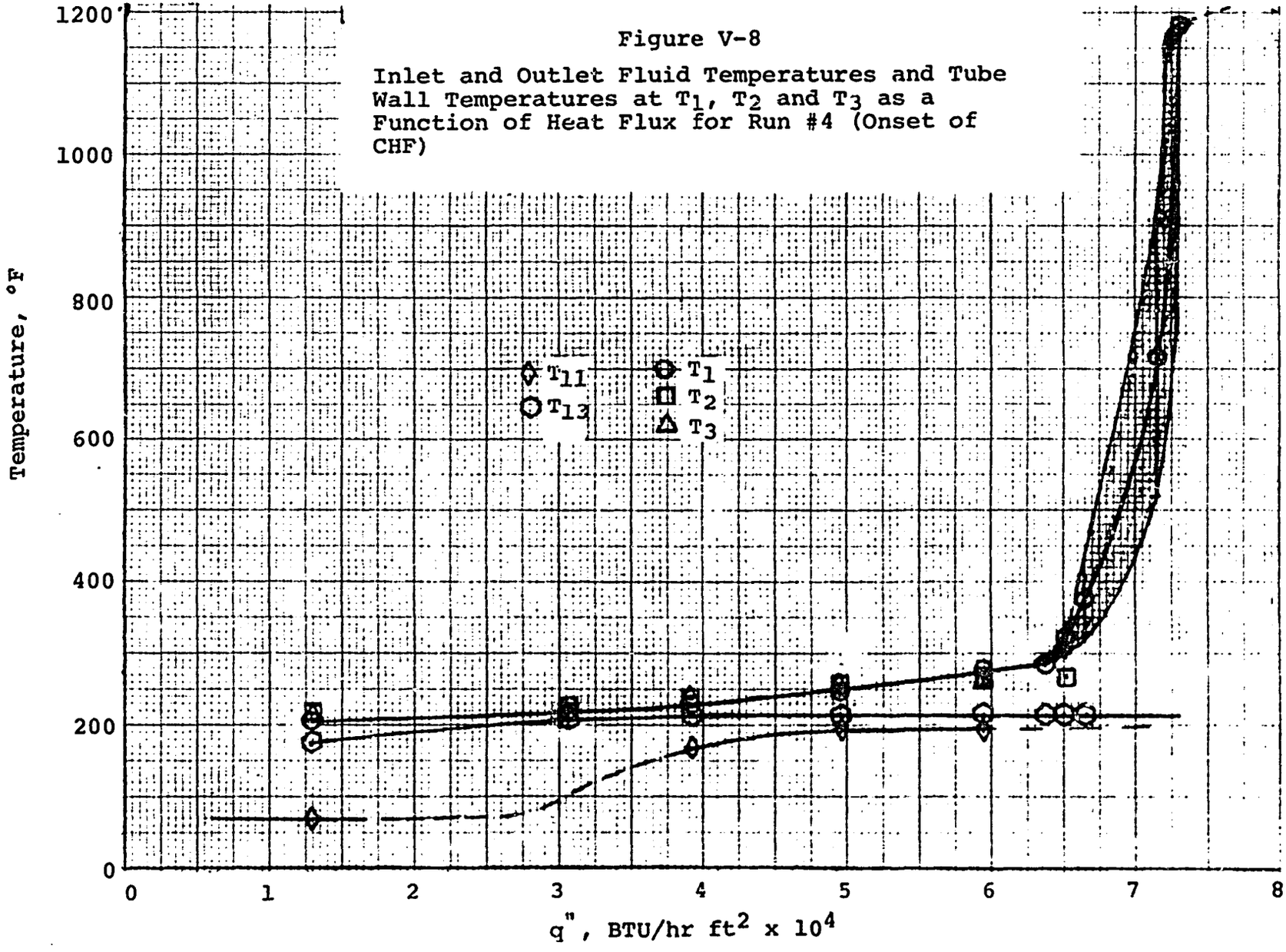

is substantially greater than the lower plenum temperature. This is due to the periodic expansion of steam from the heated section into the inlet section and the resulting condensation and mixing. At heat fluxes above 5×10^4 BTU/hr ft^2, the inlet temperature appears to be relatively constant at 190-195°F. However, this is based on only two data points, the last being at a heat flux of 5.93×10^4 BTU/hr ft^2.

The fact that the exit fluid temperature remained at the saturation temperature for heat fluxes beyond the CHF, added to the observation that water was present at the upper sight flow indicator, shows that there is entrained liquid present at the top of the test section even beyond CHF. Thus CHF occurs at an average exit quality of less than 1.0; and, if rewetting were possible above 7.3×10^4 BTU/hr ft^2, the water would be present to do it.

The heat transfer coefficient calculated from the temperature data at the top of the heated section (see Table IV-4) is plotted as a function of heat flux in Figure V-9. (Also shown on this graph are the heat transfer coefficients calculated from data obtained in Runs 1, 2, and 3 discussed in Sections V.A.1 and V.A.2.) For comparison, the heat transfer coefficient calculated at various heat fluxes using the Jens-Lottes correlation (Equation V-8) is also shown.

Figure V-9 shows that at low heat fluxes near 1×10^4 BTU/hr ft^2, corresponding to the onset of subcooled boiling, the measured heat transfer coefficient is less than predicted by the Jens-Lottes correlation. However, for this heat flux condition, nucleate boiling has probably not yet become fully developed. At a heat flux of 1.75×10^4 BTU/hr ft^2 the measured heat transfer coefficient is in very good agreement with the Jens Lottes correlation, indicating that, for this condition, nucleate boiling is fully developed.

Figure V-9

Heat Transfer Coefficient at Location T_1 as a Function of Heat Flux for Run #4 (Onset of CHF)

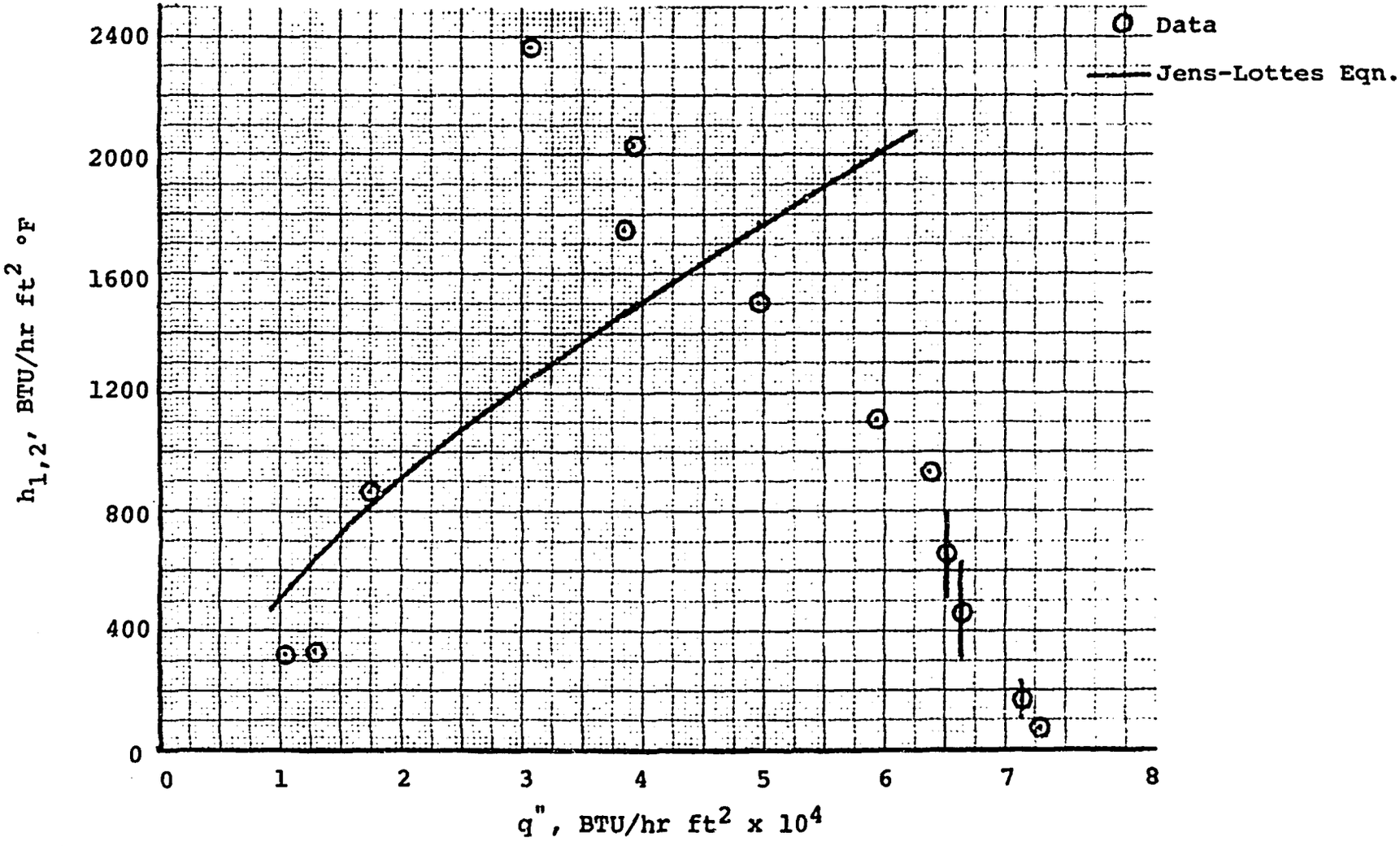

At heat fluxes between 3×10^4 BTU/hr ft^2 and 4 to 4.5×10^4 BTU/hr ft^2, the measured heat transfer coefficient is greater than predicted from the Jens-Lottes correlation. But, for this range of conditions, the heat transfer coefficient is decreasing; and, above 4.5×10^4 BTU/hr ft^2, the measured heat transfer coefficient becomes less than predicted by the Jens Lottes correlation. This comparison indicates that a nucleate boiling heat transfer correlation such as Jens-Lottes doesn't apply for flow conditions at heat fluxes above 3×10^4 BTU/hr ft^2. The proper correlation for this range of conditions would probably be a two-phase convection heat transfer correlation such as Schrock-Grossman (9). However, for these correlations, the heat transfer coefficient depends on flow rate and quality; and no information regarding flow and quality was obtained for heat fluxes above 3×10^4 BTU/hr ft^2. Therefore, no comparison can be made. Nevertheless, it is probable (on the basis of the discussion of pressure oscillation data and observations in Section V.A.3, part C) that, as the heat flux increases above 3×10^4 BTU/hr ft^2, the average flow into the test section decreases and the average exit quality increases. These effects would result in a decreasing two phase convection heat transfer coefficient for this range of test conditions, as was observed.

At a heat flux of 7.3×10^4 BTU/hr ft^2 (for which the tube wall temperature remains above the Liedenfrost temperature) the heat transfer coefficient at the top of the heated section is still 75 BTU/hr ft^2°F. Assuming a mass flow rate of 2.25×10^{-3} lb_m/sec (from Figure V-5 for a heat flux of 7.3×10^4 BTU/hr ft^2) and an exit quality of 1.0 (neglecting the effect of any liquid present) and using the Dittus Boelter correlation gives 88 BTU/hr ft^2°F. Thus the magnitude of the heat transfer coefficient beyond dryout is approximately what would be expected as a result of convection to steam with a

quality of 1.0 and a flow rate predicted from the analysis presented in Section V.A.1.

c. Discussion of CHF Mechanism

The preceding results indicate that CHF was due to dryout. However, the CHF of 6.4×10^4 BTU/hr ft^2 was significantly higher than would be predicted from a simple homogeneous flow model. This can be seen from Figure V-5 which shows that a stable flow condition corresponding to an exit quality of 1.0 is predicted at a heat flux 4.25×10^4 BTU/hr ft^2. However, this prediction assumes dryout does not occur as long as any water is present; since, if it were assumed that some of the water is entrained in the steam and does not help to keep the wall wet, dryout would occur at a lower quality. If it is assumed that dryout occurs at an outlet quality of 0.5, for example, Figure V-5 would predict dryout at 3.5×10^4 BTU/hr ft^2.

The fact that dryout occurs at 6.4×10^4 BTU/hr ft^2, rather than 4.25×10^4 BTU/hr ft^2 or below, is probably a result of the pressure and flow oscillations. As discussed in Section V.A.3, these oscillations appear to maintain an average quality at the top of the heated section which is lower than predicted from Figure V-5. Moreover, even at heat fluxes above CHF, these oscillations continue to provide enough water for periodic rewetting of the tube wall; and the Leidenfrost temperature is not exceeded until the heat flux is above 7.3×10^4 BTU/hr ft^2.

5. Transient Tests (Runs #5 and #6)

a. Step Increase in Heat Flux to Beyond CHF (Run #5)

This test was discussed in Section IV.B.1. The heat flux was increased from zero to 7.3×10^4 BTU/hr ft^2 using a knife switch. The result is shown in Figure IV-6. This Figure and the visual observations at the sight flow indicators indicate that the equilibrium

flow condition (Run #4) was reached within a few seconds. The equilibrium tube wall temperature at T_6 (upstream of the CHF location) was reached in 10 seconds. However, the equilibrium tube wall temperature at the CHF location was not reached until about 135 seconds after the power was turned on.

This result provides evidence that the flow oscillations corresponding to CHF would develop very quickly in a transient situation. Moreover, the CHF condition appears to result in the same tube wall temperatures regardless of whether it is approached slowly from lower heat fluxes or very rapidly in a single step.

b. Liedenfrost Temperature (Run #6)

This test was discussed in Section IV.B.2. The heat flux was increased to about 8×10^4 BTU/hr ft^2 and the temperature was allowed to increase to about 1547°F. Then the power was decreased to well below the power corresponding to CHF. The resulting temperature transient (Figure IV-5) shows a sharp increase in the cooldown rate once the temperature drops below 900°F. This provides additional evidence that the Liedenfrost temperature is about 900°F for the steam-water system used for these tests.

B. Analysis of LMFBR

1. Flow-Pressure Drop Characteristics of Reactor Loop

In Section V.A.1, an analysis was done to determine the flow-pressure drop characteristics of the water test loop. A similar analysis can be done for the reactor loop shown in Figure II-1a. Therefore steady state solutions for Equation (V-2) for the reactor loop can be obtained as described in Section V.A.1, providing the numerical values used for fixed parameters involving geometry and fluid properties are those appropriate to the reactor loop. The results of

such an analysis are shown in Figures V-10, V-11, and V-12.

The numerical values of fixed parameters involving geometry and fluid properties were those listed for the FTR in Tables II-1A and II-1B. These values were the following:

$$\rho_f = 46.4 \text{ lb}_m/\text{ft}^3$$

$$x_1 = -0.165$$

$$\frac{\rho_f}{\rho_g} = 1865$$

$$f = 0.0055$$

$$D = 0.128 \text{ in.}$$

$$A = 0.0154 \text{ in.}^2$$

$$L_1' = 131 \text{ in.}$$

$$L_H = 36 \text{ in.}$$

$$L_2 = 48 \text{ in.}$$

$$L_2' = 57 \text{ in.}$$

The values of D, A, and L_1' were obtained from data and information taken from Reference (9). D and A are, respectively, the equivalent diameter and flow area for an average subchannel of the reactor and were obtained from Appendix I of Reference (9). L_1' was obtained from information in Table 3.4 of Reference (9) which indicates that, for an average assembly (Zone 1), the ratio of the rated single phase flow pressure drop across the inlet nozzle and orifice block to the pressure drop across the core region of the bundle is 60.6/16.7 or 3.63. Thus:

$$L_1' = 3.63(36) = 131 \text{ in.}$$

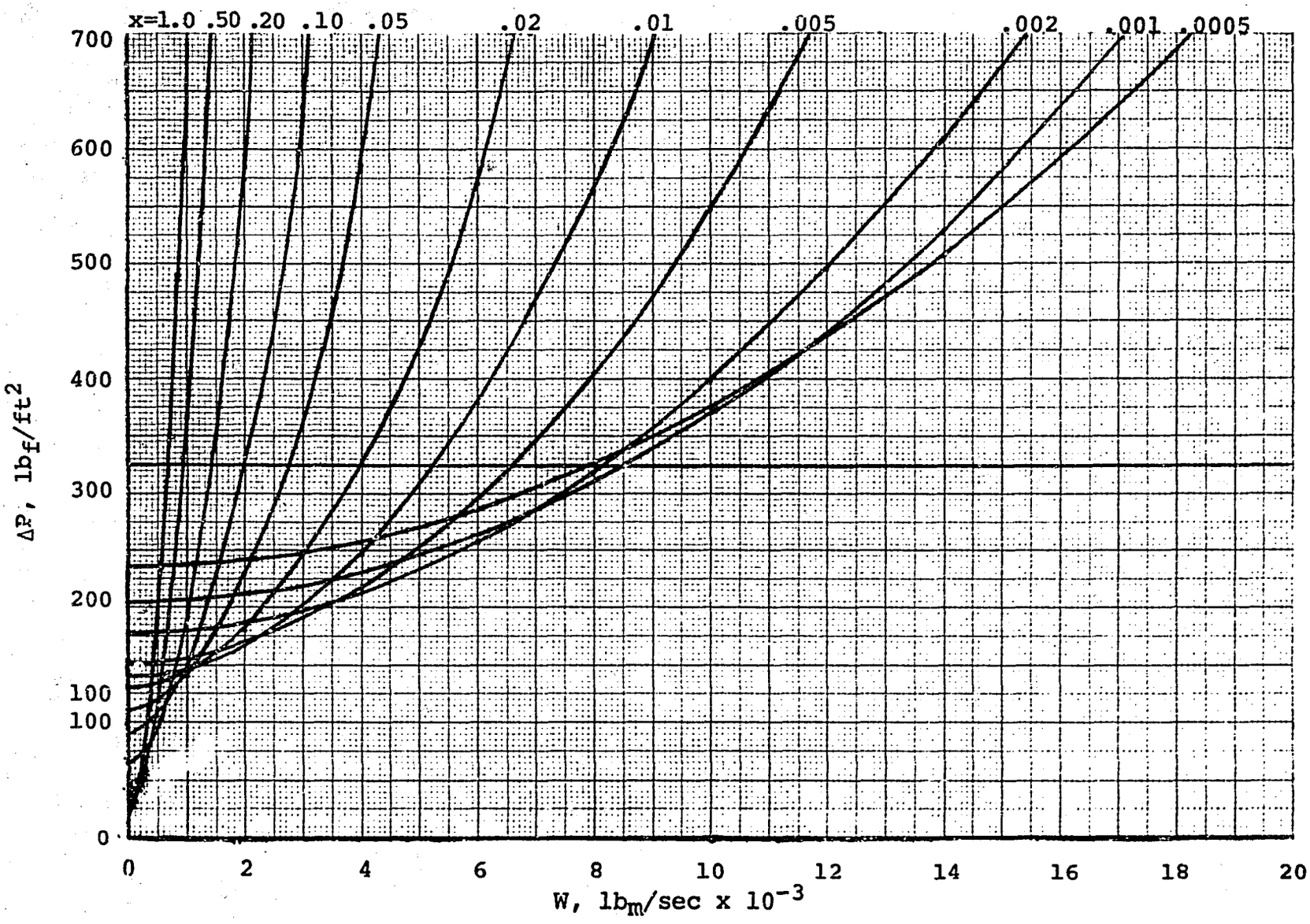

Figure V-10
Flow-Pressure Drop Characteristics of LMFBR
(FTR) with Exit Quality as a Parameter

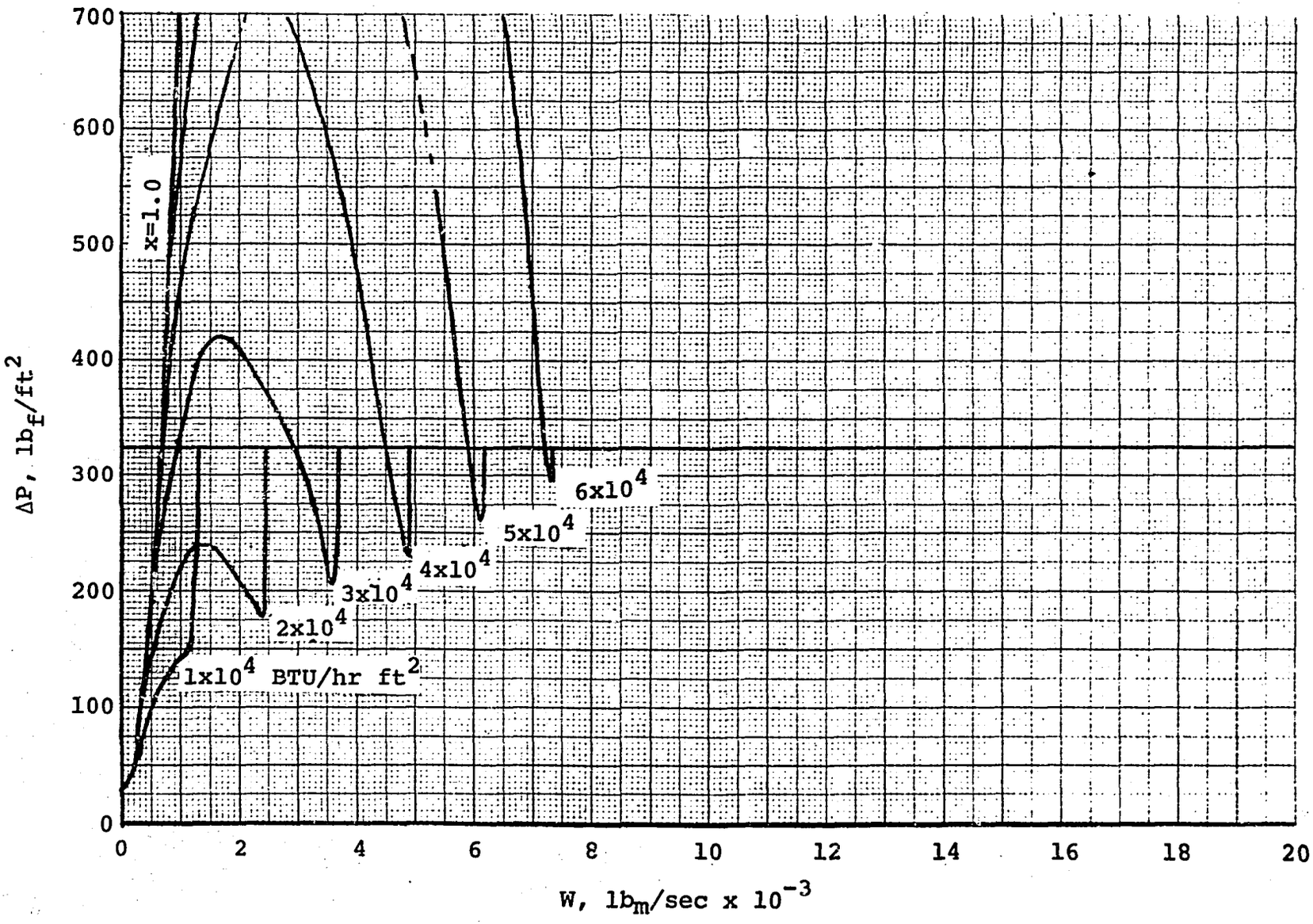

Figure V-11
Flow-Pressure Drop Characteristics of LMFBR (FTR) with Heat Flux as a Parameter

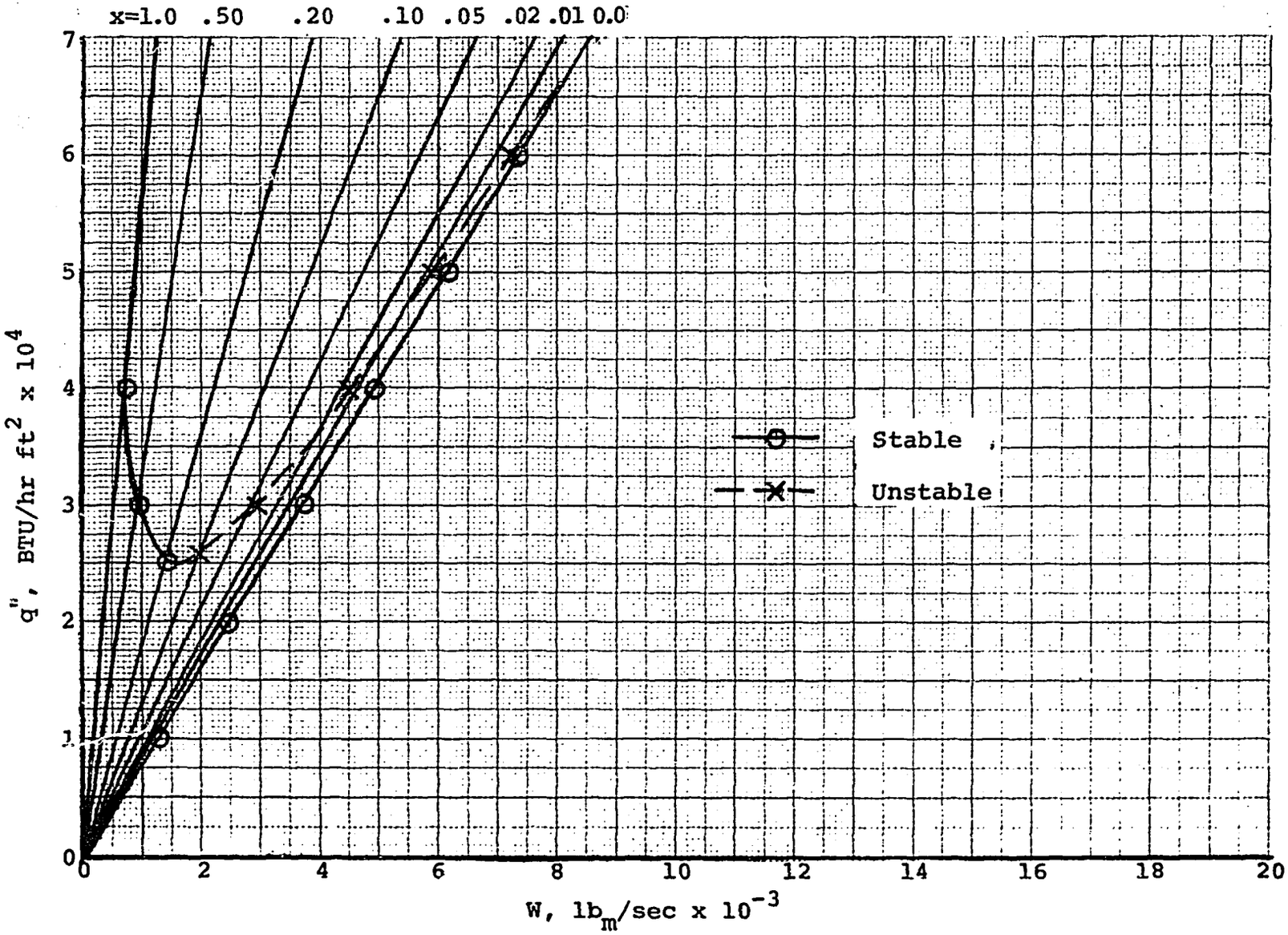

Figure V-12

Steady State Flow Conditions for LMFBR (FTR)
Determined from Figures V-10 and V-11

Similarly, the ratio of the single phase pressure drop across the part of the bundle associated with the fission gas plenum and the exit hardware to the pressure drop across the core region is $\frac{26.4}{16.7}$ or 1.58. Thus

$$L_2' = 1.58 \times 36 = 57 \text{ in.}$$

as listed above.

2. Subcooled Boiling

In the LMFBR, under LOPI accident conditions subcooled boiling would probably not occur. This is because of the fact that, in sodium cooled systems such as the LMFBR, a substantial amount of bulk liquid superheat is needed before vapor generation can take place (10). The superheat required for boiling in sodium may range as high as 500°F; but it is expected to be on the order of 30-50°F in a reactor environment (11).

3. Bulk Boiling

For the reason given above, boiling during a LOPI accident would probably be bulk boiling. Therefore, a flow condition would probably develop which is essentially the same as described in Section V.A.3 for the water tests. Specifically, vapor generated in the core region would probably be generated faster than it could be forced through the top of the fuel assembly to the upper plenum. Thus a vapor bubble would expand downward through the fuel assembly and into the region below the core. However, upon contacting the subcooled liquid trying to enter from the lower plenum, this bubble would condense and collapse, allowing liquid to reenter the core. An oscillatory flow condition would thus develop in which a vapor bubble alternately grows and collapses and liquid periodically enters the core in slugs.

Once the reactor coolant pumps coast down to an extent such that flow through core is driven only by the buoyancy force caused by the

density difference between the hot assembly and the colder assemblies on the periphery of the core, a natural circulation loop such as shown schematically in Figure IV-1a would be established. The flow condition would then depend on the heat flux; and the oscillations described above would probably result in an average mass flow rate somewhere between the high and low quality stable flow rates predicted by Figure V-12. The reasoning behind this assertion is the same as given in Section V.A.3 for the water tests.

4. Onset of CHF

As described in Section II, the water test loop was designed so that its flow rate-pressure drop characteristics would be similar to the LMFBR (FTR) under both steady state and transient flow conditions. Thus, if Q/h_{fg} is the same for the two systems, the mass flow rate (due to natural circulation) and exit quality should be about the same. Also, the rate of change of mass flow rate and quality under oscillatory conditions should be about the same. Therefore, for natural circulation boiling conditions, CHF should occur at about the same value of Q/h_{fg} for the two systems.

But, as can be seen from Tables II-1A and II-1B, all of the geometry and fluid property parameters of the LMFBR were not matched exactly. Therefore an estimate of the CHF condition for the LMFBR can be made more accurately by using Figures V-5 and V-12, rather than by just using the value of Q/h_{fg} corresponding to CHF in the water tests. Figure V-5 shows that lowest heat flux which gives a stable flow condition corresponding to an exit quality of 1.0 is 4.25×10^4 BTU/hr ft^2. The corresponding heat flux for the LMFBR is 4.0×10^4 BTU/hr ft^2. Using the ratio of these two heat flux values as a scale factor and multiplying by the CHF of 6.4×10^4 BTU/hr ft^2 observed in the water tests then gives 6×10^4 BTU/hr ft^2 as the predicted CHF for the LMFBR.

If it is assumed (as discussed in Section II.A) that the CHF mechanism in the LMFBR under LOPI accident conditions is dryout and that non-uniform heat flux effects would not be of major importance, the average fuel assembly power per subchannel corresponding to CHF would be of more interest than the heat flux. The average subchannel power for a LMFBR (FTR) fuel assembly with an average heat flux equal to the CHF is given by the following equation:

$$Q_{critical} = \frac{(CHF)(\pi d L_H)(N)}{3413} \qquad \text{(V-9)}$$

where

d is the outside diameter of the fuel rod cladding

N is the number of fuel rods per assembly

Thus (using data and information from Reference [9]):

$$Q_{critical} = \frac{(6 \times 10^{4})(\pi)(.23)(36)(217)}{(144)(3413)} = 690 \text{ kw}$$

or

$$Q'_{critical} = \frac{(690)}{(217)(3)} = 1.06 \text{ kw/ft}$$

For comparison with this result, the average linear power for the LMFBR (FTR) hot assembly during normal operation (initial condition for the LOPI accident), according to Reference (9), would be approximately:

$$(7.3)(1.4) = 10.2 \text{ kw/ft}$$

or, if it is assumed that the heat flux at the time boiling starts during a LOPI accident is 25 to 50 percent of its initial value (as indicated by the calculations described in Section I.A), the equivalent linear power at that time would be:

$$(.25 \text{ to } .5)(10.2) = 2.55 \text{ to } 5.1 \text{ kw/ft}$$

On the basis of this comparison, the results of the water tests indicate that CHF would occur in the LMFBR (FTR) hot assembly at the time boiling begins during a LOPI accident, if the only flow is due to natural circulation. But, it should be recognized that the water test results and therefore this conclusion are probably conservative (pessimistic) for the following reasons:

1) The results of the water tests indicate that when CHF occurs there is still a substantial amount of entrained liquid present at the CHF location. But the fact that this amount of liquid could no longer keep the heated surface wet at the CHF location in the water tests does not mean it would not do so in the reactor under similar conditions. This is because the surface tension for water is substantially less than for sodium. Therefore, in the reactor, the amount of entrainment should be less; and the critical quality (and CHF) would be higher than indicated by the tests.

2) The fact that the flow is oscillating when CHF occurs indicates that the film flow rate at the CHF location could be very small for short periods of time. Under such conditions, the CHF would depend on the conductivity of the liquid. Specifically, it would be expected that for similar time periods between arrival of slugs of liquid from the lower plenum, the heat flux required to disrupt the film would be less for a liquid of lower conductivity. Therefore, since sodium has a substantially higher conductivity than water, a higher CHF would be expected, other conditions being the same.

3) Calculational results discussed in Section II.A indicate that the pump induced flow through the reactor core at the time boiling is initiated would be 20 to 30 percent of the flow during normal operation. Therefore, even accounting for the fact that the increased pressure drop in the hot assembly would tend to divert flow, it is likely that the flow would be significantly above that due to natural circulation. This additional flow would also help to increase the CHF above that indicated by the tests.

4) It has been suggested (2) that, because of fission gas pressure, the fuel rod clad would swell as it gets hot during a LOPI transient. If this is the case the gap conductance would decrease and the rate stored heat is transferred from the fuel would decrease. This would result in a lower reactor heat flux at the time boiling begins than assumed in the above comparison.

5. Beyond CHF

The results of the water tests indicated that, until the heat flux was increased significantly above the CHF (7.3×10^4 BTU/hr ft^2 compared to CHF of 6.4×10^4 BTU/hr ft^2) periodic rewetting kept the maximum tube wall temperature below the Liedenfrost temperature. Similar effects could occur in the LMFBR. In addition, because of the lower surface tension (better wetting characteristics) and higher thermal conductivity of sodium as compared to water, post CHF heat transfer in the LMFBR could be even better than observed in the water tests. Also, as the clad temperature rises during a temperature excursion, the gap conductance effect could become even more important. On the other hand, if the CHF does occur at higher quality for the reasons given above, there may not be much liquid available for rewetting beyond CHF. Also, since the saturation temperature for sodium is 1670°F compared to 212°F for water, the initial temperature for the periodic temperature excursions would be higher in the LMFBR. And, the difference between the dimensions of the electrically heated tube and the fuel clad combined with the higher CHF would result in a dT/dt for the reactor about 6 times that observed in the tests. Thus the amount of time available for rewetting before the Liedenfrost temperature is exceeded (or melting occurs) would be very short. The overall conclusion to be drawn from these positive and negative factors is that post-CHF heat transfer in the LMFBR could be better or worse than observed in the water tests. More prototypical tests with sodium would be needed to determine which it is.

BLANK PAGE

VI. CONCLUSIONS AND RECOMMENDATIONS

A. Conclusions

As stated in Section I.B, it was expected that data and information obtained from the tests described in this report would help to answer several questions concerning the nature and effect of natural circulation flow oscillations on post-voiding heat transfer under conditions similar to those predicted to exist during an LMFBR LOPI accident. Therefore, it is appropriate to conclude this report by summarizing some of the principal results and conclusions from these tests within a framework provided by these questions.

> What types of oscillations occur? What appears to be the cause of these oscillations? How do they affect post-voiding, pre-CHF heat transfer?

For subcooled flow boiling, both pressure oscillations and oscillations of the heated surface temperature were observed; but the pressure oscillations were not observed continuously (Sections IV.A.1 and IV.A.2). At a heat flux of about 1×10^4 BTU/hr ft^2 (corresponding approximately to the onset of subcooled boiling) the time interval between appearance of the pressure oscillations was about 45 seconds; but as the heat flux/flow condition approached bulk boiling, this time interval decreased. At a heat flux of 1×10^4 BTU/hr ft^2 the period of the pressure oscillations was less than 1 second; but as the heat flux/flow condition approached bulk boiling, the period increased. The period of the temperature oscillations was approximately the same as the time interval between appearance of the pressure oscillations.

The pressure oscillations were probably due to vapor bubble formation and collapse associated with the subcooled boiling process. The periodic appearance of the pressure oscillations at the onset of subcooled boiling was probably due to a periodic change in the heat transfer process at the top of the heated section from single phase convection to nucleate boiling (Section V.A.2.b). Calculations indicate that this change would result in an increased flow (Section V.A.1). After a few seconds this increased flow, combined with the improved heat transfer would cause a decrease in the heated surface temperature. Then, once the surface temperature decreased below that needed to maintain nucleate boiling, boiling would stop and the heat transfer mechanism would revert back to single phase convection. Also, the flow would decrease. This change then results in a gradual increase in heated surface temperature back to the temperature required for onset of nucleate boiling and the cycle would repeat. As the heat flux/flow condition approaches bulk boiling the time period required for this cycle of events would decrease, as was observed.

For bulk boiling conditions, at a heat flux of 3.83×10^4 BTU/hr ft^2, pressure oscillations were observed continuously. However, the heated surface temperatures were relatively steady (Section IV.A.3). The period of the pressure oscillations was 1 - 2 seconds.

The pressure oscillations observed for bulk boiling were similar to those observed for subcooled boiling and probably also relate to vapor (bubble) formation and collapse (Section V.A.3c). Calculations indicate that, for a given heat flux in the bulk boiling range, there are two stable flow conditions (Section V.A.1). One of these is a high flow, low quality condition and the other is a low flow, high quality condition. But, the high flow low quality condition tends to

be unstable; since, only a relatively small, momentary decrease in flow would create an unstable situation resulting in a further decrease in flow. As a result, the rate of vapor generation would increase and the quality would increase. However, observations indicate that a condition quickly develops where the rate of vapor generation is greater than the rate at which it can flow out the top of the heated section. Thus the pressure builds up and the excess vapor pushes downward through the heated section. At the same time, the liquid flow into the test section decreases and the void fraction within the test section increases. Eventually, enough of the test section is voided so that the steam being generated can flow out the top of the heated section as fast as it is being generated. However, this flow condition is not in thermal equilibrium in the upstream half of the test section due to the presence of a substantial amount of subcooled water. As a result the steam in this part of the test section begins to condense and the water flow into the test section increases, causing still further condensation and a return toward the original high flow, lower void fraction condition from which the transient initially started. Then, since this flow condition tends to be unstable the sequence begins again.

> Under what conditions does CHF occur? What is the mechanism? What is the role of the observed oscillations? How is rewetting and post-CHF heat transfer related to the oscillations? How does the power corresponding to CHF compare to the power it takes to completely vaporize a steady homogeneous flow driven by the hydrostatic pressure difference between the inlet and outlet of the test section (or the appropriate length)?

As the CHF condition was approached the average water temperatures entering the heated section increased to a temperature well above the liquid temperature in the lower plenum. This was due to the observed periodic downward expansion of vapor from the heated section into the

inlet section, and the resulting condensation and mixing (Section IV.A.4). Thus the average quality of the vapor-liquid mixture leaving the top of the heated section also increased. The flow regime appeared to be annular and the film flow rate at the top of the heated section was probably oscillating with time as a result of the pressure and flow oscillations.

CHF was observed at a heat flux of 6.4×10^4 BTU/hr ft^2. It occurred at the top of the heated section; and the mechanism was probably due to dryout of the liquid film during a pressure oscillation when vapor was expanding downward through the test section. However, rewetting occurred after a few seconds, apparently because of reentry of a slug of liquid into the test section as the vapor bubble collapsed at the other end of a pressure oscillation. Then CHF occurred again and the cycle repeated. As the heat flux was increased the maximum surface temperature during each oscillation increased; until, at a heat flux of 7.15×10^4 BTU/hr ft^2, the maximum temperature exceeded 900°F and could no longer be rewetted.

Calculation based on a homogeneous, steady flow model indicated that the heat flux required to completely vaporize a flow driven only by the hydrostatic pressure difference between the inlet and outlet of the test section is 4.25×10^4 BTU/hr ft^2 (Section V.A.1). The test results as stated above, indicate that the CHF is 6.4×10^4 BTU/hr ft^2. Moreover, even at this heat flux, liquid was observed in the flow stream downstream of the CHF location (Section IV.A.4). Thus the oscillating flow condition observed in the tests is able to maintain the exit quality below the CHF quality at a substantially higher heat flux than predicted from a homogeneous, steady flow model.

To what extent are the answers to the previous questions applicable to the LMFBR during the first few seconds of a LOPI accident?

In the LMFBR, subcooled boiling would probably not occur. This is because of the fact that, in sodium cooled systems such as the LMFBR, a substantial amount of bulk liquid superheat is needed before vapor generation can take place (10). The superheat required for boiling in sodium may range as high as 500°F; but it is expected to be on the order of 30 - 50°F in a reactor environment (11). Therefore, the first boiling during a LOPI accident would probably be bulk boiling; and a flow condition would probably develop similar to that observed in the water tests. Specifically, vapor generated in the core region would probably be generated faster than it could be forced through the top of the fuel assembly to the upper plenum. Thus a vapor bubble would expand downward through the fuel assembly and into the region below the core. However, upon contacting the subcooled liquid trying to enter from the lower plenum, this bubble would condense and collapse, allowing liquid to reenter the core. An oscillatory flow condition would thus develop in which a vapor bubble alternately grows and collapses and liquid periodically enters the core in slugs.

Once the reactor coolant pumps coast down to an extent such that flow through core is driven only by the buoyancy force caused by the density difference between the hot assembly and the colder assemblies on the periphery of the core, a natural circulation loop such as shown schematically in Figure IV-1a would be established. The flow condition would then depend on the heat flux.

The water test loop was designed (Section II) so that its flow rate-pressure drop characteristics would be similar to the LMFBR (FTR)

under both steady state and transient flow conditions. Thus, if Q/h_{fg} is the same for the two systems, the mass flow rate (due to natural circulation) and exit quality should be about the same. Also, the rate of change of mass flow rate and quality under oscillatory conditions should be about the same. Therefore, for natural circulation boiling conditions, CHF should occur at about the same value of Q/h_{fg} for the two systems.

But, as can be seen from Tables II-1A and II-1B, all of the geometry and fluid property parameters of the LMFBR were not matched exactly. Therefore, analysis results based on a homogeneous flow model (Sections V.A.1 and V.B.1) were used to obtain a scale factor (Section V.B.4). Multiplying this factor times the CHF of 6.4×10^4 BTU/hr ft^2 observed in the water tests then gives 6×10^4 BTU/hr ft^2 as the predicted CHF for the LMFBR.

If it is assumed (as discussed in Section II.A) that the CHF mechanism in the LMFBR under LOPI accident conditions is dryout and that non-uniform heat flux effects would not be of major importance, the average linear power of the hot fuel assembly corresponding to the CHF would be of more interest than the heat flux. This critical linear power is 1.06 kw/ft, which compares to an estimated 2.55 to 5.1 kw/ft being transferred to the coolant at the time boiling begins (Section V.B.4).

On the basis of this comparison, the results of the water tests indicate that CHF would occur in the LMFBR (FTR) hot assembly at the time boiling begins during a LOPI accident, if the only flow is due to natural circulation. But, it should be recognized that the water test results and therefore this conclusion are probably conservative for the following reasons.

1) The results of the water tests indicate that when CHF occurs there is still a substantial amount of entrained liquid present at the CHF location. But the fact that this amount of liquid could no longer keep the heated surface wet at the CHF location in the water tests does not mean it would not do so in the reactor under similar conditions. This is because the surface tension for water is substantially less than for sodium. Therefore, in the reactor, the amount of entrainment should be less; and the critical quality (and CHF) would be higher than indicated by the tests.

2) The fact that the flow is oscillating when CHF occurs indicates that the film flow rate at the CHF location could be very small for short periods of time. Under such conditions, the CHF would depend on the conductivity of the liquid. Specifically, it would be expected that for similar time periods between arrival of slugs of liquid from the lower plenum, the heat flux required to disrupt the film would be less for a liquid of lower conductivity. Therefore, since sodium has a substantially higher conductivity than water, a higher CHF would be expected, other conditions being the same.

3) Calculational results discussed in Section II.A indicate that the pump induced flow through the reactor core at the time boiling is initiated would be 20 to 30 percent of the flow during normal operation. Therefore, even accounting for the fact that the increased pressure drop in the hot assembly would tend to divert flow, it is likely that the flow would be significantly above that due to natural circulation. This additional flow would also help to increase the CHF above that indicated by the tests.

4) It has been suggested (2) that, because of fission gas pressure, the fuel rod clad would swell as it gets hot during a LOPI transient. If this is the case the gap conductance would decrease and the rate stored heat is transferred from the fuel would decrease. This would result in a lower reactor heat flux at the time boiling begins than assumed in the above comparison.

The results of the water tests indicated that, until the heat flux was increased significantly above the CHF (7.15×10^4 BTU/hr ft^2 compared to CHF of 6.4×10^4 BTU/hr ft^2) periodic rewetting kept the maximum tube wall temperature below the Liedenfrost temperature. Similar effects could occur in the LMFBR. In addition, because of the lower surface tension (better wetting characteristics) and higher thermal conductivity of sodium as compared to water, post-CHF heat transfer in the LMFBR could be even better than observed in the water

tests. Also as the clad temperature rises during a temperature excursion the gap conductance effect could become even more important. On the other hand, if the CHF does occur at higher quality for the reasons given above, there may not be much liquid available for rewetting beyond CHF. Also, since the saturation temperature for sodium is 1670°F compared to 212°F for water, the initial temperature for the periodic temperature excursions would be higher in the LMFBR. And, the difference between the dimensions of the electrically heated tube and the fuel clad combined with the higher CHF would result in a dT/dt for the reactor about 6 times that observed in the tests. Thus the amount of time available for rewetting before the Liedenfrost temperature is exceeded (or melting occurs) would be very short. The overall conclusion to be drawn from these positive and negative factors is that post-CHF heat transfer in the LMFBR could be better or worse than observed in the water tests. More prototypical tests with sodium would be needed to determine which it is.

B. Recommendations

Recommendations for further work based on the results of the tests and analyses described in this report are the following:

1) Experimental and analytical work should continue using the low-pressure water loop used for the tests described in this report. Additional experiments should focus on pre-CHF conditions. More detailed measurements should be made relating to pressure oscillations near CHF. In addition, flow measurements should be made in order to verify some of the conclusions arrived at in this study. Further experiments might also include modifications of test section geometry to allow better visualization of flow conditions near the CHF location. A transient experiment might also be run to simulate the LOPI flow transient and the effect of pump induced flow remaining at the time boiling starts. Analytical work should include development of a more detailed model of the oscillating flow conditions leading to CHF. This model should include transient effects, slip flow and non-equilibrium effects.

2) Similar tests should be run with sodium. Initially, it is suggested that such tests be done using a simple loop geometry similar to the water test loop. Measurements should be the same as in the water tests, except that measurement of test section flow should also be included. Also, the focus should be on heat flux conditions near CHF. Both steady state and transient tests (of the type included in the water tests) should be done. The results should be compared with the water tests and the analysis in Section V.B of this report (or some improvement on this analysis). Once the tests with the simple geometry are completed, more prototypical tests should be conducted using rod bundle geometry.

REFERENCES

1. Driscoll, M., P. M. Magee, and Y. S. Tang, Unpublished papers and analyses prepared for ERDA LMFBR Loss of Pipe Integrity Working Group, February - August, 1975.

2. Griffith, P., "An Overview of LMFBR Voiding," Unpublished paper prepared for ERDA LMFBR Loss of Pipe Integrity Working Group, March, 1975.

3. Blaisdell, J. A., L. E. Hochreiter, and J. P. Waring, "PWR FLECHT-SET Phase A Report," WCAP-8239, December, 1973.

4. Bonilla, C. F., "Nuclear Engineering," McGraw Hill, 1957, Chapter 8.

5. Bouve, J. A., A. E. Bergles, and L. S. Tong, "Review of Two Phase Flow Instabiltiy," ASME Paper 71-HT-42, Paper presented at the ASME-AIChE Heat Transfer Conference held in Tulsa, Oklahoma, August 15-18, 1971.

6. Bergles, A. E., and W. M. Rohsenow, "The Determination of Forced Convection Surface Boiling Heat Transfer," ASME Paper 63-HT-22. Paper presented at the 6th ASME-AIChe Heat Transfer Conference held in Boston, August 11-14, 1963.

7. Bonilla, C. F., "Nuclear Engineering," McGraw Hill, 1957, Chapter 9.

8. Schrock, V.E. and L. M. Grossman, "Forced Convection Boiling Studies," Final Report on Forced Convection Vaporization Project, TID-14632, 1959.

9. Calamai, G. J. et al., "Steady State Thermal and Hydraulic Characteristics of the FFTF Fuel Assemblies," FRT-1582, June 1974.

10. Collier, J. G., "Boiling of Liquid Alkali Metals," Chemical Process Engineering Heat Transfer Survey, 1968.

11. Graham, J., "Fast Reactor Safety," Academic Press, 1971, p. 26.

12. McAdams, W. H., Heat Transmission, McGraw Hill, Third Edition, 1954, p. 19, Equation (2-14d).

BLANK PAGE

NOMENCLATURE

A	Cross sectional flow area of tube or average reactor fuel assembly subcahnnel, ft^2.
C_f	Specific heat of saturated liquid, $BTU/lb_m°F$.
C_s	Specific heat of stainless steel, $BTU/lb_m°F$.
CHF	Critical heat flux, $BTU/hr\ ft^2$.
D	Diameter of tube or equivalent diameter of average reactor fuel assembly subchannel, ft.
d	Outside diameter of reactor fuel rod clad, ft.
F_1	Quantity in Equation V-7 defined as fraction of one cycle of temperature oscillation for which flow is single phase, dimensionless.
F_2	Quantity in Equation V-7 defined as fraction of one cycle of temperature oscillation for subcooled boiling occurs, dimensionless.
f	Fanning friction factor, dimensionless.
g	Gravitational acceleration, $32.2\ ft/sec^2$.
g_c	Dimensional constant, $32.2\ lb_m ft/lb_f sec^2$.
h	Enthalpy of liquid or liquid-vapor mixture, BTU/lb_m.
h_{fg}	Enthalpy of vaporization, BTU/lb_m.
$\bar{h}$	Heat transfer coefficient corresponding to average test section flow, $BTU/hr\ ft^2°F$.
$\bar{h}_{1,2}$	Heat transfer coefficient at top of test section heated length, as calculated from Equation (III- 6), $BTU/hr\ ft^2\ °F$.
J	Mechanical equivalent of heat, $778\ ft\ lb_f/BTU$.
K_1	Friction coefficient associated with flow area contraction at test section inlet, dimensionless.
K_2	Friction coefficient associated with flow area expansion at test section outlet, dimensionless.
k_f	Thermal conductivity of saturated liquid, $BTU/hr\ ft°F$.
k_s	Thermal conductivity of stainless steel, $BTU/hr\ ft°F$.

L	Total length of vertical tube test section or reactor fuel assembly, ft.
L_1	Length of unheated inlet section of the test section or reactor fuel assembly, ft.
L'_1	Equivalent length of the unheated inlet section of the test section or reactor fuel assembly, including the effect of the inlet contraction and orifice, ft.
$L_{1\phi}$	Length of the single phase region within the test section or reactor fuel assembly, ft.
$L'_{1\phi}$	Equivalent length of the single phase region of the test section or reactor fuel assembly, including the effect of the inlet contraction and orifice, ft.
L_H	Length of the heated section of the test section or reactor fuel assembly, ft.
L_2	Length of the unheated outlet section of the test section or reactor fuel assembly, ft.
L'_2	Equivalent length of the unheated outlet section of the test section or reactor fuel assembly, including the effect of the outlet expansion, ft.
$L_{2\phi}$	Length of the two-phase region of the test section or reactor fuel assembly, ft.
$L'_{2\phi}$	Equivalent length of the two-phase region of the test section or reactor fuel assembly, ft.
L_B	Boiling length within the test section or reactor fuel assembly, as defined by Equation (II-14), ft.
N	Number of fuel rods per reactor fuel assembly, dimensionless.
P	Static pressure, psia.
ΔP	Pressure drop, lb/ft^2.
P_1, P_2 and P_3	Pressures at various locations in the test loop (see Figure II-9), psig.
Pr_f	Prandtl number of saturated liquid, $\mu_f C_f/k_f$, dimensionless.
Q	Power of test section or average reactor fuel assembly subchannel, BTU/hr or kw.
$Q_{critical}$	Power of test section or average reactor fuel assembly corresponding to CHF, BTU/hr or kw.
$Q'_{critical}$	Linear power of average reactor subchannel corresponding to CHF, kw/ft.

q''	Average heat flux to test section or reactor fuel assembly heated length, BTU/hr ft^2.
$q''(z)$	Heat flux at a specific distance, z, from the inlet of the test section or reactor fuel assembly, BTU/hr ft^2.
q''_{ONB}	Heat flux required for onset of nucleate boiling at $(\Delta T_{sat})_{ONB}$ according to Equation (V-4), BTU/hr ft^2.
$\bar{R}$	Average two-phase friction multiplier along the two-phase length of the test section or reactor fuel assembly, defined in relation to Equation (II-8), dimensionless.
R_1	Inside radius of vertical tube test section, ft.
R_2	Outside radius of vertical tube test section, ft.
Re_f	Reynolds number, $4W/\pi D\mu_f$, dimensionless.
T_1 through T_{15}	Temperatures at various locations in the test loop (see Figure II-9), °F.
T_i	Temperature of the inside surface of the vertical tube test section, °F.
T_o	Temperature of the outside surface of the vertical tube test section, °F.
T_s	Average temperature of stainless steel tube wall or fuel rod clad, °F.
T_{sat}	Liquid saturation temperature, °F.
ΔT_{sat}	Difference between temperature of heated surface and liquid saturation temperature, °F.
$(\Delta T_{sat})_{ONB}$	ΔT_{sat} required for the onset of nucleate boiling at q''_{ONB} according to Equation (V-4), °F.
u	Internal energy of liquid or liquid-vapor mixture, BTU/lb_m.
V_L	Velocity of single phase liquid, ft/sec.
V_m	Velocity of liquid-vapor mixture in homogeneous flow, as defined in relation to Equations (II-1), (II-2) and (II-3), ft/sec.
v_f	Specific volume of saturated liquid, ft^3/lb_m.
v_g	Specific volume of saturated vapor, ft^3/lb_m.
v_{fg}	Difference, $v_g - v_f$, ft^3/lb_m.
v_m	Specific volume of liquid-vapor mixture in homogeneous flow, lb_m/ft^3.

W	Mass flow rate of liquid or liquid-vapor mixture, lb_m/hr.
$\overline{W}$	Average mass flow rate of liquid or liquid-vapor mixture, lb_m/hr.
x	Flowing or thermodynamic equilibrium quality, dimensionless.
x_1	Quality of liquid in lower plenum of test loop or reactor, $C_f\frac{(T_{sat}-T_1)}{h_{fg}}$, dimensionless.
x_{out}	Quality of liquid-vapor mixture leaving heated section of test section or reactor fuel assembly, dimensionless.
x_2	Quality of liquid in upper plenum of test loop or reactor, $C_f\frac{(T_{sat}-T_2)}{h_{fg}}$, dimensionless.
z	Distance from inlet of test section or reactor fuel assembly, ft.

Greek Letters

δ	Thickness of test section tube wall or reactor cladding, ft.
μ_f	Viscosity of saturated liquid, $lb_m/ft\ hr$.
π	Constant, 3.14.
ρ_f	Density of saturated liquid, lb_m/ft^3.
ρ_g	Density of saturated vapor, lb_m/ft^3.
ρ_L	Density of subcooled liquid, lb_m/ft^3.
ρ_m	Density of liquid-vapor mixture in homogeneous flow, lb_m/ft^3.
$\overline{\rho}_m$	Average density of liquid-vapor mixture along the two-phase length of the test section or reactor fuel assembly, defined in relation to Equation (II-8), dimensionless.
ρ_s	Density of stainless steel, lb_m/ft^3.
σ_f	Liquid surface tension, lb_f/ft.
τ	Wall shear stress, lb_f/ft^2.
ϕ	Dimensionless quantity, $x_{out}\frac{\rho_f}{\rho_g}$, defined in relation to Equation (V-2).